Mobility Control for CO_2 EOR in Heterogeneous Reservoirs

Master Thesis in Reservoir Physics

Kristine Bø

Department of Physics and Technology

University of Bergen

June 2014

Summary

This experimental thesis investigates enhanced oil recovery (EOR) by secondary and tertiary CO_2 and/or CO_2-foam injections at miscible conditions in fractured and whole core plugs using different rock types. Injection of CO_2 for EOR has in recent years received increased attention because it may 1) reduce CO_2 concentration in the atmosphere to reduce global warming, and 2) significantly improved oil recovery. A major challenge is the low viscosity of the injected CO_2, which may lead to poor sweep efficiency and low oil recovery. Poor sweep is a general challenge in fractured reservoirs, where the fractures control flow and matrix blocks are saturated with oil. Mobility control by the use of CO_2-foam will increase the apparent gas viscosity and provide a more favorable mobility ratio and lead to incremental oil recovery by adding a viscous component to the transport of CO_2 from the fracture to the matrix.

Laboratory experiments have been carried out on Portland chalk cores and Edward limestone cores, as analogues to reservoir rocks, in addition to reservoir cores. From a total of 52 cores prepared, 28 cores were used for CO_2 and/or CO_2 foam injections conducted with different setups that was designed tested and used, located in three different laboratories: Department of Physics and Technology, Haukeland University Hospital and Texas A&M University.

Secondary miscible CO_2 and CO_2-foam flooding experiments were performed on both fractured and non-fractured, strongly water-wet core material to study recovery performance. Mineral oil was used in all experiments to ensure miscibility with CO_2, at both liquid and supercritical conditions. Eight supercritical CO_2 experiments were conducted in strongly water-wet fractured and non-fractured Edward limestone and Portland chalk outcrops. Results showed high recoveries in the range of 81.5 – 89.9 % of OOIP for the whole cores and lower recoveries in the range of 57.5 – 68.4 % of OOIP for the fractured cores. Less amount of CO_2 was required to reach end point oil saturation in the whole cores compared to the fractured cores. To investigate if the recovery performance by CO_2 diffusion could be improved in a fractured system a subsequent CO_2-foam injection for mobility control were conducted in six additional experiments. The results from experiments in Edward limestone cores suggested that strong foam is generated and accelerated the oil production, whereas no significant effect was observed in the Portland chalk. General observations from the secondary CO_2 and CO_2-foam injection indicate that oil recovery by diffusion is more prominent in chalk material and foam is more efficient in limestone material, suspected to be caused by differences in pore characteristics.

Integrated EOR, by combing proven EOR methods in a smart sequence, was evaluated in strongly water-wet, fractured limestone cores at supercritical conditions. The core plugs were first waterflooded, then CO_2–injection and subsequent CO_2-foam injections were performed. The oil recovery was increased for each injection step, and an accelerated oil recovery was observed

during CO_2-foam injections due to in-situ generation of foam in fractured systems. Tertiary CO_2 injections were also performed in unpreserved reservoir cores from a heterogeneous carbonate field in the USA, leading to an oil recovery above 90% of OOIP.

A “best practice” was developed to measure permeability using CO_2 and re-saturate unpreserved reservoir shale core plugs with crude oil. Using PET/CT, shale rock structure and flow behavior during CO_2 injections were evaluated.

Acknowledgements

First, I would like to thank Professor Arne Graue and Associated Professor Martin Fernø at the Department of Physics and Technology at University of Bergen for guidance, support and valuable feedback throughout the work of this thesis and for the opportunity to travel abroad to do research.

I would also like to thank Associated Professor Geir Ersland for his help and contribution to my thesis and for interesting conversations.

Thanks to Associated Professor David Schechter at the University of Texas A&M, College Station, for being able to participate in relevant experiments for my thesis. I would also like to thank Francisco Tovar for his help and collaboration in the laboratory.

I would like to thank PhD students Bergit Brattekås and Marianne Steinsbu for their contribution and collaboration in the experimental work, and thanks to Inez Buzdugan for always being helpful in the laboratory.

I would also like to express my gratitude to my fellow lab associates Rebecca Tunli and Ingrid Eikemo Opdal for a successful teamwork in the laboratory. Thank you both for always being cheerful and for making my time here a pleasure. Also thanks to all fellow MSc students for a great year.

Thanks to Geir Espen Abel for his help and expertise with experiments in the PET/CT scanner.

Also thanks to PhD student Øyvind Eide and former MSc students Stig Langlo and Tom Ydstebø for their educational guidance in early experimental work.

Finally, I would like to thank my parents and my brother for their motivation and support throughout my years of study.

Bergen, June 2014

Kristine Bø

Table of Contents

Summary 3
Acknowledgements 5
Introduction 9
1 Fundamental Principles 11
1.1 Fractured reservoirs 11
1.1.1 Fracture characterization 11
1.1.2 Fluid flow in fractured reservoirs 13
1.2 Interfacial tension (IFT) and Miscibility 14
1.1.1 Minimum miscible pressure (MMP) 16
1.2.2 Oil swelling 18
1.3 Mobility Ratio 19
1.4 Wettability 19
1.5 Capillary Pressure 20
1.6 Dispersion in porous media 22
1.6.1 Diffusion 22
1.6.2 Convection 24
1.7 Enhanced Oil Recovery 24
2. CO_2 and CO_2 Foam 25
2.1 EOR from CO_2 injection 25
2.1.1 Features of CO_2 as an EOR fluid 28
2.1.2 Secondary and Tertiary CO_2 injection 29
2.2 CO_2 Foam 31
2.2.1 Foam Mobility in heterogeneous porous media 33
2.2.2 Foam regimes/Foam stability 33
2.3 CO_2 and CO_2 foam injection on field scale 35
3. Experimental Procedure 38
3.1 Rock material 38
3.2 Fluids 40
3.3 Core Plug Preparations 41
3.3.1 Fractured cores 42
3.3.2 Wettability alteration 42
3.4 Experimental Design 43
3.5 Experimental procedure 47
3.5.1 Supercritical CO_2 injection in whole and fractured core plugs 48

3.5.2 Supercritical CO_2 and CO_2-foam injection in fractured core plugs 48
3.5.3 Secondary Liquid CO_2-foam injection in whole core plugs 49
3.5.4 Tertiary CO_2 injection and CO_2-foam injection in fractured core systems 49
3.5.5 Tertiary CO_2 injection on reservoir carbonate cores 52
3.5.6 Reservoir shale rock experiments 53
4 Results and discussion 57
4.1 Routine core analysis 57
4.2 Experimental processes 60
4.2.1 Supercritical CO_2 injection in whole and fractured core plugs 60
4.2.2 Supercritical CO_2 and CO_2-foam injection in fracture cores plugs 63
4.2.3 Secondary Liquid CO_2-foam injection in whole core plugs 69
4.2.4 Tertiary CO_2 injection and CO_2 foam injection in fractured core systems 70
4.2.5 Tertiary CO_2 injection in reservoir carbonate cores 76
4.2.6 Reservoir shale rock experiments 78
4.2.7 Uncertainties related to experiments 82
5 Concluding remarks 84
5.1 Conclusion 84
5.2 Future work 85
6 Nomenclature 86
7 References 87
Appendix A – Uncertainty calculations 94

Introduction

The high oil price and the increasingly demand for petroleum as a source of energy from limited reserves has accelerated the effort to further extend the life of hydrocarbon reservoirs. The majority of the effort is aimed at developing and implementing Enhanced Oil recovery (EOR). The objectives of EOR methods are to recover additional oil by other techniques after the conventional primary and secondary recovery methods (Katz, 1980). The aim is to increase the macroscopic sweep efficiency and to enhance the microscopic displacement efficiency in the reservoir compared to water flooding. Microscopic sweep can be increased by lowering the interfacial tension between the displacing fluid and the oil. In homogeneous reservoirs this could be done with surfactant injection or a miscible CO_2 flood. In heterogeneous reservoirs, it is desirable to reduce flow in high permeable zones or reduce the viscosity in the injected fluids to increase the macroscopic sweep area in the reservoir. Macroscopic sweep can be increased by altering the mobility ratio between the displacing and the displaced fluid and may be achieved by polymer or foam injection.

Residual oil will only be produced if profitable. Average annual U.S. natural gas prices have remained relatively low over the past several years as a result of the availability of abundant resources and the application of improved production technologies. Relatively low natural gas prices make natural gas an attractive candidate for EOR (Administration, 2014). Using miscible gas injection as an EOR method has received considerable attention in the oil industry because the oil may be displaced with maximum efficiency and the result is high recoveries. Due to economics and availability reason, carbon dioxide (CO_2) may be a potential source of gas for this process.

CO_2 is considered the primary greenhouse gas and account for about 84% of all U.S. greenhouse gas emissions from human activities (National Research Council, 2010). It is naturally present in air, and the increasing concentration of CO_2 in the atmosphere causes the temperature on Earth to rise. For this reason Carbon Capture and Storage (CCS) is a potential technology to reduce large amount of CO_2 emission. Subsurface hydrocarbon reservoirs have the required properties to trap CO_2 and are good candidates for geological sequestration. This involves capturing, transporting and compressing the CO_2 and further injecting it into a geological reservoir and monitoring its movement and behavior after sequestration (Nguyen, 2003).

CO_2 injection has been used to improve oil recovery for the past four decades. Several CO_2 injection tests have been conducted since the first commercial CO_2 injection for enhanced oil recovery at the SACROC Unit in Texas in 1974 (Graue and Blevins, 1978). The results have proven to increase oil production and indicate that CO_2 for EOR is a promising method for commercial applications. In recent years, the improved recovery method has become more

attractive because of the dual effect by CO_2 injection in the subsurface and include: 1) reduction of CO_2 concentration in the atmosphere to reduce global warming, and 2) improved oil recovery (Nasrabadi et al., 2009). It have been estimated that the "next generation" of CO_2 EOR may produce additional 67 billion barrels of oil by implementing new technology and increase macroscopic sweet by introducing thickeners and foams (Enick et al., 2012).

As most hydrocarbon reservoirs are affected in some way by natural fractures (Nelson, 2001), and 60% of hydrocarbon reservoirs worldwide have significant fracture components (Ardèvol and Gutmanis, 2008), it is important to get a better understanding of these structural features to reduce risk in development and to increase production. Because CO_2 is a low viscosity fluid, it may cause poor sweep efficiency in fractured reservoirs. Mobility control by the use of CO_2-foam may provide a more favorable mobility ratio, by adding a viscous component to the transport of CO_2 foam from the fracture to the matrix, and thus improve oil recovery (Kovscek and Bertin, 2002, Farajzadeh et al., 2009).

Prediction of field's performance undergoing miscible displacement is generally conducted by laboratory core flood experiments or reservoir simulation. In this thesis a series of laboratory experiments will be presented. The motivation of the work conducted has been to study CO_2 and CO_2-foam injection in heterogeneous reservoirs. Previous research from the Reservoir Physics Research Group at the Department of Physics and Technology has set the groundwork for experiments conducted in this thesis. The aim of this thesis have been to study recovery mechanism in heterogeneous reservoirs by CO_2 injection and CO_2-foam for mobility control on both outcrop and reservoir core plugs in idealistic systems (with miscibility between CO_2 and mineral oil) and realistic systems (with miscibility between CO_2 and crude oil). Experiments with CO_2 injection on tight shale core plugs have also been performed to study the complexity of fluid flow behavior in tight unconventional reservoirs. Visualization of the fluid flow behavior has been conducted with the use of CT and PET/CT scanners.

This thesis consists of 7 chapters. Chapter 1 gives an introduction to the basic parameters that are relevant for this thesis. Chapter 2 is more focused on CO_2 and CO_2 foam as displacements mechanism. Chapter 3 gives an overview of the experimental procedure, and includes information about rock material and fluid utilized as well as a detailed description of the experimental design. The results and discussion of the experiments is presented in Chapter 4, and Chapter 5 gives the general conclusions of this thesis as well as proposed future work. Chapter 6 and 7 presents the nomenclature and the references used in this thesis. Appendix A shows the formulas used in uncertainty calculations.

1 Fundamental Principles

This chapter gives a short theoretical introduction to some of the fundamental principles controlling fluid flow and distribution in the reservoir.

1.1 Fractured reservoirs

Fractured reservoirs represent a significant fraction of the unexploited oil and gas reserves in our nation (Kleppe and Morse, 1974). Nearly all hydrocarbon reservoirs are affected in some way by natural fractures. “A fractured reservoir is any reservoir in which naturally or occurring fractures have, or are predicted to have, a significant effect of flow rates, anisotropy, recovery, or storage” (Nelson, 2001). Fractures are found in all rock formations, both subsurface and outcrop. Many types of fracture have no major impact for fluid flow performance, yet in some reservoirs the fracture may have significant impact on fluid flow behavior, but they are often difficult to describe and to evaluate (Nelson, 2001, Ersland, 2008). One reason for this is because heterogeneity limits the validity of the relationship between recovery and time (Kleppe and Morse, 1974).

In naturally fractured reservoirs the storage capacity exists in the pore space between the mineral grains and in the fractures. To be able to extract the hydrocarbons, flow capacity is needed, which requires a continuity between the void spaces over distance (Ersland, 2008). The displacement process in a fractured reservoir occurs when the matrix block saturated with oil is partially or entirely surrounded by another phase (Golf-Racht, 1982a). In carbonate reservoirs, natural fractures help create secondary porosity and increase communications within different reservoir zones. These high permeability zones sometimes lead to channeling of the injected fluid, and thus an ineffective recovery. Natural fractures are the main driving force in a wide range of less conventional reservoir, including shale gas (Nelson, 2001).

1.1.1 Fracture characterization

A fracture is a macroscopic planar discontinuity in a rock, as a result of deformation or physical diagenesis that may modify the rock characteristics. Orientation, density and aperture are the three main fracture features of importance to create a realistic understanding of the fracture network (Ersland, 2008). It may be due to compactive or dilatant processes, thus having either a positive or negative effect on fluid flow (Nelson, 2001). The fractures may be open, sealing or partly sealing depending on the degree of mineralization and precipitation (Golf-Racht, 1982b).

When developing and modelling fractured reservoirs, the ability to understand and predict the characteristics of fracture and fracture network is essential. In the laboratory, fracture types are divided into two groups related to their mode of formation: shear fractures that form with shearing parallel to the created fracture, and tension fractures that form with tension perpendicular to the created fracture. Shear and tension fractures defined from laboratory experiments have clear counterparts that occur in nature. Shear fractures corresponds to faults and tension fractures correspond to joints. Most faulting occurs through tectonic events when differential stress is high. Joints, or fractures, form perpendicular to bedding (Bratton et al., 2006).

The stress state is important in natural fractured reservoirs because it largely dictates whether fractures are open to conduct fluids. Stress is defined as the force per unit area acting on a plane. Figure 1.1 shows a block of rock having constant stress throughout. Any stress state at a point in a solid body can be described completely by the orientation and magnitudes of three principal stresses. The principal stresses are oriented perpendicular to each other and to the three planes of no resolved shear stress at the point. In the laboratory, shear and tension fractures form in consistent orientation with respect to the three principal stress directions, namely the maximum compressive principal stress, σ_1, the minimum compressive stress, σ_3, and the intermediate stress, σ_2. Shear fractures form when all the three principal stress forces are compressive. Tension fractures form perpendicular to σ_3 and at relatively low differential stresses (Bratton et al., 2006).

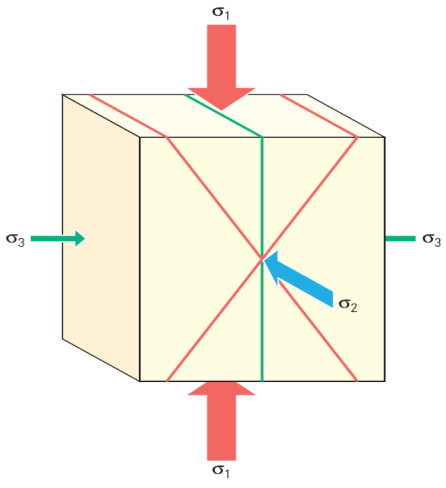

Figure 1.1 Illustration of the principal stresses and the creation of fractures that could develop during laboratory tests (Bratton et al., 2006).

1.1.2 Fluid flow in fractured reservoirs

Most reservoirs contain fractures, but it is the degree to which fractures influence fluid flow through a reservoir that should dictate the level of resources needed to identify, characterize and model fractures (Bratton et al., 2006). The heterogeneous flow in a fractured reservoir depends on the nature of fluids saturating the matrix and surrounding fracture network, as well as on the relationship between a rock and fluids at various stages of the saturation history during the displacement process. For this reason, the wettability, average pore size and pore size distribution will have a high impact on the flowing conditions in the matrix-fracture network (Golf-Racht, 1982a). In fractured reservoirs there are four principal recovery processes, and include: 1) fluid expansion, 2) capillary imbibition, 3) diffusion and 4) gravity controlled displacement (Golf-Racht, 1982b).

Generally the reservoir is at high pressure with oil in both fracture and matrix initially. During primary recovery the pressure will drop rapidly in the fractures because they are well connected, whereas the lower permeability matrix will remain at high pressure. The pressure difference will lead to influx of oil from the matrix rock to the fractures as the fluids expand. When the pressure drops below the bubble point, gas will evolve from solution and the expanding gas will lead to further recovery from the matrix. This process is effective until gas breakthrough, and then mostly gas will be produced, leaving significant volumes of oil in the matrix (Golf-Racht, 1982b).

To avoid oil production decline, it is important to maintain pressure in the fractured reservoir. One way to do this is by injecting water. Because the fractures have a high permeability, the water will rapidly invade the fractures, and if the matrix block has water-wet characteristics, water may enter it by capillary imbibition. Oil will then be displaced from the block and recovered from the fractures. The efficiency of this process depends on the amount of water that will imbibe into matrix and the rate at which this occurs. Imbibition is a primary mechanism of oil production in a fractured reservoir as a result of the drastic variations in permeability between fractures and matrix helping the fractures water to imbibe the matrix (Golf-Racht, 1982a, Golf-Racht, 1982b).

Another way to maintain reservoir pressure is by injecting gas into the fractured reservoir. Like water, the gas will invade the fractures. Due to gravity, most of the low-density gas will flow the top part of the formation. The gas may overcome the threshold capillary pressure to push the oil to the bottom until oil and gas are in capillary/gravitational equilibrium (Golf-Racht, 1982b).

The final recovery process is diffusion where the injected gas and oil can mix to form a single hydrocarbon phase that may be swept into the fracture and produced. Diffusion will be described in detail in section 1.6.1 (Golf-Racht, 1982b).

1.2 Interfacial tension (IFT) and Miscibility

When two fluids are in contact with each other there exists an interfacial tension (σ) between the molecules of the two fluids. The interfacial tension depends on the relative magnitude of the intra- and interfluid cohesive forces (intermolecular attraction), and represents the amount of energy that keeps the two fluids apart. The interfacial tension may result in three different outcomes (Zolotuchin and Ursin, 2000):

- A *positive* interfacial tension ($\sigma > 0$) occurs when the molecules of each fluid are more attracted to the molecules of their own kind, and thus the two fluids are immiscible.
- A *neutral* interfacial tension ($\sigma \approx 0$) occurs when the molecules of each fluid are attracted equally to the molecules of their own kind as to those of the other kind, hence the two fluids are miscible. The fluids will mix by diffusion until equilibrium is reached.
- A negative interfacial tension ($\sigma < 0$) occurs when the molecules of one fluid are more attracted to the molecules of the other fluid. The process is called dissolution and means that the chemical reaction between the two fluids will result in a new stable fluid.

The fundamental criteria for attaining miscibility between two phases are the conditions of zero interfacial tension (Rao and Lee, 2003). The petroleum industry defines miscibility as "*the ability of two or more substances to form a single homogenous phase when mixed in all proportions*" (Holm, 1986). Miscibility describes how well different phases mix, and depends on which force is the stronger, the intermolecular force or the intramolecular force. Intermolecular force is the force that holds the atoms or ions together in a compound. The molecules in a phase attract each other to stay together by van der Waals forces, an electrostatic force. Intramolecular force is attractive forces that act between discrete molecules. If the intramolecular force is stronger than the intermolecular force, the phases are miscible (Holm, 1986). In an oil recovery process, miscibility between the displaced and displacing phase may increase the displacement efficiency and the total oil recovery. Miscible enhanced oil recovery processes have estimated additional 10-15% recovery of OOIP (Original oil in place), compared to immiscible displacement processes that with 5-10% additional recovery (Lake, 1989). Miscible gas flooding applications usually

employ an injection gas with lower viscosity than reservoir oil. This may lead to unfavorable mobility ratio and sweep efficiency (Walsh et al., 1989).

There are two types of miscible gas displacement: first-contact miscible process and a multi-contact miscible process. The latter can be developed by three processes: condensing gas drive, vaporizing gas drive and combined condensing vaporizing gas drive (Rao and Lee, 2003). In this thesis experiments are conducted with first contact miscibility between CO_2 and mineral oil (n-Decane or paraffinic oil) and multi-contact miscibility between CO_2 and crude oil. To explain the different processes in miscible flooding, ternary diagrams are common to use. Figure 1.2 illustrates a ternary diagram and summarize the different miscibility processes.

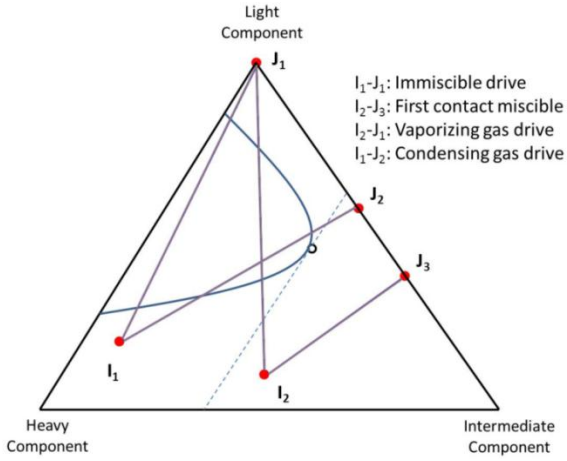

Figure 1.2 Conditions for miscible displacements modified from (Mathiassen, 2003). Two phases are first contact miscible when the dilution path (I_2-J_3) does not cross the two phase region or the critical tie line. When the dilution path lies entirely on the two phase region (I_1-J_1) an immiscible displacement is present. If the initial and the injected fluid composition are on the opposite side of the critical tie line, the displacement is either a vaporization gas drive (I_2-J_1) or a condensing gas drive (I_1-I_2).

First contact miscibility is a displacement process where any amount of the solvent can be injected and exist in one single hydrocarbon phase. The concept of a first contact miscible process may be explained by a ternary diagram as shown in Figure 1.2, and occurs when the linear dilution path between the injection gas and the oil do not intersect the two phase region (I_2-J_3). The displacement will consist of one single hydrocarbon phase that change composition from oil to undiluted gas through the gas-oil mixing zone. (Lake, 1989, Rao and Lee, 2003, Orr, 2007).

During multi-contact miscible processes, the injected gas vaporizes the lighter oil components and/or condenses into the oil phase. Both processes, individually or combined, may develop multi-contact miscibility. The miscibility is achieved by mass transfer of components witch results from multiple and repeated contact between the oil and the injected fluid through the reservoir. The difference between CO_2 and natural gas is that the dynamic miscibility with CO_2

does not require the presence of intermediate molecular weight hydrocarbons in the reservoir fluid (Mathiassen, 2003).

In the gas vaporization process a lean gas is injected and as it flows through the reservoir it vaporizes intermediate components (C_2-C_6) from the crude oil. The process takes place at the interface between the phases. The displacement will not be a first contact miscibility process because the dilution path crosses the two phase region (I_2-J_1 on Figure 1.2). The composition of the injected gas is modified as it moves through the reservoir. Miscibility will develop in this process as long as the injected gas and the crude oil are on the opposite sides of the critical tie line (Lake, 1989, Rao and Lee, 2003, Orr, 2007). The pressure required for achieving dynamic miscibility with CO_2 is usually significantly lower than the pressure required for other gases such as natural gas, flue gas or nitrogen. By using CO_2, also heavier hydrocarbon components may be extracted. The lower pressure and the extraction of higher hydrocarbon components are key advantages of the CO_2 miscible process (Holm, 1986).

During a condensing gas drive process (I_1-J_2 on Figure 1.2), an enriched gas containing significant amount of intermediate components (C_2-C_6) is injected. As this gas flows through the reservoir, the intermediates condense from the gas phase into the oil phase. The miscibility now develops at the rear of the gas-oil mixing zone as a consequence of the enrichment of the liquid phase of the intermediate components. The leading gas in the front of the displacement will be immiscible with the crude, because both the solvent and the crude are on the same side of the critical tie line, and thus cannot develop miscibility (Lake, 1989, Rao and Lee, 2003, Orr, 2007). CO_2 cannot form miscibility by condensing gas drive alone, but through a vaporizing drive were injected CO_2 vaporizes some of the light components in the oil. These are subsequently re-condensed at the displacement front generating an enriched zone with favorable mobility characteristics, referred to as a combined vaporizing and condensing drive (Mathiassen, 2003).

1.1.1 Minimum miscible pressure (MMP)

"The minimum miscible pressure is the lowest pressure at which miscibility between the injected gas and reservoir oil is achieved when the interfacial tension between oil and gas vanishes" (Teklu et al., 2013). MMP depends on both crude oil and solvent composition and is typically determined experimentally using slim tube tests. This method involves displacement of oil with a miscible agent at a given reservoir temperature through a small diameter tube packed with sand or glass beads. The pressure is regulated and MMP is determined based on the oil recovery and visual observations (Elsharkawy et al., 1992). However, the slim tube experiments have several drawbacks. The porous media in the slim tube test may not resemble the same

characteristics as the reservoir rock, and often the MMP value depends on the number and choices of test pressure and may result in large discrepancy in interpreted values (Watkins, 1978). Other methods to determine the MMP include (Williams et al., 1980, Christiansen and Haines, 1987, Elsharkawy et al., 1992, Teklu et al., 2013):

- Empirical correlations
- Rising bubble apparatus (RBA) measurements
- Tertiary representation / Restricted tie line
- Single- and multi-cell simulations
- Semi-analytical approach using the method of characteristics (MOC)
- Vanishing interfacial tension

Empirical MMP correlations may give a good indication of the potential with miscible gas processes for oil recovery in the reservoir. They are rapid and cheap to conduct, but because MMP correlation typically err by 10%, they are not appropriate for a final decision (Elsharkawy et al., 1992). Numerical modeling of slim tube displacement tests is a popular alternative to using MMP correlations (Williams et al., 1980). To accurately estimate the MMP for a gas-oil pair with these simulators, detailed compositional data as well as reliable phase behavior data are required. This may be a sufficient way for predicting consequences of small changes in gas composition when all the required data is already available, but the cost to obtain such data may exceed the cost of measuring an MMP with another method (Williams et al., 1980).

Development of miscibility between a gas bubble and oil, when both are miscible at first contact, can be observed visually in the Rising Bubble Apparatuses measurement. This approach to measure MMP's is much more rapid than the commonly accepted slim-tube technique. The measurements of the MMP with the RBA compare favorably with those based on the slim-tube experiments and predictions from phase-behavior studies. However, measurement of CO_2 and oil MMP's with RBA at lower temperatures (< 120 F) is less precise because of complexities of CO_2- oil behavior (Christiansen and Haines, 1987).

Accurate predictions of MMP are especially important in reservoir evaluation to determine the necessary conditions for miscible displacement processes. CO_2 has major advantages compared to other miscible agents because it achieves miscibility with reservoir oil at lower pressure compared with natural or inert gases. (Holm and Josendal, 1974, Holm, 1986)

Figure 1.3 illustrates the determination of MMP of CO_2 and oil, for a displacement process of oil with 1.2 hydrocarbon pore volume of CO_2 by the use of slim-tube experiments. If miscibility is achieved, it is characterized by a plateau on the pressure vs. recovery curve. Oil recovery from

slim tube tests are typically high at pressures above the MMP and decline steeply as pressures are reduced below the MMP. This bend-over point in the recovery versus pressure is the MMP (Shyeh-Yung, 1991). The MMP corresponds to the pressure, at which the critical tie line passing through the crude oil composition. This pressure is significantly lower than what is needed for a first contact miscibility. A further increase of pressure does not increase oil recovery, because above the MMP the displacement tend to develop into a first contact miscibility (Holm and Josendal, 1974, Lake, 1989).

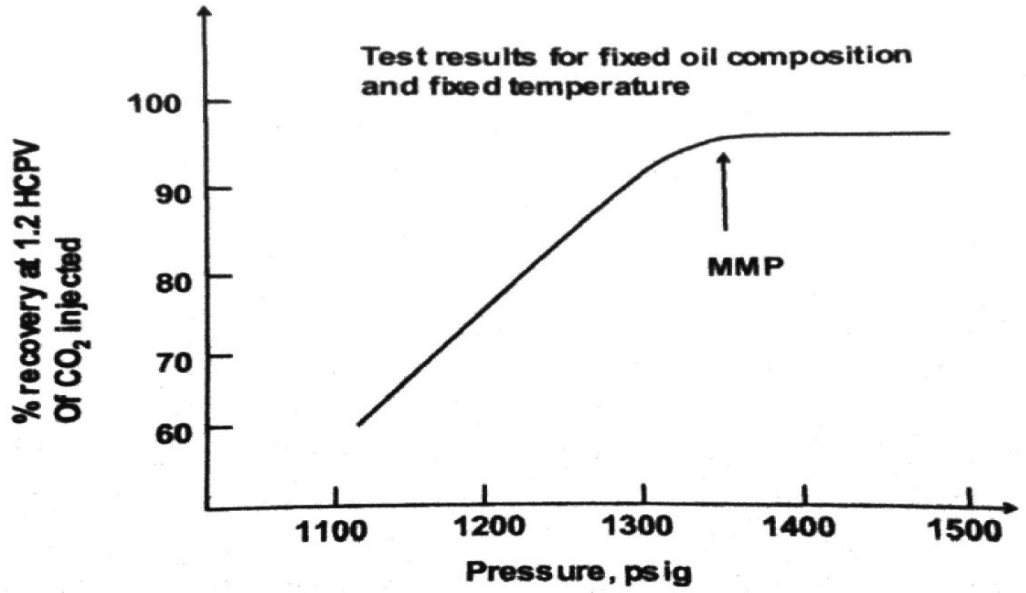

Figure 1.3 Minimum miscible pressure for CO_2 for a fixed oil composition (Skarrestad and Skauge, 2010)

1.2.2 Oil swelling

The solubility of CO_2 may decrease oil viscosity and can result in swelling of the oil volume and increased mobility. Dissolution of CO_2 may cause oil to swell up to 50-60% and thereby increases the contact area between the oil and CO_2 in which increase diffusion rate and recovery efficiency for the CO_2 injection (Moortgat et al., 2011). Swelling of the oil is also more dominant in crude oils with heavier components than in n-Decane and paraffinic oil.

Gas and oil viscosities are often measured in swelling tests as these are very important in determining fluid mobilities and mobility ratios. In a swelling test the selected injection gas is mixed with the oil at various proportions at constant reservoir temperature (Hand and Pinczewski, 1990). The test is used to determine: 1) how much gas that dissolves in the oil at a given pressure, 2) how much the oil will swell as intermediate components in the gas are dissolved by the oil, and 3) the resulting saturation pressure as injection gas is progressively added.

1.3 Mobility Ratio

Mobility is defined as the relationship between the endpoint relative permeability and the viscosity of the fluid, and is strongly dependent on the fluid saturation. It is an important factor for flow patterns of two or more fluids in a porous media (Zolotuchin and Ursin, 2000). The mobility, λ, of a phase, *i*, is given by:

$$\lambda_i = \frac{k_{r,i}}{\mu_i}, i = oil, water, gas \quad (1.1)$$

where μ is the viscosity and *k* is the end point relative permeability of the fluid.

The mobility ratio, M, is defined as the ratio between the mobility of the displacing fluid and the mobility of the displaced fluid (Zolotuchin and Ursin, 2000).

$$M = \frac{\lambda_{displacing}}{\lambda_{displaced}} \quad (1.2)$$

1.4 Wettability

The wettability of a reservoir rock can be defined as "the tendency of one fluid to spread on, or to adhere to, a solid's surface in the presence of another immiscible fluid" (Craig, 1971). In an oil- water system it is a measure of the preference the rock has for either oil or water (Anderson, 1986b). The wettability within a reservoir determines the microscopic fluid distribution in the reservoir or the core sample. For a water-wet rock, water has a tendency to occupy the small pores and most of the rock surface, and vice versa for an oil-wet system. The wettability may also be heterogeneous, classified as either fractional- or mixed wet system (Skarrestad and Skauge, 2010). In fractional wet cores, the wettability distributions are uncorrelated to pore size, whereas in mixed wettability conditions indicate that wettability distribution is related to pore size, that is either that the large pores are oil-wet and the small pores are water-wet or vice versa (Skauge et al., 2007). Changes in wettability influence the electrical properties, capillary pressure, water flood behavior, relative permeability, dispersion, irreducible water saturation and residual oil saturation (Anderson, 1987).

Three procedures are commonly used to measure wettability. One way is to estimated wettability quantitatively by measuring the contact angle, giving wettability for a specific surface (Anderson, 1986a). The two other methods, the Amott Harvey method (Amott, 1959) and the USBM method (Donaldson et al., 1969), are based on the brine/oil displacement behavior, looking at water saturation related to flow conditions or capillary pressure to quantify wettability (Morrow, 1990).

The wettability may range from strongly oil-wet to strongly water-wet. In this thesis mostly strongly water-wet cores were used. Petroleum reservoirs are rarely (if ever) strongly water-wet (Sorbie and van Dijke, 2004). A series of studies has proven the tendency of a CO_2-wet system (Chi et al., 1988, Siemons et al., 2006a, Siemons et al., 2006b, Plug et al., 2008). The main reason for the wetting alterations from water-wet to CO_2-wet is related to the difference in stability of the water film between the matrix surface and the CO_2 (Siemons et al., 2006a, Siemons et al., 2006b). Such a film must be ruptured before the coal becomes CO_2-wet (Hirasaki, 1991, Plug et al., 2008). It has been observed that by increasing system pressure, the wettability changes from water-wet to CO_2-wet (Chi et al., 1988, Siemons et al., 2006b). Fast water breakthrough during the imbibition process indicates CO_2-wet behavior (Plug et al., 2008).

1.5 Capillary Pressure

Capillary pressure, P_c, is the molecular pressure difference across an interface between the wetting phase (P_j) and the non-wetting (P_i) phase. When the curvature of the interface is at static conditions, the capillary entry pressure for a phase *i* displacing a phase *j* is given by the Young-Laplace equation (Schubert, 1982):

$$P_c = \Delta P = P_i - P_j = \sigma_{ij}\left(\frac{1}{R_1} + \frac{1}{R_2}\right) \tag{1.3}$$

where σ_{ij} denotes the interfacial tension, and R_1 and R_2 are the principal radius of the interface curvature. In a capillary tube, where R_1=R_2=r, the capillary pressure can be expressed as:

$$P_{c,ij} = \sigma_{ij}\left(\frac{1}{R_1} + \frac{1}{R_2}\right) = \frac{2\sigma_{ij}\cos\theta_{ij}}{r} \tag{1.4}$$

where θ_{ij} denotes the contact angel between the phase *i* and phase *j*, and *r* is the radius of the capillary tube.

Capillary pressure may also be described by the height of capillary rise in a tube:

$$P_c = (\rho_j - \rho_i)gh \tag{1.5}$$

where ρ_j - ρ_i is the density difference between the non-wetting and the wetting phase, g is the gravity force and h is the height of the capillary rise.

Capillary pressure is dependent on saturation, saturation history, wettability, pore structure and pore size, and is therefore important for the pore filling sequence of fluids in porous media. The static capillary pressure has conventionally been used to interpret two-phase fluid flow in porous media and to describe the dynamic capillary pressure, although the Laplace law is valid only under static conditions.

There are two types of capillary pressure processes: drainage and imbibition. Imbibition describes an increase in the wetting phase saturation, whereas drainage refers to an increase in saturation of the non-wetting phase. For an imbibition process, two displacement mechanisms occur at the pore level, and include piston-like displacement and snap-off. Snap-off occurs when the flow of the wetting phase through films swell around the oil to form a "collar". At a certain P_c, continuity of the oil phase snaps off and thus occupying the space with water. In reality, when P_c rises, snap-off ceases. Snap-off frequently occurs when foam is introduced to a system (Kovscek and Radke, 1996).

Capillary pressure for piston-like displacement versus snap-off can be compared in magnitude as shown in equation (1.6).

$$P_{C,drain}^{(piston)} \geq P_{C,imb}^{(piston)} \geq P_{C,imb}^{(snap-off)} \tag{1.6}$$

Spontaneous imbibition is an important factor controlling oil recovery mechanism in fractured reservoirs, and is dependent on the wettability of the media. The amount of water imbibed depends on the spontaneous (positive) part of the capillary pressure curve, which in addition to wettability is closely correlated to the pore structure. In addition to spontaneous imbibition, the capillary continuity is an important factor to oil recovery in fractured reservoirs because it provide fluid communication between isolated matrix blocks and increase the recovery by gravity drainage or viscous displacement. Applying a viscous component to the water may enhance recovery, depending on wettability, fracture permeability and fracture aperture. A surfactant solution is often added to the water and co-injected with gas to generate foam for mobility control. The stability of foam lamellae is also limited by capillary pressure (Khatib et al., 1988). The capillary pressure will increase as the as the fractional flow of gas in foam increase until a critical capillary pressure is reached, after this point coalescence coarsens foam texture and the liquid saturations remains constant and the relative gas mobility becomes proportional to the ratio of gas-to-liquid fractional flow.

There exist several methods today for capillary pressure measurements, but the centrifuge method may be the most frequently used method (Fernø et al., 2009). Many of the naturally fractured carbonate reservoirs characterize a mixed-wet or oil-wet wettability (Downs et al., 1989), and waterflooding will not necessarily perform as well as for water-wet fractured reservoirs, because spontaneously imbibition will be less efficient, resulting in poor recoveries and early water breakthrough.

1.6 Dispersion in porous media

Dispersion is defined as the mixing of two miscible fluids, caused by diffusion and convection (Lake, 1989). Dispersion occurs when one fluid is decomposed into small microscopic particles or droplets (dispersive phase), that float around in the other fluid (continuous phase). These are not mixed, but finely distributed in each other because they have different polarity. Two fluids will slowly diffuse into one another if the contact area between two miscible fluids is initially a sharp interface, caused by random motion of the molecules (Perkins and Johnston, 1963). In reservoir engineering dispersion is of particular importance in miscible displacements (Skjæveland and Kleppe, 1992), such as miscible CO_2 injection for EOR as will be discussed in this thesis.

1.6.1 Diffusion

Molecular diffusion is the mixing of miscible phases to form one single phase by molecular transfer due to concentration gradients (Jha et al., 2011). The two phases reach thermodynamic equilibrium through diffusion, caused by movement of molecules from high-concentration areas to low-concentration areas, as illustrated in Figure 1.4. Due to the concentration differences, molecular diffusion of inert gas normally favors displacement of hydrocarbons over dry gas (da Silva and Belery, 1989). The molecular diffusion process is mainly governed by three mechanisms depending on the matrix structure and pressure. These are: 1) bulk diffusion where fluid-fluid molecular interactions dominate, 2) Knudsen diffusion for which fluid molecule collide with pore walls, and 3) surface diffusion which correspond to molecules transported along an adsorbed film (Smith and Williams, 1984). Unless there is a large amount of adsorption, surface diffusion plays a minor role. Knudsen type of transport is independent of fluid pressure as opposed to bulk diffusion for which the diffusion coefficients are inversely proportional to pressure (Smith and Williams, 1984).

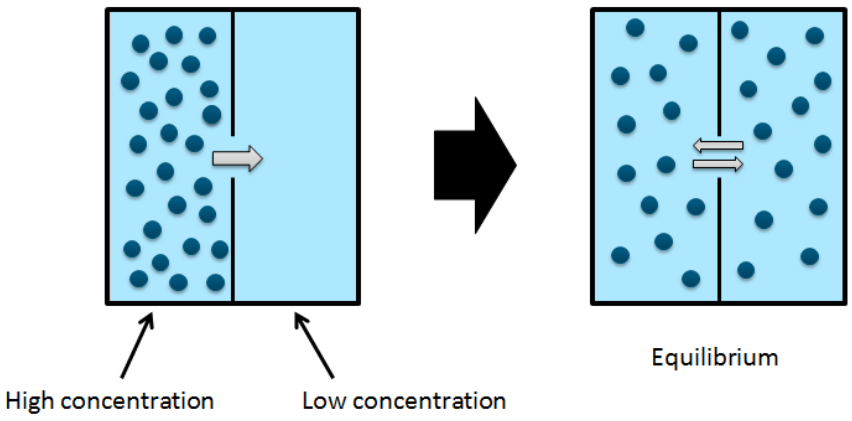

Figure 1.4 The concept of diffusion: Mixing of two miscible fluids in contact with each other through random motion of molecules until equilibrium is reached (Lie, 2013)

The diffusional flux is possible to determine by Flick's law:

$$J = -D\frac{\partial C}{\partial x} \tag{1.7}$$

where J is the diffusional flux, D is the molecular diffusion coefficient, C is the concentration and x is the position.

By taking time, t, into account Fick's second law describes the one-dimensional unsteady state diffusion between two miscible fluids, and is given by:

$$\frac{\partial C}{\partial t} = D\frac{\partial^2 C}{\partial x^2} \tag{1.8}$$

From Fick's second law, with a constant concentration as the boundary condition, it is possible to determine the concentration of each fluid component as a function of time and distance. Modification to account for the texture of the matrix is required. It has been proven that for a porous media the ratio between the absolute diffusion coefficient, D_a, and the effective diffusion coefficient, D_e, is given by (Perkins and Johnston, 1963):

$$\frac{D_a}{D_e} = \frac{1}{F\phi} \tag{1.9}$$

where F is the formation electrical resistivity factor and φ is the porosity.

Phase behavior effects by molecular diffusion in a miscible CO_2 displacement in porous media depends on contact time, length of diffusion and rate of diffusion (Bird et al., 1976). As opposed to porous media, where molecular diffusion generally is small, it may be very important in naturally fractured reservoirs, as the dispersive flux through fractures rapidly increases the contact area for diffusion (da Silva and Belery, 1989). Fick's molecular diffusion potential may override the viscous force when injecting a phase, if the fractured spacing is small (da Silva and Belery, 1989).

1.6.2 Convection

Convective mixing describes the mechanic mechanism of fluid mixing in porous media resulting from heterogeneities, and occurs when the fluid is flowing through a porous media and particles are mixing on a microscopic scale (Perkins and Johnston, 1963, da Silva and Belery, 1989, Sahimi, 2012). The rate of mixing depends on the interstitial velocity. Convective dispersion may be described by two mechanism that include longitudinal dispersion and transverse dispersion (Sahimi, 2012). Longitudinal dispersion represents spreading of a solute concentration front in the mean-flow direction as it passes through a porous media, whereas transverse dispersion means cross-spreading at a given transverse plane in a porous media.

1.7 Enhanced Oil Recovery

The main objective of all methods of enhanced oil recovery (EOR) is to increase the volumetric (macroscopic) sweep efficiency and to enhance the displacement (microscopic) efficiency after the conventional primary and secondary recovery. The volumetric sweep may be increased by reducing the mobility ratio between the displacing fluid and the displaced fluid. In order to enhance the microscopic sweep, a reduction of the interfacial tension between the displacing and displaced fluid will lower the amount of oil trapped due to the capillary force, and result in a lower residual oil saturation and hence higher ultimate recovery (Katz, 1980, Lake, 1989).

During oil and gas production from a reservoir, several measures may be implemented in order to improve the recovery. Implementation of EOR techniques will have impact on the production profile. The definition of EOR is linked to the use of unconventional recovery methods, such as injection of materials not normally present in the reservoir like surfactants and polymers. Therefore, the injection of water and hydrocarbon gas is not regarded as EOR methods. CO_2 and WAG (Water-Alternating-Gas) injection falls outside the strict definition of EOR, but these are unconventional techniques that usually are defined as EOR (Lake, 1989).

2. CO_2 and CO_2 Foam

The use of carbon dioxide (CO_2) for enhanced oil recovery (EOR) is considered one of the most promising methods for commercial application, and has been used to recover oil for over 40 years (Enick et al., 2012). Both laboratory and field studies have proven CO_2 to be an efficient oil-displacement agent (Holm and Josendal, 1974, Abrishami and Hatamian, 1996, Enick et al., 2012). Recoveries are observed to be high provided that the effects of gravity segregation, viscous fingering, and bypassing are minimized (Holm and Josendal, 1974, Gardner et al., 1981). The most efficient use of CO_2 for EOR is obtained at flooding pressures at which miscible displacements is achieved (Holm and Josendal, 1974). If fractures are present in the reservoir, CO_2 may be less efficient. Because CO_2 is a low viscosity fluid, it may channel into the high permeable fractured network and may result in an early breakthrough and low sweep efficiency. By introducing foam to the fractured network promising results for controlling gas mobility in an EOR process have been recognized (Bernard and Holm, 1964, Bernard and Jacobs, 1965, Holm, 1968, Wang, 1984).

2.1 EOR from CO_2 injection

CO_2 is naturally stored in plants, subsea and beneath the Earth surface where the crust is thin. It can also be found in small portions in the atmosphere. CO_2 is a naturally occurring gas at standard temperature and pressure, composed of 2 oxygen (O) atoms and one carbon atom (C). At such conditions it is very stable and no process other than photosynthesis having been discovered to effectively decompose it (Energy Institute, 2010).

For many years, the oil industry has injected CO_2 into oil reservoirs to increase the oil production. CO_2 gas has many favorable properties as displacing fluid and accounted for 0.3% of the world's oil production in year 2000 (Freund, 2000). In 2012 CO_2 provided about 280 000 barrels of oil per day in the U.S., which is just over 5% of the total U.S. crude oil production (Enick et al., 2012). To increase the interest for CO_2 EOR and storage projects, they have to be economical beneficial. The increased focus on CO_2 emission and taxation contributes to make Carbon Capture Storage (CCS) more attractive (Energy Institute, 2010). The number of CO_2 flooding projects has increased steadily in recent years, compared to other EOR methods. The limiting factor for the expansion of CO_2 projects is in transitioning from a low oil price to the quantities of high-pressure CO_2 needed (Abrishami and Hatamian, 1996, Enick et al., 2012). Despite the fact that CO_2 has a well-established ability to recover oil, the CO_2 EOR process could be improved if the high mobility of CO_2 relative to reservoir oil and water can be effectively affordable reduced (Vikingstad et al., 2005, Enick et al., 2012).

With recent environmental concerns like pollution, acidic rain, greenhouse effects and global warming, not only the cost of injection schemes but also their environmental aspects have to be considered by the industry (Abrishami and Hatamian, 1996). Recently, CO_2 flooding has become so technically and economically attractive that CO_2 supply, rather than CO_2 price, has been the limiting factor (Enick et al., 2012). CO_2 flooding for EOR requires a large amount of pure CO_2.

The Sleipner field in the North Sea is considered the world's first CCS project, and became a fully operational offshore gas field with CO_2 injection in August 1994, where CO_2 is sequestrated 1000 meters below the sea bed. 14 Mt CO_2 is injected to this date, and in 2014 it is expected that the carbon capture facilities at Sleipner also will separate additional gas from the Gudrun field, and is currently under development (GCCSI, 2014).

It is important to understand the properties and behavior of CO_2 because it may represent a very attractive EOR method at optimum conditions. The phase behavior of the reservoir oil and gas, depending on pressure and temperature, combined with reservoir rock type, wettability and presence of fracture and their permeability, are crucial factor which determine the efficiency of the CO_2 injection. The CO_2 phase diagram is illustrated in Figure 2.1.

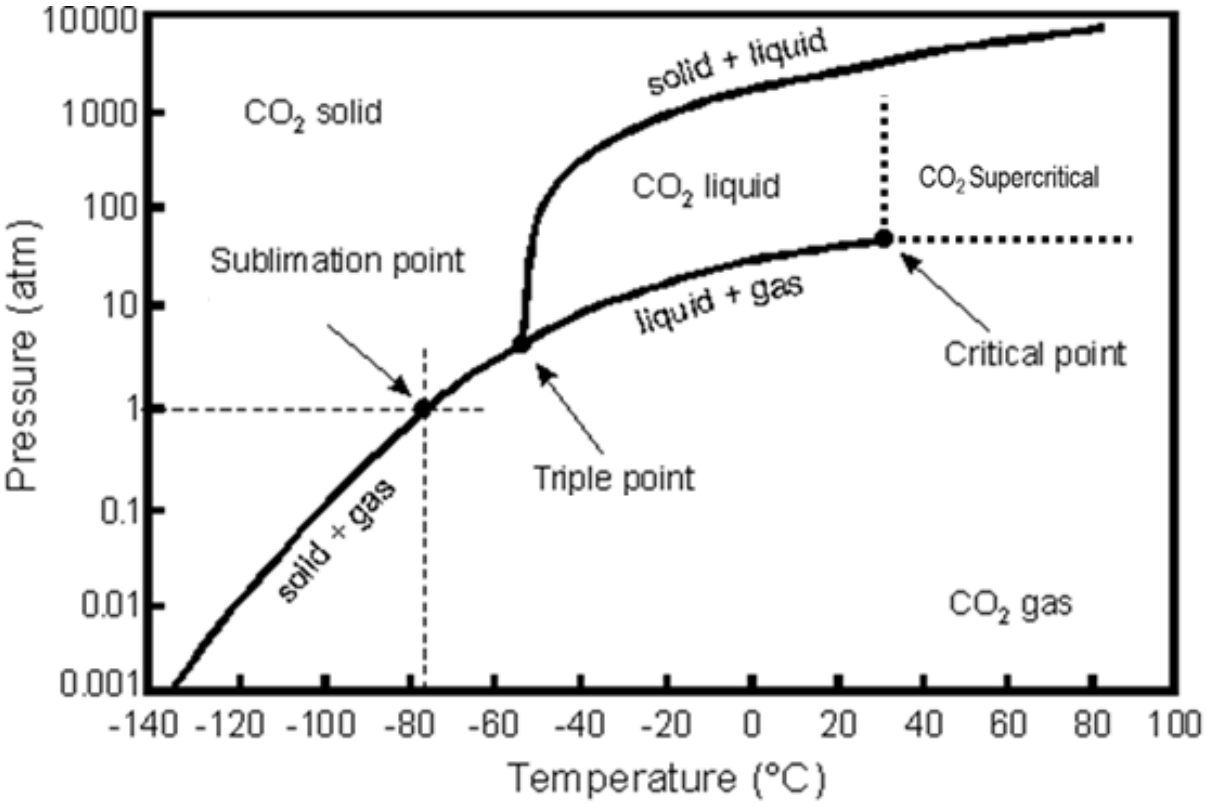

Figure 2.1 Phase diagram for CO_2 for different temperatures and pressures, including the sublimation point (78.5 °C, 1 bar), the triple point (-56.6 °C, 5.11 bar) and the critical point (31.1°C, 73.83 bar). The triple point is defined as the temperature and pressure where the three phases can exist simultaneously in thermodynamic equilibrium (Energy Institute, 2010).

The behavior of CO_2 with respect to density and viscosity are shown in Figure 2.2 and Figure 2.3, respectively. The CO_2 becomes denser and more viscous with increasing pressure. The increased density behavior means that CO_2 has favorable properties to reduce gravity segregation.

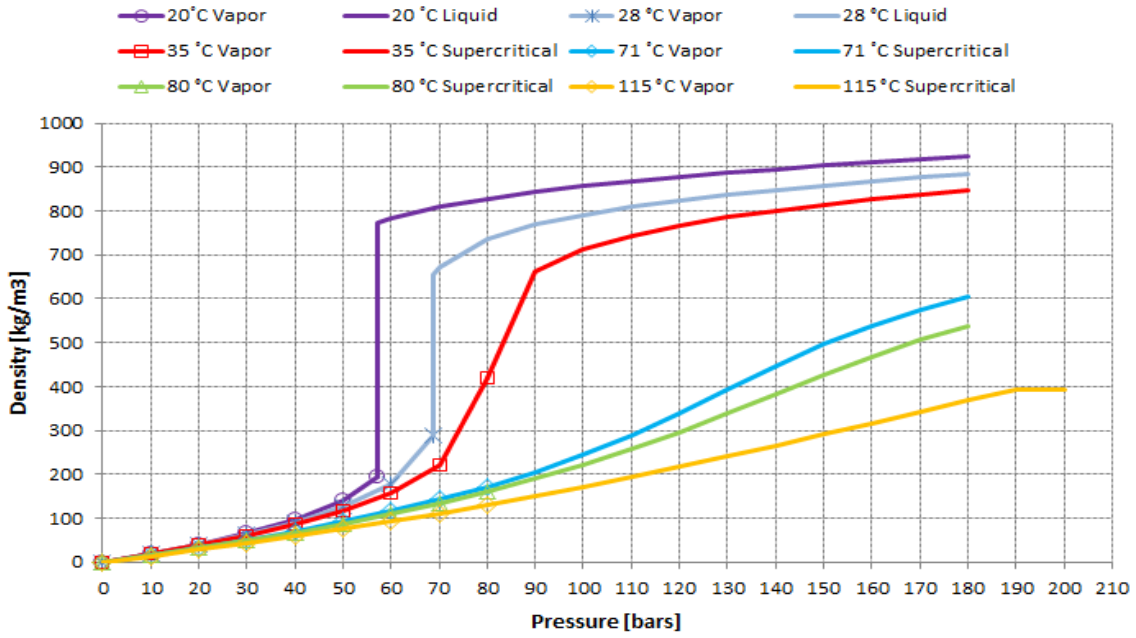

Figure 2.2 CO_2 densities as a function of pressure at temperature conditions for experiments conducted in this thesis.

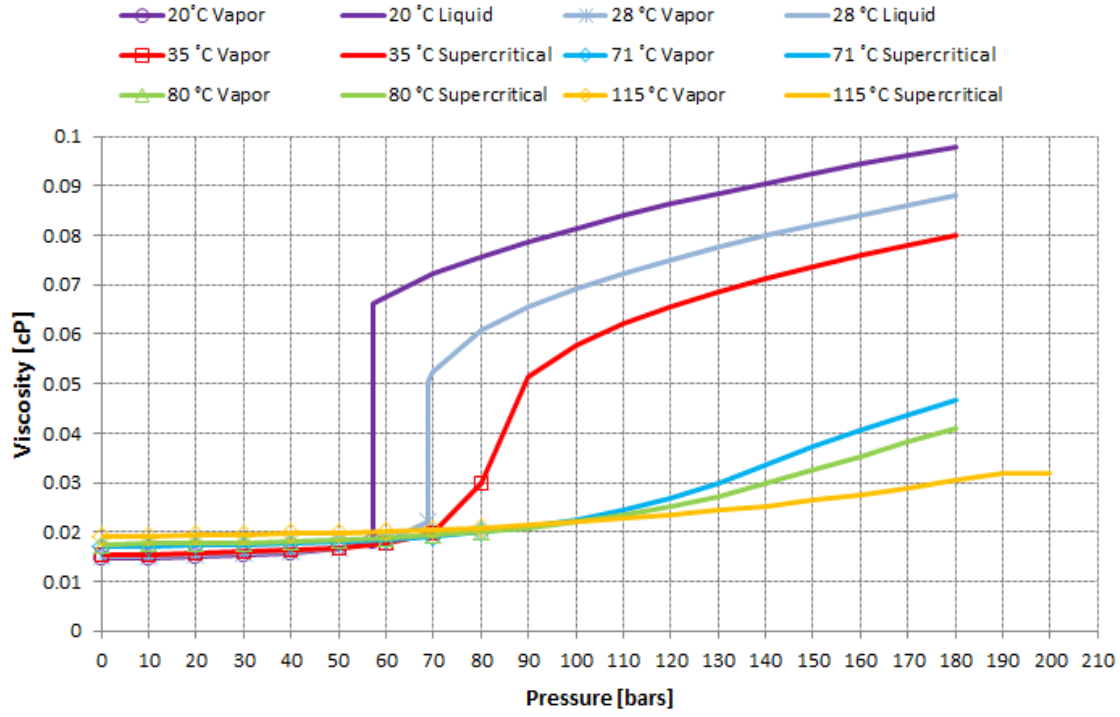

Figure 2.3 CO_2 viscosities as a function of pressure at temperature conditions for experiments conducted in this thesis.

In the laboratory a simplified situation may be constructed to study CO_2/oil miscibility and displacement at constant temperature and pressure in core samples. Maintaining a high pressure exceeding the MMP is crucial conditions for additional oil recovery. In this thesis experiments were conducted at liquid or supercritical CO_2 conditions.

CO_2 cannot exist as liquid at atmospheric pressure, but at a pressure above 5.11 bar and a temperature between -56.6°C and 31.1°C the CO_2 becomes liquefied, and its density rises with temperature to 1180 kg/m^3 (Energy Institute, 2010). CO_2 at pressure and temperature conditions above the critical point is described as a supercritical phase. Supercritical fluids have the low viscosity of a gas and the high density of a liquid. Thus, it may diffuse into a solid matrix faster than liquid, yet possess the strength to displace other fluids from the matrix. However, it is possible to go from gas to a liquid without crossing the boundary between the vapor and liquid phase using a supercritical fluid just by lowering the temperature (Energy Institute, 2010).

2.1.1 Features of CO_2 as an EOR fluid

Depending on the reservoir conditions and fluid composition, CO_2 may have different recovery performances like increasing oil density, high solubility in water, promoting oil swelling, reducing interfacial tension, extraction or vaporization portions of the oil, reducing oil viscosity and exerting an acidic effect on rock (Holm and Josendal, 1974, Abrishami and Hatamian, 1996, Nasir and Amiruddin, 2008). There is also some expansion of water (2-5 %) when CO_2 goes into solution and the water density decreases. As a consequence, the densities of oil and water becomes closer to each other, hence lessens the chance of gravity segregation of these fluids and the overriding effect of the CO_2-water mixture (Holm and Josendal, 1974). The acidic effect of CO_2 on the rock has proven to stimulate injectivity of water by direct action on carbonate portions of the rock and by a stabilizing action on clays in the rock (Crawford et al., 1963) .

CO_2 flooding can either be miscible or immiscible depending on the Minimum Miscibility Pressure (MMP). Miscible flooding forms a single phase solution with the hydrocarbons in the reservoir when injected and in contact with the hydrocarbon at a pressure above the MMP, whereas immiscible flooding occurs when the pressure is below the MMP where CO_2 does not form a single phase solution with the hydrocarbons in the reservoir (Holm, 1986). Miscible CO_2 displacements include all the performance enhancements mentioned above, whereas immiscible CO_2 displacements relies more on the reduction of viscosity of the oil phase, reduction of interfacial tension (IFT) and swelling of oil in contact with CO_2. It has been recognized that CO_2 and light hydrocarbon gas are completely miscible at relatively low pressure. Miscibility can be attained at lower pressure by injecting CO_2 gas than hydrocarbon gas (Holm and Josendal, 1974). Unlike the high-pressure gas-miscible process, the displacement of oil by CO_2 does not

depend upon the presence of light hydrocarbons (C_2-C_4) in the reservoir oil. Hence, the CO_2 process is applicable to reservoirs which the oil has been depleted of its lighter components (Holm and Josendal, 1974, Brock and Bryan, 1989).

In addition to the environmental and the economical aspect, the main challenge for a successful CO_2 flood is related to its density and viscosity. The major challenge associated with gas injection is its poor volumetric sweep efficiency, as the result of which gas does not contact a large fraction of oil and, thus, the low overall recovery remains low (Wellington and Vinegar, 1985, Rossen and van Duijn, 2004). This happens because of the channeling (flow of gas in the high permeability streaks in heterogeneous reservoirs), viscous fingering that occurs because of the viscosity difference between the oil and gas, and gravity override due to the large density contrast between the gas and oil (Koval, 1963). CO_2 is capable of displacing nearly all the oil in the local areas where it flows, but yet CO_2 flooding does not recover all of the oil in the formation. Miscible CO_2 floods typically recover 10%-20% of the OOIP (Original Oil In Place), whereas immiscible CO_2 floods only recover 5%-10% of the OOIP, due to the interfacial tension between the CO_2 and the more viscous oil. This may result in high residual oil saturation in the reservoir, between 35%-65% of the OOIP (Koval, 1963, Enick et al., 2012).

2.1.2 Secondary and Tertiary CO_2 injection

Displacement efficiency in fractured and non-fractured reservoirs during both secondary and tertiary CO_2 flood is strongly influenced by achieving miscibility between the CO_2 and the oil. For a secondary CO_2 displacement, the CO_2 is injected into a porous media without previously waterflooding. For a miscible, secondary CO_2 displacement, the oil recoveries are observed to be high and rate-intensive, provided that the effect of gravity segregation, viscous fingering and bypassing are minimized (Watkins, 1978, Gardner et al., 1981, Wang, 1982).

For a tertiary CO_2 displacement, the CO_2 is injected into a previously water flooded porous media. The recoveries tend to be considerable lower than for a secondary CO_2 displacement, depending on flow rate, core length and wettability (Stalkup, 1970, Watkins, 1978, Spence and Watkins, 1980, Wang, 1982). However, tertiary CO_2 injection projects may be more interesting than secondary CO_2 injection projects on field scale, because many fields are at tail production after been water flooded. The lower recovery is usually explained by the high water saturation present in a tertiary CO_2 flood and its effect on the microscopic displacement efficiency. The highly unfavorable mobility ratio for the immiscible CO_2-water displacement may lead to CO_2 bypassing considerable volumes of water, leaving high water saturations behind the displacement front in water-wet rock. The water blocks or shields the residual oil from direct contact with the CO_2 injected (Stalkup, 1970, Spence and Watkins, 1980).

Water shielding or bypassing is an important factor that may influence the oil recovery efficiency of a CO_2 flood. Having water present in the system may lead to lack of complete and uniform contact between oil and CO_2, leading to decreased oil recovery efficiency. The effect is more pronounced in strongly water-wet systems, compared with oil-wet systems where the effect is insignificant (Gardner et al., 1981, Walsh et al., 1989). Walsh et al. proved experimentally that water shielding is controlled by the trapping function and oil and solvent mobilities, and that trapping by water shielding occurs for the non-wetting phase. This prevents development of miscibility and results in a considerable reduction in microscopic displacement efficiency (Grogan and Pinczewski, 1987).

Other research supported the idea that presence of a water phase in the core weakens CO_2 flood oil recovery performance, because water causes the oil to be less connected. It was found that water shielding of oil extraction by CO_2, at initial water saturations in the range of S_w=0.4 to S_w=0.75 had an effect on the oil bank development and hence on oil recovery even in a mixed-wet core. At initial water saturations lower than S_w=0.4, CO_2 flood behavior was not affected by water shielding, explained by water receding in smaller, water-wet pores (Shyeh-Yung, 1991).

Bypassing may occur at both microscopic and macroscopic levels. Microscopic bypassing might be due to the presence of oil in dead-end pores and/or shielding of oil by water in the tertiary mode. Macroscopic bypassing, on the other hand, may result from viscous fingering, paths of least resistance on a visible scale, gravity over- or underide, and/or simply poor distribution of injection fluid at the inlet of the system (Gardner et al., 1981).

Molecular diffusion of CO_2 through the water phase has been proposed as an important factor in the mobilization and recovery of the residual oil in water-wet rock. Swelling of the oil causes changes in pore-scale phase distribution, and can be effective in recovering residual oil as long as enough time is available for diffusion of CO_2 to swell the oil significantly (Orr and Taber, 1983, Campbell and Orr, 1985). It is unlikely that molecular diffusion play a significant role in reducing the adverse effect of large-scale bypassing resulting from gravity segregation, reservoir stratification, and unfavorable mobility ratio in tertiary field flooding (Grogan and Pinczewski, 1987). Even though local displacement efficiencies are high as a result of the large contact times, overall recoveries may be low due to the presence of large-scale bypassing. For core scale experiments, diffusion may be sufficiently rapid, depending on size, to effectively reduce the adverse effect of bypassing on overall recovery efficiency. However, on a field scale, bypassing of oil by injecting CO_2 may be expected to occur on a much higher level (Grogan and Pinczewski, 1987).

2.2 CO_2 Foam

Foaming of the injected gas is a potential solution for the density and viscosity challenges identified above with CO_2 as an EOR method, because it may decrease its mobility (Boud and Holbrook, 1958, Kovscek and Bertin, 2002, Farajzadeh et al., 2009, Enick et al., 2012). Foam consists of gas bubbles dispersed in liquid and a continuous liquid film called lamellae separates the gas bubbles (Bikerman, 1973), and are illustrated in Figure 2.4.

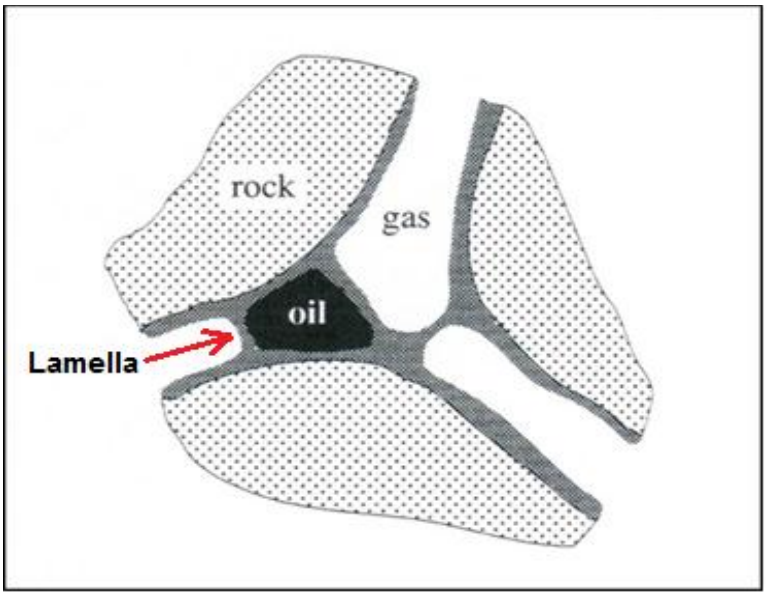

Figure 2.4 Foam forming and flowing in porous media (Skjæveland and Kleppe, 1992)

Foam is generated when gas and a solution of a surface active agent are injected to a porous media, and may have several advantages that include: 1) reduce the gas mobility in the fractured rock, 2) increase differential pressure, and 3) divert flow into the oil-saturated matrix. (Bernard and Holm, 1964, Holm, 1968). Foam can be useful in water floods, where highly permeable layers or unfavorable mobility ratio are present (Bernard and Jacobs, 1965). When foam is present in a porous media, the effective permeability of the porous medium to each phase is greatly reduced compared with permeabilities measured in the absence of foam (Bernard and Holm, 1964). It has been proven experimentally that foaming gas is a promising technique for achieving mobility control and diverting injected fluid to low permeable strata within porous media (Kovscek and Bertin, 2002).

By injection of a slug of surfactant prior to CO_2 injection it may reduce the CO_2 mobility, below and above its critical point (Farajzadeh et al., 2009). CT images have shown that by adding surfactant to the injected brine it prevents gravity and viscous instabilities, and enables CO_2 to displace the oil from cores in a piston-like manner (Wellington and Vinegar, 1985).

Foam texture, a measure of bubble volume, has been recognized as the key parameter in determining foam flow (Hirasaki and Lawson, 1985). Four mechanisms have been identified to explain how fluid flow in the presence of foam:

1. A large portion of the gas is trapped in the porous medium and a small fraction flows as free gas, following Darcy's law (Kolb, 1964).
2. The foam structure moves as a body, as the rate of gas flow is the same as the rate of liquid flow (Fried, 1961).
3. Gas flows as a discontinuous phase by breaking and re-forming films, and liquid flows as a free phase (Bernard and Jacobs, 1965).
4. A portion of the liquid and gas move as a foam body whereas excess surfactant solution moves as a free phase (Holm, 1968).

The apparent viscosity of foam is the sum of three contributions (Hirasaki and Lawson, 1985): 1) that from slugs of liquid between bubbles, 2) the resistance to deformation of the interface of a bubble passing through the media and 3) the surface tension gradient that results when surface active material is swept from the front of a bubble and accumulates at the back of it.

There have been several successful laboratory tests capable of stabilizing CO_2-foams that led to 13 published reports of pilot tests conducted between 1984 and 1994. Five of these projects were assumed to be successful considering the technical effort and favorable economic assessments (Enick et al., 2012). A large number of laboratory studies were directed at the design of in-depth mobility control foams. This led to two pilot tests aimed solely at CO_2 mobility control, one which indicated that a 60% increase in the apparent viscosity of CO_2 occurred where the foam is formed, and several pilot tests that were designed to both increase the apparent viscosity of CO_2 and block a high permeable zone, one of which clearly demonstrated that CO_2 foams could simultaneously enhance conformance control and mobility control (Enick et al., 2012).

Research results have proven that surfactant-induced CO_2-foam is an effective method for mobility control in CO_2 flooding, but have potential weaknesses. Because foam is unstable by nature, its long-term stability during a field application is difficult to maintain. Foam stability will be described in detail in section 2.2.2. Carbon dioxide-soluble surfactants ensure that the surfactant appears only where the CO_2 flows. These surfactants may be capable of providing a modest degree of conformance and mobility control, and are easy to implement even for operators who only employ continuous CO_2 injection, and may greatly reduce the need for alternating slugs of brine. New nano -science technologies may also provide an alternative for the generation of stable CO_2-foam. Using nanoparticles to stabilize CO_2 mobility control foam

may overcome the long-term instability and surfactant adsorption loss issues that affect surfactant-based CO_2 EOR processes (Enick et al., 2012).

2.2.1 Foam Mobility in heterogeneous porous media

Gas, as a bulk fluid, has a very low viscosity compared with oil and water. The high mobility of gas in the reservoir frequently leads to poor conformance in gas flooding processes. In a reservoir scale, results have shown poor sweep efficiency. Localized problems such as gravity override, gas channeling in high permeable zones, and gas coning into production wells have also lead to problems. The conventional practice of using water-alternating-gas (WAG) injection is not always effective, and may create other problems by retrapping mobilized oil. By introducing foam in problem wells or deep into the reservoir, may be a good alternative to WAG. A properly designed foam may reduce gas mobility by several orders of magnitude (Tanzil et al., 2000). It may improve injection conformance in two directions; in a horizontal direction by increasing areal sweep efficiency and in a vertical direction by diverting fluids to other unswept zones (Stevens, 1995). Foam selectively reduces gas flow, leaving the relative permeability of the liquid phase unchanged, hence foam is selective to permeability and reduces the gas mobility relatively more in higher-permeable regions smoothing out reservoir heterogeneities (Hirasaki and Lawson, 1985, Kovscek and Bertin, 2002).

Experiments in homogeneous and heterogeneous sand-packed columns showed that the foam mobility in the two cases could differ by two orders of magnitude (Tanzil et al., 2000). The difference is due to the generation of foam lamella by snap-off for flow across an abrupt increase in permeability. This mechanism is shown to be dependent on the degree of permeability contrast and the gas fractional flow. It has important implications for the degree of gravity segregation of gas and liquid in field-scale recovery processes. (Tanzil et al., 2000)

2.2.2 Foam regimes/Foam stability

Two different foam-flow regimes have been identified and have later been supported by newer research and proven this behavior to be general. “Dry” foam is considered as a high-quality regime where steady-state pressure gradient is independent of gas flow rate, and “wet” foam as a low-quality regime, where pressure gradient is independent of liquid rate. Foam at higher qualities is dominated by capillary pressure and coalescence, whereas lower quality foam is dominated by bubble trapping and mobilization (Osterloh and Jante Jr., 1992).

Foam stability in porous media is limited by capillary pressure, P_C*. (Khatib et al., 1988). In the high quality Pc* regime (limiting capillary pressure), foam bubble change size as needed to maintain foam at the limiting capillary pressure and thus to control gas mobility. For the low quality regime, the Pc* model does not apply. The bubble size is fixed, and the pressure gradient

depends on the porous medium, and less on the surfactants ability to stabilize the foam (Alvarez et al., 1999). The transition zone between the two regimes occurs at the point of limiting capillary pressure. If it is higher than the limiting capillary pressure, the foam is in the high quality foam regime, and vice versa. This was characterized by a specific value of gas fractional flow, f_g, which is the gas velocity, u_g divided by total velocity, u_T.

$$f_g = \frac{u_g}{u_T} \tag{2.1}$$

Foam "quality" is f_g rescaled from the range from 0 to 1 or to the range from 0 to 100%. (Osterloh and Jante Jr., 1992)

The efficiency of a foam displacement process is affected by stability of foam films, and is greatly influenced by the presence of oil and the nature of the core material in addition to surfactant selection (Hirasaki, 1991, Vikingstad et al., 2005, Farajzadeh et al., 2012).

To characterize the strength of the generated foam, the mobility reduction factor (MRF) is often defined (Schramm and Wassmuth, 1994):

$$MRF = \frac{\Delta P(foam)}{\Delta P(no-foam)} \tag{2.2}$$

where MRF is the mobility reduction factor, ΔP (foam) and ΔP (no-foam) are the pressure drop across the porous media with and without the presence of foam, respectively.

One of the most important factors in EOR application of foam is the influence of oil on foam stability. To have efficient oil displacement in the presence of foam it is crucial that foam remains stable in contact with oil (Jensen and Friedmann, 1987, Farajzadeh et al., 2012). The effect of foam in the presence of an oil phase has been found to be strongly surfactant-specific (Jensen and Friedmann, 1987) as the presence of oil reduce the foam mobility reduction factor of different surfactants to different degrees (Mannhardt et al., 1998). The foam stability in the presence of alkane-type oil is related to molecular weight of the oil molecules, and the foam generation and stability is possibly connected to the surfactant ability to solubilize oil molecules. Alkanes that solubilize in the micelles seem to have a defoaming effect, but alkanes with higher molecular weight than n-Decane are too large to be solubilized in the micelles, and thus have less ability to be transported out of the foam and oil seems to stabilize the foam Short chain alkanes tend to destabilize foam, whereas long chain alkanes give stable foam (Vikingstad et al., 2005, Simjoo et al., 2013).

The nature of the porous media may affect foam stability. Surfactant selection for practical foam performance relates to both foam formation and foam persistence, which in turn depend on the alteration of surface properties including surface tension lowering, surface elasticity, surface viscosity and disjoining pressure (Huang et al., 1986, Schramm and Wassmuth, 1994, Schramm and Green, 1995).

A foam film is always in contact with a meniscus from the solution used to generate the foam. The disjoining pressure, Π, is the force acting between two interfaces separated by a thin film (Hirasaki, 1991). A positive disjoining pressures imply strong repulsive forces between the film interfaces and a stable film, whereas negative attractive forces produce unstable films (Exerowa and Kruglyakov, 1997). There are three major factors contributing to the disjoining pressure: electrostatic interactions, van der Waals interactions and hydrations forces (Hirasaki, 1991). The disjoining pressure increases as the film thickness decreases. When the local maximum value, Π_{max}, is reached, this corresponds to a critical capillary pressure, P_c^*, for film rupture, and when the capillary pressure for the system, $P_{c,bulk}$ exceeds P_c^* the film becomes unstable and break. At equilibrium the disjoining pressure of a flat film equals to the capillary pressure, and can be defined by the Young-Laplace equation as:

$$\Pi = P_c = \frac{2\sigma}{r} \tag{2.3}$$

where σ is the interfacial tension and r is the radius.

From Formula 2.3 it follows that the smaller the pore size the higher the disjoining pressure, and thus film rupture will be more pronounced in porous media with small pores than bigger pores, hence a more stable foam film in larger pores (Hirasaki, 1991).

2.3 CO_2 and CO_2 foam injection on field scale

The East Vacuum Grayburg/ San Andreas Unit (EVGSAU) became the site of the first full-scale tertiary miscible CO_2 flood project in the state of New Mexico, when injection began in September 1985 (Stevens, 1995). Due to over thirty years of primary production, reservoir pressure in the unit was below the minimum miscibility pressure, and reservoir pressurization by water flooding was conducted for five years prior to the CO_2 injection (Brownlee and Sugg, 1987). The 5-spot pattern for the CO_2 project was chosen from the southern parts of the unit, with a 2:1 water-alternating-gas (WAG) ratio, with each of the three WAG injection areas in the unit receiving 4 months of CO_2 injection followed by 8 months of water injection. The first results were encouraging with a large percentage of the wells exhibiting no CO_2 breakthrough. However, some wells in the more heterogeneous section of the unit reached an early CO_2 breakthrough. At an early state of the project, the overall oil production decline had been greatly

reduced, and later the oil production started to increase. Some of the severe problems that occurred were increased calcium sulfate scale formation, precipitation of asphaltenes and paraffins in wells with CO_2 breakthrough, and increased of corrosion problems in injection well casing (Brownlee and Sugg, 1987, Stevens et al., 1992, Stevens, 1995).

In light of the CO_2 breakthrough that occurred in the EVGSAU and as the increase of gas production volumes continued, different methods of mobility control were investigated. The applicability of foams was studied as it would reduce permeability resulting in a more evenly distributed injection profile (Brownlee and Sugg, 1987). A 4 years pilot test for foam injection was conducted at the EVGSAU for improving the effectiveness of a CO_2-flood. The overall CO_2 project results at EVGSAU looked promising, but certain wells had shown very high CO_2 production, which was suspected to be caused by channeling of injected fluid through high permeability zones. The goal of the field test was to investigate foam for conformance control to reduce rapid CO_2 breakthrough, and to prove that foam could be generated and change the mobility of CO_2 in the reservoir. The selected pattern for the CO_2 foam pilot was chosen as a result of: 1) excessive CO_2 breakthrough in one of the production wells, 2) representative reservoir for most of the EVGSAU reservoir for up scaling and 3) an injection well with sufficient injectivity to reduce the chance of the well becoming pressure limited during foam injection (Stevens et al., 1992, Stevens, 1995).

Foam generation began in 1992, and the injection pressure increased dramatically when CO_2 was injected, which indicated generation of foam. To estimate in-situ fluid mobilities at various points during the baseline and foam generation periods Hall plots and falloff testing were used. The techniques compared favorably, and suggested that the foam treatment reduced CO_2 mobility by amount one-third to one-half of the pre-foam value. Because the observed injection pressure increased and remained high for several months, the foam appears to have persisted or continued to be formed in the reservoir. The favorable production response that was observed at the offset production wells experienced a positive effect of CO_2-foam, and showed an improved oil response and reduced CO_2 production. Although a large amount of surfactant was injected, the revenue and savings produced from the test hold promise that foam could be an economical method for sweep improvement (Stevens et al., 1992, Stevens, 1995).

Field applications for CO_2 and CO_2-foam have also been conducted in the SACROC Unit, Scurry County, Texas. Oil recovery by tertiary CO_2 flooding was pilot tested during 1974-1975, where CO_2 was injected into six wells in two adjacent, five-spot patterns in a watered-out portion of the reservoir over a period of nine months. Residual oil was displaced by the CO_2 and approximately 3% of OOIP was recovered (Graue and Blevins, 1978). Implementation of a CO_2 foam pilot test is

currently being tested in the field at SACROC. The project include two stages: 1) a single injection test to validate an infectivity response and a change in the vertical conformance and 2) involving a four injector area to determine the effect of mobility solution on oil production and the gas-oil-ratio (GOR). The single injection test showed a significant reduction in the amount of CO_2 injected and a 30% increase in oil production. By injecting surfactant into the CO_2 phase directly after a water cycle, the amount of CO_2 injected decreased by more than 50% compared to CO_2 alone. Three subsequent cycles of CO_2/surfactant were conducted and proved the same effect. The foam caused an improvement in the vertical conformance at the injector and changes in the flow profiles. Stage two is currently in progress and emphasizes the need of understanding of the reservoir and foam behavior for CO_2 foam to be effective. This requires the development of a history matched model to forecast. However, the results through the end of the project indicate that CO_2 foam injection may be having an effect on the pilot area, and is currently being utilized in development of further trials (Enick et al., 2012, Sanders et al., 2012).

3. Experimental Procedure

This chapter describes the experimental procedure and setups used in this thesis, including core preparations, experimental conditions and information of fluids and rock material.

3.1 Rock material

To better understand and evaluate petroleum reservoirs one may conduct experimental work on reservoir core plugs to obtain important reservoir properties. However, reservoir cores may be expensive and hard to obtain so it is common to perform experimental work on outcrop analogues similar to the reservoir rock, especially when numerous experiments for research purpose is conducted. Reservoir core plugs may not be representative for the actual reservoir as changes in pressure and temperature may impact core properties to a various degree, but are still more representative than outcrop analogues. Using outcrop rocks of a selected rock type may be a good way to single out different effects by changing one parameter at the time. In this thesis four types of rock have been used: 1) Edward limestone, 2) Portland Rørdal chalk 3) reservoir carbonate rock and 4) reservoir shale rock. They were all standard cylindrical core plugs of 1.5" or 2" diameter.

Edward limestone

The Edward limestone is collected from Garden City in Texas and is a grainstone that contains well sorted fossil shells cemented by sparry calcite (Morrow and Buckley, 2006). Previous experimental work reports poor reproducibility between identical tests as a result of heterogeneous core material, regarding pore size, pore geometry and mineralogy (Johannesen et al., 2007, Riskedal et al., 2008). The pore throat is relatively narrow with average throat radius of 2 μm, and a majority of the pore diameter at about 150 μm (Morrow and Buckley, 2006, Johannesen et al., 2007). The permeability and porosity ranged from 6-33 mD and 19-26%, respectively.

Portland Rørdal chalk

Rørdal outcrop chalk is obtained from the Portland cement factory in Denmark. Previous experimental work reports a good reproducibility between identical tests and indicate that the Rørdal chalk is a homogeneous rock (Graue et al., 1999a, Haugen, 2012) . It mainly consists of coccolith deposits, with a composition of calcite (99%) and some quartz (1%). The permeability and porosity range from 1-10 mD and 40-50%, respectively (Lie, 1995).

Reservoir carbonate cores plugs

The nature of carbonate rock material is generally heterogeneous as the complex pore system creates significant scatter in the porosity -permeability relationship (Liu et al., 2009). Generally, carbonates have complex pore size distribution and contain different types of porosity. The pore scale range from 0.5 microns to over 5 microns (Schlumberger, 2014).

Reservoir shale rock

Shale is fine-grained laminated sediments that mainly consist of silt and clay particles. Physical properties such as porosity and permeability are largely depended on the grain size of the constituent minerals (Britannica, 2014). Permeability of shale vary in the range of 0.01- 10 μD (CSUR, 2014). Commonly, horizontal drilling coupled with multi-stage fracturing is used to produce shale reservoirs (CSUR, 2014). A picture of one of the shale core samples used in this thesis is shown in Figure 3.1.

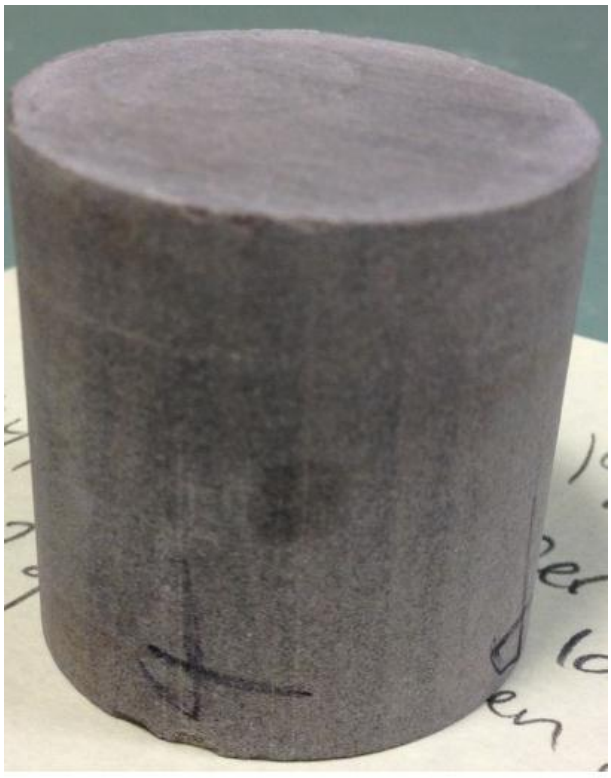

Figure 3.1 Reservoir shale core plug used for experimental test in this thesis.

3.2 Fluids

Table 3.1 lists fluids used in this thesis, and include densities, viscosities and salts. Change in viscosity and density of CO_2 at various temperature and pressure is shown in Figure 2.2 and Figure 2.3.

Table 3.1 Fluid properties including fluid type, salt, densities and viscosities.

Fluid	Salts	Density, 1 bar, 20°C [g/cm³]	Viscosity, 1 bar, 20°C [cP]	Comments
Chalk Brine[1)]	Distilled water 50 g/m³ NaCl 50 g/m³ $CaCl_2 \cdot H_2O$ 0.05 cm³ NaN_3	1.05	1.09	To avoid bacterial growth 0.05 ml/l NaN_3 is added. $CaCl_2$ was added to avoid dissolution of the carbonate rock (Graue et al., 1999a)
Brine C	5.2362 g/m³ Na_2SO_4 4.576 g/m³ KCl 5.8247 g/m³ $CaCl_2 \cdot 2H_2O$ 2.7599 g/m³ $MgCl_2 \cdot 6H_2O$ 22.7968 g/m³ NaCl	n/a	n/a	Five salts were identified from field water analysis, and Brine C composition was suggested as the closest approximation to the formation brine.
n-decane	$C_{10}H_{22}$	0.73	0.92	Purity > 95%
Paraffinic oil	n-paraffin	0.74	1.43	Purity > 98%
Surfactant solution: AOS $C_{14/16}$ (Petrostep C-1)	Distilled water 50 g/l NaCL 0.05 ml/l NaN_3 1wt% AOS $C_{14/16}$	n/a	n/a	To avoid bacterial growth NaN_3 is added.
Surfactant solution: Surfonic L24-22	Brine C 1 wt% Surfonic L24-22	n/a	n/a	To avoid bacterial growth 0.05 ml/l NaN_3 is added
Ekofisk-crude oil[2)]	53 wt% saturated HC 35 wt% aromatic HC 12 wt% resins 0.9 wt% asphaltenes	0.849	14.5 2.5 [90°C]	Acid number: 0.094 Base number: 1.79
CO_2[3)]	> 99.999 % CO_2	0.40	29.2	

[1)] The salts used in the chalk brine were from Sigma Aldrich and used as received and the purity of these salts are: NaCl 99.5%, $CaCl_2$ 99.5%. The sodium azide, NaN_3, has a purity of 99.5% (Graue et al., 1999a).

[2)] Composition of Ekofisk crude oil is from (Graue et al., 1999a).

[3)] Properties are from NIST web book

3.3 Core Plug Preparations

Evaluating rock- and fluid parameters for the core samples is important when predicting the reservoir production performance. Reservoir core samples are obtained from small core plugs drilled out perpendicular to the well bore core, i.e. along the fluid production direction. Two essential characteristics were measured prior to the experiments: 1) porosity, and 2) rock permeability. Porosity is one of the most important rock parameter in reservoir engineering, because it determines the storage capacity of fluid that a reservoir rock can hold, whereas permeability of a porous media is its capability to transmit fluid through its network of interconnected pores.

After cylindrical cores were drilled out from a larger block of rock, they were dried in a heating cabinet at 90 °C for at least 24 hours before the core dimensions were measured. The porosity was determined by the increase in weight after the core plug was saturated with water under vacuum (>1mBar). Assuming 100% water saturation, the porosity is found by equation 3.1.

$$\varphi = \frac{(m_s - m_d)}{\rho \cdot V_b} \tag{3.1}$$

where m_s and m_d is the weight of the saturated and dry sample respectively, ρ is the density of the brine and V_b is the bulk volume of the sample.

The permeability was measured by flushing the 100% brine saturated core sample at a constant flow rate (Q) whereas measuring the differential pressure (ΔP) across the core sample. By plotting the measured data, Q and ΔP, and fitting the regression line for the projection points, the rock permeability was calculated using the line slope and Darcy's law:

$$Q = \frac{K \cdot A}{\mu} \cdot \frac{\Delta P}{L} \tag{3.2}$$

where Q is the fluid flow rate, μ is the viscosity of the fluid, ΔP is the pressure drop across the length, L, and A is the cross-sectional area of the sample.

Subsequent primary drainage was conducted on all core plugs. The saturated strongly water-wet cores were drained with n-Decane or refined paraffinic oil until the irreducible water saturation was reached. The cores were drained with 5 pore volumes of brine in both directions, to eliminate end-effects, with a constant pressure drop equivalent to 2 bar/cm for the chalk core plugs and 1.5 bar/cm for the limestone core plugs.

3.3.1 Fractured cores

To study recovery mechanism of CO_2 and CO_2-foam in fractured reservoir, some of the cores were split down the long axis to represent a smooth surface fracture. A 1 mm thick polyoxymethylene (POM) spacer was inserted between the two halves as illustrated in Figure 3.2. The spacer had a known volume of void space, and its purpose was to resemble a fracture opening where fluid has enhanced access to the porous media. The porosity and fluid distribution were assumed constant before and after the core were cut.

Figure 3.2 POM spacer used in experiments to maintain a constant fracture aperture.

The mass of the core plug was measured before and after the cutting process, and the void volume in the spacer was subtracted as dead volume. The pore volume was modified to account for the volume that was lost in the cutting process, and the new pore volume was calculated by:

$$PV_{frac} = PV_{inital} \times \frac{M_{frac}}{M_{inital}} \tag{3.3}$$

where PV_{inital} and PV_{frac} are the pore volumes before and after fracturing respectively, and M_{inital} and M_{frac} is the measured mass of the core plug before and after fracturing respectively.

3.3.2 Wettability alteration

One core sample was aged to an oil-wet wettability condition. The core sample was aged by continuously injecting oil into the core to expose the core sample to crude oil over an extended period of time at low constant rate and high temperature (Graue et al., 1999a, Graue et al., 2002, Aspenes et al., 2003). The 100% saturated core plug was drained with 2.5 PV of filtered crude oil in each direction to eliminate end effects and create a uniform wetting distribution. After irreducible water saturation was established, the injection rate was set to a constant injection rate of $3cm^3/h$ and maintained for 2-4 days in each direction.

3.4 Experimental Design

A series of experiments have been conducted to study recovery mechanism by CO_2 and CO_2-foam injection in different core material at various experimental conditions and include both liquid and supercritical CO_2. During this experimental work 3 different setups have been designed, tested and used. All cores were wrapped with aluminum folio to protect the sleeve from CO_2, and assembled in the core holder and placed horizontally in the heating cabinet.

Setup 1

Figure 3.3 shows a schematic illustration of "Setup 1", used for supercritical CO_2 and/or CO_2-foam experiments conducted at Department of Physics and Technology. The equipment used in this setup is listed below. The CO_2 and CO_2-foam injection on this setup was performed on limestone or chalk outcrops. Prior to experiment all outcrops were prepared as described in section 3.3. Some cores were cut as described in section 3.3.1, and the fracture aperture was held constant with POM spacers. When a fracture was present, the core system was placed horizontally such that the open fracture was aligned with gravity.

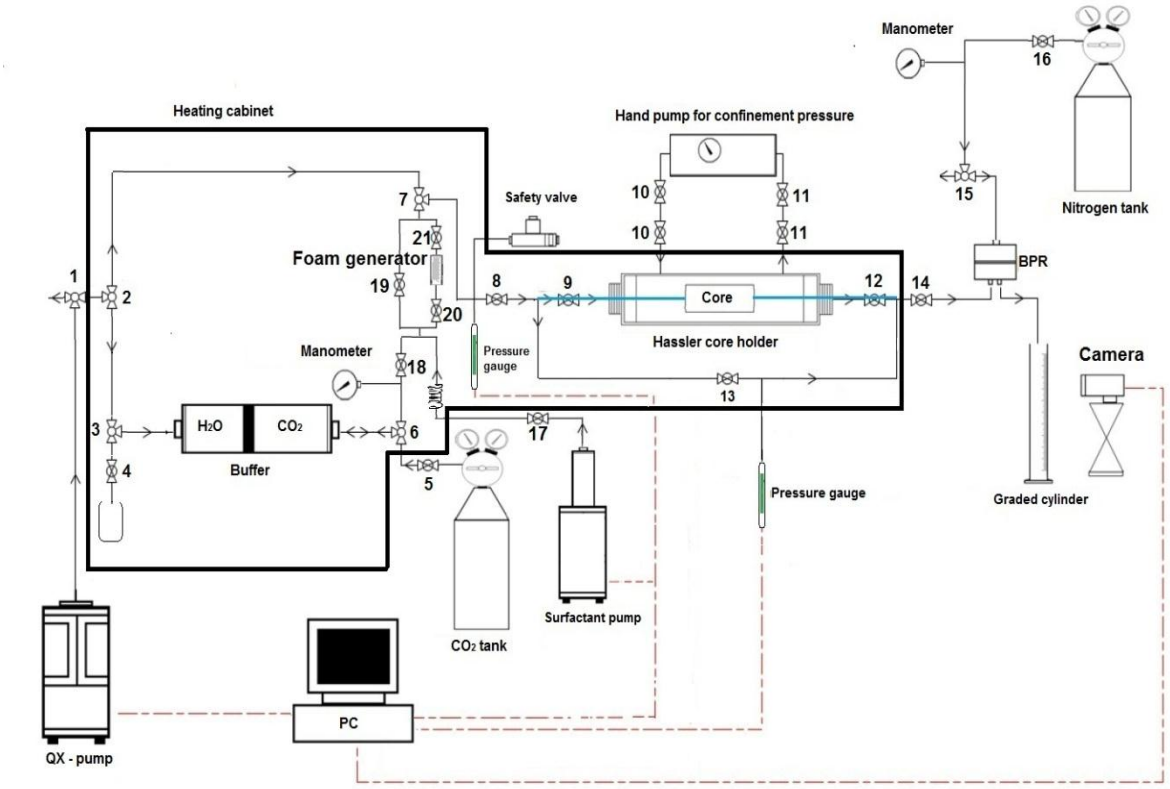

Figure 3.3 Setup 1: Schematic illustration of experimental set up for supercritical CO_2 and CO_2-foam experiments at Department of Physics and Technology. The thinner black lines represent the coil tubing and the arrows shows flow direction. The thicker black line represents the heated area. The back pressure regulator was at the first located outside the heating cabinet and later moved inside the heating cabinet to improve stable CO_2 flow. The blue line denotes the dead volume.

Equipment used:

- Back Pressure regulator controlled by nitrogen to adjust the pore pressure
- Computer for logging and operating pumps
- *ESI 200* pressure transducers for measuring pore pressure at inlet and outlet
- Hassler steel core holder
- Heating cabinet
- POM spacers to simulate a fracture
- *Quizix QX-1500* pump for pressurizing the system with paraffinic lamp oil and driving the accumulator with water and CO_2
- *Quizix SP-5200* pump for confinement oil
- *Quizix QX-1500* pump for driving the accumulator with surfactant
- Steel accumulator (buffer) to store heated and pressurized CO_2
- *Swagelock* tubings, fittings and valves
- Web camera for monitoring production

In advance, the CO_2 accumulator was pressurized and stabilized at experimental conditions (P = 90 bar T = 35 °C). At these conditions the CO_2 is in a supercritical state and assumed first contact miscible with the mineral oil used (n-Decane or paraffinic lamp oil). A gas doomed back pressure regulator, using nitrogen, was set to the desired pressure to control pore pressure during the experiment. The system was flushed and pressurized with mineral oil to experimental conditions, keeping the confinement pressure at 10 bar over the pore pressure at all time during the experiment to avoid core damages and to prevent any leaks between the core holder sleeve and the confinement chamber. CO_2 was then flooded through the system, bypassing the core holder to flush out the oil to minimize dead volume before starting the CO_2 injection through the core. For the pure CO_2 injection experiments, the CO_2 bypassed the foam generator, as no foam was present. For experiments with subsequent CO_2-foam injection the foam generator was included, and foam was generated by co-injecting surfactant and CO_2, with a 9:1 ratio to generate strong foam based on previous experience (Haugen et al., 2012).

Setup 2

Figure 3.4 shows a schematic illustration of "Setup 2" that was built in collaboration with Stig Langlo and Tom Ydstebø, and used for secondary liquid CO_2-foam experiments conducted at Texas A&M University. The equipment used in this setup is listed below. Three experiments were conducted on whole Edward limestone cores, all saturated with n-Decane to S_{wi}.

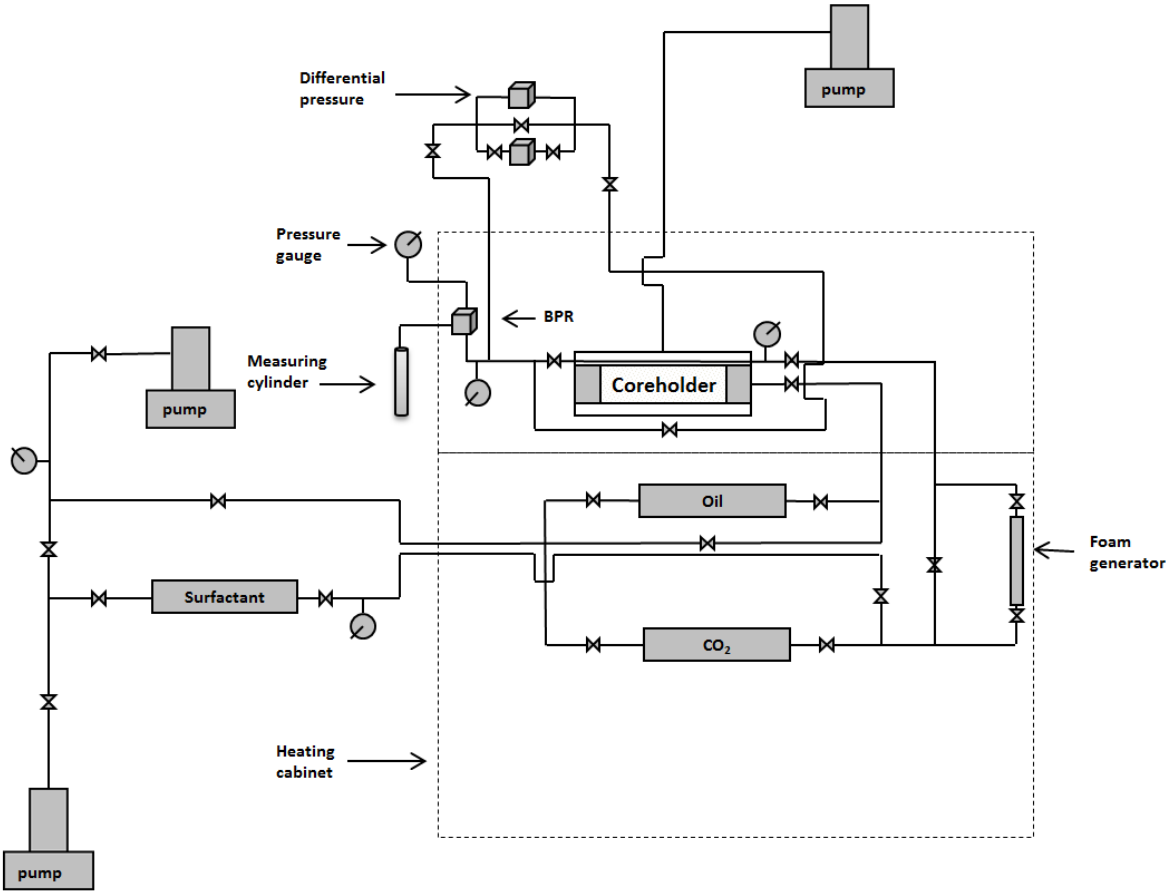

Figure 3.4 Setup 2: Schematic illustration of experimental set-up for the CO_2-foam experiments at Texas A&M University (Langlo, 2013).

Equipment used:

- Back Pressure regulator controlled by nitrogen to adjust the pore pressure
- Bi-axial (hydrostatic) core holder
- Enclosed sand pack for pre-generating foam
- Heating cabinet
- *ISCO* pump x 3 (for confinement pressure, and driving the accumulators)
- Pressure gauges
- Steel accumulators x 3 (to store heated and pressurizing CO_2, surfactant and n-Decane)
- *Swagelock* tubings, fittings and valves
- *Validyne DP15* differential pressure
- Web camera for monitoring production and differential pressure

In advance, the surfactant, n-Decane, CO_2 accumulators were pressurized and stabilized at experimental conditions (P = 99 bar T = 20 °C). At these conditions the CO_2 is in a liquid state and is assumed first contact miscible with n-Decane. Properties for the fluids are given in Table 3.1. A back pressure regulator was set to the desired pressure to control pore pressure during the experiment. The system was flooded and pressurized with n-Decane to experimental conditions, bypassing the foam generator because oil has a destabilization effect on foam. The confinement pressure was kept 20 bar over the pore pressure at all time during the experiment to avoid core damages and to prevent any leaks from between the core holder sleeve and the confinement chamber. Prior to the foam injection the lines were flushed with surfactant solution (Petrostep C1), bypassing the core holder to minimize dead volume. CO_2 and surfactant solution was then co-injected through the foam generator and pre-generated foam was injected through the core sample.

Setup 3

Figure 3.5 shows a schematic illustration of "Setup 3", used for supercritical CO_2 and CO_2-foam experiments conducted on reservoir core plugs at higher pressure and temperature conditions. The equipment used in this setup is listed below. "Setup 3" is based on the same idea as "Setup 1", with some modifications on the equipment. Due to the pressure limitations on swagelock valves (166 bar), autoclave fittings were used as they are resistant to higher pressure (10 000 bar).

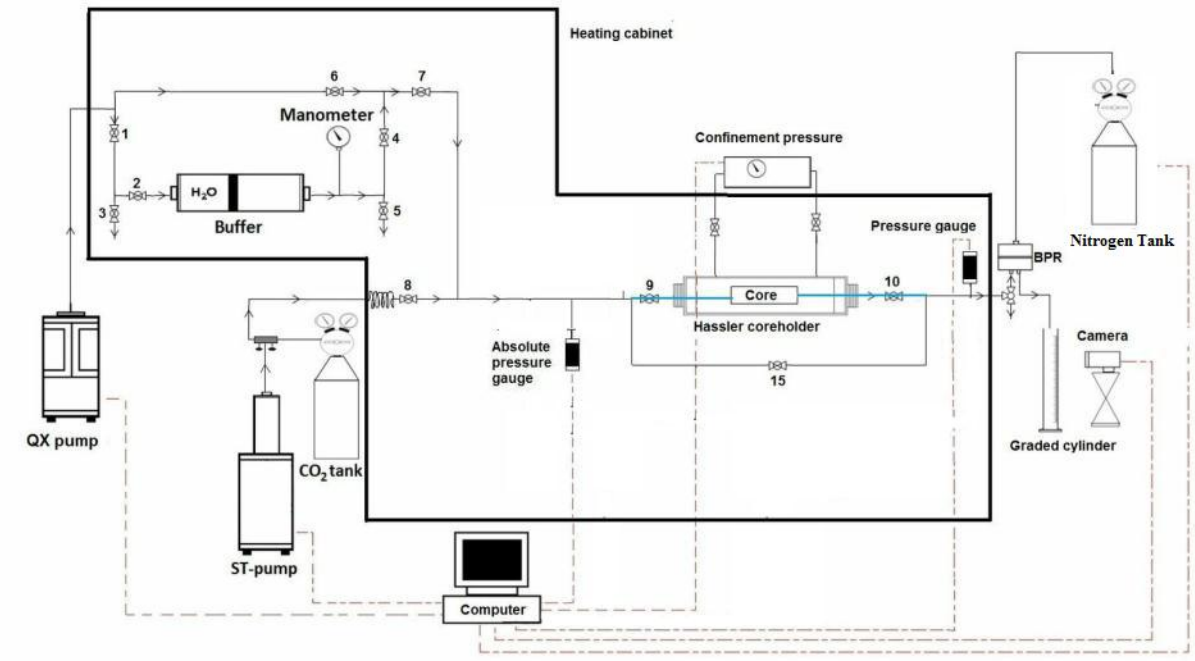

Figure 3.5 Setup 3: Experimental set up for supercritical CO_2 experiments conducted on reservoir cores at high temperature and pressure at the Department of Physics and Technology. The thinner black lines represent the coil tubing and the arrows shows flow direction. The thicker black line represents the heated area. The blue line denotes the dead volume.

Equipment used:

- Autoclave tubings, fittings and valves
- Back Pressure regulator controlled by nitrogen to adjust the pore pressure or an ST pump (retracting syringe pumps) at outlet for improved pressure and flow control
- Computer for logging and operating pumps
- *ESI 200* pressure transducers for measuring pore pressure at inlet and outlet
- Heating cabinet
- Hassler steel core holder
- *Quizix SP-5200* pump for confinement oil
- ST pump (retracting syringe pumps) for pressurizing the system with CO_2
- Steel accumulator (buffer) to store heated and pressurized CO_2
- Web camera for monitoring production

3.5 Experimental procedure

A series of experiments have been conducted to study enhanced oil recovery (EOR) by secondary and tertiary CO_2 and/or CO_2-foam injections at miscible conditions in fractured and whole core plugs using different rock types. In addition, studies of structure and flow behavior in shale cores have been performed in a PET/CT scanner. Table 3.2 summarizes the experimental processes studied in this thesis, and includes location and setups used. A detailed description of the experimental procedure for the different processes is presented in the following sub-sections.

Table 3.2 Experimental Overview, including type of experiments, location and setup.

Experiment type	Location	Setup
Secondary Supercritical CO_2 injection	Department of Physics and Technology, UoB	Setup 1
Secondary Supercritical CO_2 injection + foam	Department of Physics and Technology, UoB	Setup 1
Secondary Liquid CO_2-foam injection	Texas A&M University	Setup 2
Tertiary supercritical CO_2 injection + foam	Department of Physics and Technology, UoB	Setup 1
Tertiary supercritical CO_2 injection	Department of Physics and Technology, UoB	Setup 3
Secondary Supercritical injection CO_2	Department of Physics and Technology, UoB	Setup 3
Secondary Liquid CO_2 injection	Haukeland University Hospital (HUS)	-

3.5.1 Supercritical CO_2 injection in whole and fractured core plugs

Eight supercritical CO_2 experiments were performed on strongly water-wet outcrop carbonate rock, to study recovery mechanism through CO_2 injection, and its effect on whole versus fractured cores samples. Figure 3.3 show a schematic overview of the experimental set up (Setup1). CO_2 was injected through the core at constant injection rate. Injection rate varied for the different experiments to study the effect of diffusion, and to account for different frontal velocity between core materials to be able to compare the results. The oil production was captured in a graded cylinder. Computers logged the pressures during the experiments. Table 3.3 gives an overview of the material balance experiments with supercritical CO_2 injection.

Table 3.3 Overview of material balance experiments with supercritical CO_2 injection.

Core ID	Rock material	Oil	Frac	S_{wi} [%]	Average P [bar]	Average T [°C]	Injection rate [ml/h]
RIK_1	Chalk	n-Decane	No	28.7	91.06	35	2
RIK_3	Chalk	n-Decane	Yes	29.2	91.47	35	10
RIK_9	Chalk	n-Decane	No	25.2	91.48	35	2
RIK_13	Chalk	n-Decane	No	22.7	95.18	35	20
L_5	Limestone	n-decane	No	22.7	93.79	35	4
RI_2	Limestone	Paraffinic	No	23	91.29	35	2
RI_3	Limestone	Paraffinic	Yes	25.8	95.06	35	5
RI_4	Limestone	Paraffinic	No	24.3	94.68	35	5

3.5.2 Supercritical CO_2 and CO_2-foam injection in fractured core plugs

Six experiments have been conducted with supercritical CO_2 with subsequent CO_2-foam injection on fractured outcrop carbonate cores. The objective was to study recovery mechanism by CO_2 diffusion and CO_2-foam for mobility control. The experimental setup is illustrated in Figure 3.3 (Setup 1), and is the same set up that was used for the supercritical CO_2 experiments. In these experiments the foam generator was included for the subsequent foam injection. All injection rates were set to 10 ml/h for the chalk cores and 5 ml/h for the limestone cores, which corresponds to approximately equivalent frontal velocity, without the presence of the fracture due to the higher porosity in chalk. Table 3.4 gives an overview of the material balance experiments with CO_2 and CO_2-foam injection.

Table 3.4 Overview of material balance experiments with CO_2 and CO_2-foam injection in fractured cores.

Core ID	Rock material	Oil	S_{wi} [%]	K_{total} [mD]	Average P [bar]	Average T [°C]	Injection rate [ml/h]
RIK_4	Chalk	n-Decane	30.9	3.77	87.21	35	10
RIK_7	Chalk	n-Decane	30.7	4.67	91.21	35	10
KIR_1[1)]	Chalk	Paraffinic	30.8	4.99	95.30	35	10
KIR_4[2)]	Chalk	Paraffinic	28.8	4.04	95.30	35	10
RI_5	Limestone	Paraffinic	24.5	20.19	92.20	35	5
RI_7	Limestone	Paraffinic	25.6	19.11	92.02	35	5

[1)] Direct foam

[2)] Aborted because of leaks

Supercritical CO_2 were injected through the core at constant injection rate, prior to the CO_2-foam injection in all experiment, except one experiment conducted with direct CO_2-foam (core plug KIR_1). For the CO_2-foam injection part, a surfactant solution was co-injected with CO_2 (90% gas fraction). The surfactant (Surfonic L24-22) was mixed with CO_2 through a sand pack mounted on the inlet side of the core to inject pre-generated foam. The oil production was captured in a graded cylinder. Computers logged the pressures during the experiments.

3.5.3 Secondary Liquid CO_2-foam injection in whole core plugs

Three experiments were performed with liquid CO_2-foam injection, in collaboration with Stig Langlo and Tom Ydstebø, on outcrop carbonate cores at Texas A&M University. The objective was to study recovery mechanism by CO_2-foam for mobility control at both water-wet and neutral-wet conditions on whole Edward limestone core plugs. The neutral-wet (NW) core was altered to this wettability by aging, as described in section 3.3.2, by Stig Langlo and Tom Ydstebø. "Setup 2" was used for this part of the thesis, see Figure 3.4. Table 3.5 gives an overview of the material balance experiments with liquid CO_2-foam injection.

Table 3.5 Overview of the material balance experiments with liquid CO_2-foam injection in whole 2" core plugs.

Core ID	Rock material	Oil	Wettability	S_{wi} [%]	Average P [bar]	Average T [°C]	Injection rate [ml/h]
L_28	Limestone	n-Decane	WW	24.3	99	20	4.2
L_33	Limestone	n-Decane	WW	29.4	98	20	4.2
L_14	Limestone	n-Decane	NW	28.5	99	20	4.2

The surfactant solution was co-injected with CO_2 and mixed in the sand pack (foam generator) mounted on the inlet side of the core to inject pre-generated foam. The injection rates were 3.72 ml/h for the CO_2 and 0.48 ml/h for the surfactant solution (90% gas fraction).

3.5.4 Tertiary CO_2 injection and CO_2-foam injection in fractured core systems

Integrated EOR, by combing proven EOR methods in a smart sequence, was evaluated in strongly water-wet, fractured limestone core systems at supercritical conditions. Three experiments were conducted to study recovery mechanism by combining three injection steps: 1) water injection, 2) CO_2 injection and 3) CO_2 foam injection.

"Setup 1" was used for these experiments and is illustrated in Figure 3.3. No foam generator was used in these experiments, and the CO_2 bypassed the foam generator, because foam was supposed to be generated in-situ in the first whole inlet core plug. All core samples were Edward limestone outcrops, saturated with refined paraffinic oil to residual water saturation, before they were cut, as explained in section 3.3.1. Paraffinic lamp oil was used because it has higher molecular weight than n-Decane, and thus may have less destabilization effect on foam, as described in section 2.2.2. The core samples consisted of three core pieces butted together, one

whole and two fractured cores. The whole core piece was placed closest to the inlet, followed by a core piece with vertical fracture orientation and a core piece with horizontal fracture orientation, as illustrated in Figure 3.6.

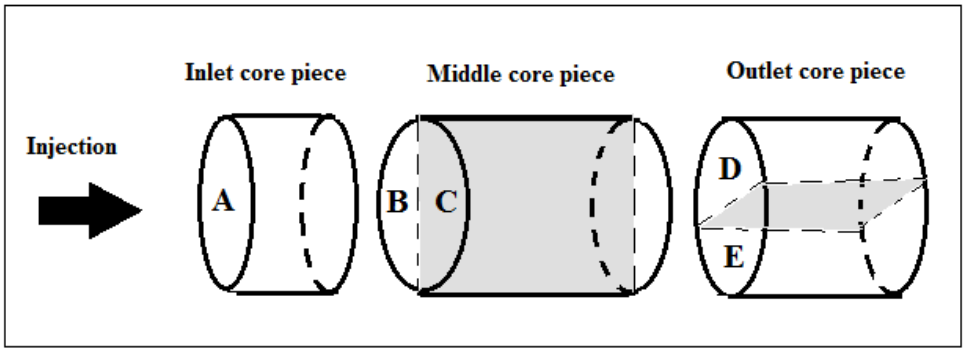

Figure 3.6 Schematic showing the fracture representation of core samples AC_1, AC_2 and AC_3. The middle and outlet core pieces are cut in half in a plane perpendicular to each other.

Table 3.6 summarizes the core dimensions measured, including core length (L) and radii (R) for the different core pieces butted together, and Table 3.7 gives an overview of the total porosity, pore volume and residual water saturation. The total pore volume was calculated by summarizing PV_{frac} from equation 3.3 for all core pieces, the total S_{wi} was found by summarizing the calculated S_{wi} for each core piece by equation 3.4, and porosity was obtain by dividing the total pore volume on the total bulk volume. The fluid properties, including brine and surfactant composition, densities and viscosities, are listed in Table 3.1.

$$S_{wi,tot} = \sum \left(\frac{PV_{frac}^{core\ i}}{PV_{total}} \times S_{wi}^{core\ i} \right) \tag{3.4}$$

Table 3.6 Summary of length (L) and radii (R) measurements of the core pieces utilized IEOR experiments. Core piece A, B, C, D and E were butted together as illustrated in Figure 3.5 to form a fractured system.

Core ID	A		B		C		D		E		Total length [cm]
	L [cm]	R[cm]	L [cm]	R [cm]	L [cm]	R[cm]	L [cm]	R[cm]	L [cm]	R[cm]	
AC_1	2.20	1.89	4.00	1.77	4.02	1.86	3.48	1.71	3.43	1.70	9.70
AC_2	2.33	1.89	3.47	1.99	3.47	1.82	3.44	1.71	3.45	1.82	9.25
AC_3	2.46	1.89	3.47	1.71	3.46	1.83	3.75	1.85	3.75	1.83	9.68

Table 3.7 Summary of properties of the core pieces utilized IEOR experiments. The uncertainties in permeability measurements are given in standard deviation, and a high uncertainty was calculated for core sample AC_1 due to problems with the BPR.

Core ID	Total φ [%]	Total PV [ml]	S_{wi} [%]	K_{frac} [mD]	Uncertainty
AC_1	21.9	21.43	23.7	85.3	56.6
AC_2	21.3	21.17	23.5	190	5.0
AC_3	23.6	23.07	24.2	146.2	9.4

The core samples were wrapped in aluminum folio, to protect the sleeve from CO_2, and assembled in a core holder placed inside the heating cabinet. The preparation of the cores is illustrated in Figure 3.7. No POM spacers were used in this experiment.

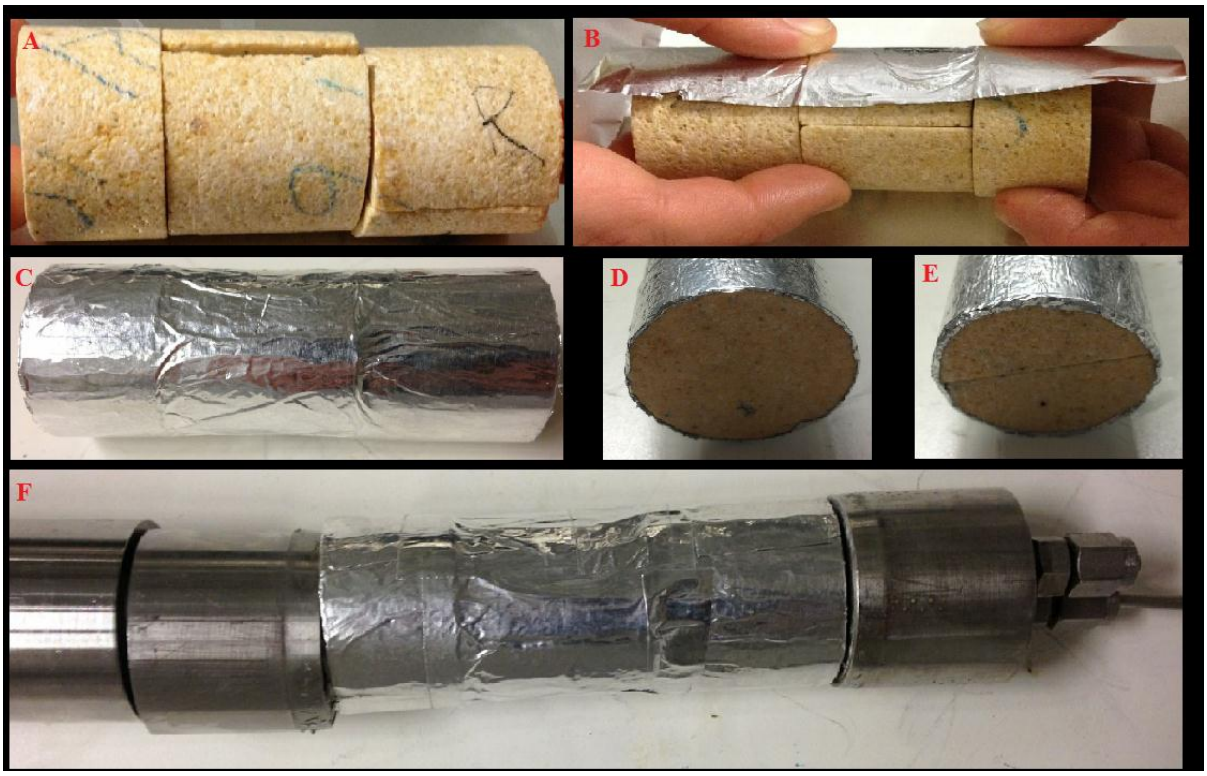

Figure 3.7 Preparation of the cores prior to experiment. The whole core piece was placed closest to the inlet, followed by a core piece with vertical fracture orientation and a core piece with horizontal fracture orientation.

Prior to water injection, water was flooded through the system, bypassing the core holder, to flush out the paraffinic oil to minimize the dead volume. Water was then injected through the core sample, followed by supercritical CO_2 injection. All injection rates were set to 10 ml/h. The subsequent co-injection of surfactant solution (Surfonic L24-22) and CO_2 was going to generate foam in the first whole core at the inlet end. The injection rates were 8 ml/h for the CO_2 and 2 ml/h for the surfactant solution (80% gas fraction). No bypass flushing of the core samples was conducted between the different injection stages in these experiments, to conserve the CO_2 to reach end-point oil saturation before terminating experiments. The oil production was captured in a graded cylinder. Computers logged the pore pressure and the confinement pressure during the experiment.

3.5.5 Tertiary CO_2 injection on reservoir carbonate cores

Four experiments were conducted on unpreserved reservoir cores from a heterogeneous carbonate reservoir in Texas, to study oil recovery by tertiary CO_2 injection, in collaboration with Marianne Steinsbu and Bergit Brattekås. The experiments were performed on setup 3, see Figure 3.5. Table 3.7 summarizes the core data including porosity, permeability, pore volume, residual water saturation after drainage and the experimental conditions. The fluid properties, including brine composition, densities and viscosities, are listed in Table 3.1.

Table 3.7 Summary of core properties and experimental conditions for experiments with tertiary CO_2 injection in reservoir carbonate cores.

Core ID	Porosity [%]	Permeability [mD]	S_{wi} [%]	Pore volume [ml]	Temperature [°C]	Average Pressure [bar]	Injection rate [ml/h]
RC_A	15.0	17.94	46.4	16.05	71	178	5
RC_B	14.1	9.14	51.7	16.25	71	178	5
RC_C	9.3	4.69	47.0	11.32	71	178	3.5
RC_D	10.8	2.32	74.9	12.56	71	178	3.5

All core samples were assumed strongly water wet as they have been cleaned by the THF (tetrahydroflourinert) method (the technique established at Rice University by Prof. George Hirasaki and Prof. Jose Lopes Salinas). The reservoir carbonate cores were prepared the same way as the outcrops, but crude oil was used instead of mineral oil. The initial water saturations, S_{wi}, were established for all core samples by drainage with Ekofisk crude oil under experimental conditions (P = 178 bar and T = 71°C). A relatively high S_{wi} was established for all core samples, especially for core sample RC_D, even with same procedure as for outcrop core plugs. This is suspected to be caused by a combination of: 1) extremely heterogeneous rock material, regarding local high permeable streaks that causes water to channel through these zones and 2) sufficient drainage pressure was not achieved and was restricted by 1 bar/cm or injection rate of 500 ml/h. Injection rates used in these experiments were 5 ml/h for the cores of higher porosity (RC_A and RC_B) and 3.5 ml/h for the lower porosity cores (RC_B and RC_D) to obtain a constant frontal velocity of 2 cm/h. Due to temperature changes from the injection pump located at room temperature to the heating cabinet, the injection rates were re-calculated based on the volume expansion of CO_2.

In advance, the CO_2 was transferred to a Sanches pump (ST-pump) located outside the heating cabinet, see Figure 3.5. Liquid CO_2, at 178 bar, was injected into the heating area and circulated through a coil to establish a supercritical CO_2 state. The system was flooded and pressurized with Ekofisk brine to experimental conditions. A back pressure regulator, adjusted with nitrogen, was used to control the pore pressure. The confinement pressure was kept at 7 bar above the pore pressure at all time during the experiment to avoid core damages and to prevent

any leaks between sleeve in the core holder and the confinement chamber. Chalk brine was injected during the waterflood, and water was injected until endpoint saturation was reached and no more oil production was observed, and corresponded to approximately 1.5 PV. CO_2 was then injected to recover additional oil.

During tertiary CO_2 injection in core plug RC_A, a sudden differential pressure increase was observed at t ≈ 2 PV injected. The abrupt increase in pressure was caused by an obstruction in the production line close to the back pressure regulator. The back pressure regulator and parts of the production line were positioned outside the heating cabinet in this experiment. A rapid decrease in pressure during production through the back pressure regulator (from 178 bar to ambient pressure conditions) caused CO_2 to expand, and the gas flow rate increased. Consequently, the back pressure regulator and production line was cooled down below room temperature. Water and gas were both present in the production line and back pressure regulator during tertiary CO_2 injection. The presence of water and gas at high pressure, and a low temperature within the hydrate stable conditions for CO_2 (11.34 °C at 178 bar)(Birkedal, 2013), may have led to hydrate formation, and was believed to be the cause of plugging. The assumed hydrate plug was removed through depressurization and thermal stimulation. For subsequent tests, the back pressure regulator was moved inside the heating cabinet to prevent similar problems.

3.5.6 Reservoir shale rock experiments

Several experiments have been conducted on three shale core samples (SC_A, SC_B, SC_C), from a shale reservoir in the USA. The objective was to study three main aspects; 1) measure permeability by injection of CO_2, 2) examine a "best practice" for re-saturating the shale cores with crude oil and 3) investigate rock structure and flow behavior by visualization techniques in a PET/CT scanner. Two of the core samples were unpreserved and one core sample was semi-preserved (covered in wax and aluminum foil). All cores were received at ambient pressure and temperature. Table 3.8 summarizes properties obtained from the shale core samples, and includes length, diameter, bulk volume and initial weight.

Table 3.8 Properties of the shale cores including core dimensions, bulk volumes and weight.

Core ID	State	Length [cm]	Diameter [cm]	Bulk volume [cm^3]	Weight [g]
SC_A	Unpreserved	3.80	3.80	43.10	111.27
SC_B	Unpreserved	3.92	3.80	44.46	114.40
SC_C	Semi-preserved	2.45	3.82	28.08	70.28

Permeability Measurements

Permeability measurements were performed on all core samples with both liquid and supercritical CO_2 injection, at various pressures, temperatures and flow rates. For the first experiment, a Back Pressure Regulator (BPR) was used at the outlet to control the pore pressure, as illustrated on the Figure 3.5. For subsequent tests, constant outlet pressure was maintained by replacing the BPR with a retracting syringe pump for improved flow and pressure control. The supercritical CO_2 experiments were conducted at the Department of Physics and Technology ("Setup 3", see Figure 3.5), whereas the liquid experiments were conducted at Haukeland University Hospital (HUS) on a similar setup. A combined PET and medical CT scanner were used to get additional information about the flow behavior of the CO_2 phase. The injected CO_2 was explicitly labeled using ^{11}C to accurately visualize flow paths within the system.

During permeability tests CO_2 was injected from the pump at experimental pressure conditions through the core. The temperature was kept constant for each experiment, whereas net confining pressure and injection rates were varied. The rates were repeated in inverse direction. Due to temperature changes from the injection pump located at room temperature to the heating cabinet, the injection rate was re-calculated based on the volume expansion of CO_2. The injection rates and the measured differential pressures were then used to calculate the effective permeability by using Darcy's law (Equation 3.2.) The experimental conditions for each experiment are listed in Table 3.9, and include temperatures and net confining pressures.

Table 3.9 Experimental conditions for different permeability tests.

Core ID	CO_2 state	Temperature T [°C]	Pore /Net confinement pressure [bar]
SC_B	Liquid	27	160 / 40
			160 / 80
SC_B	Supercritical	80	165 / 35
			165 / 85
SC_B	Supercritical	115	150 / 50
			150 / 100
			200 / 50
			200 / 100
SC_C	Supercritical	80	200/100

Rock structure

Rock structure for each core sample was obtained with a medical CT scanner located at HUS, by dry scan of all core samples. The cores were first scanned to localize their position.

Positron Emission Tomography – Computed Tomography (PET-CT)

To obtain a three-dimensional visualization of rock material and to study in-situ displacements, a Siemens Biograph TruePoint PET/CT scanner with an extended axial field-of-view of 21.6 cm and a 16-slice CT has been used (Jakoby et al., 2006). This scanner is located at the PET center and nuclear medicine at the Haukeland University Hospital in Bergen, and is illustrated in Figure 3.8.

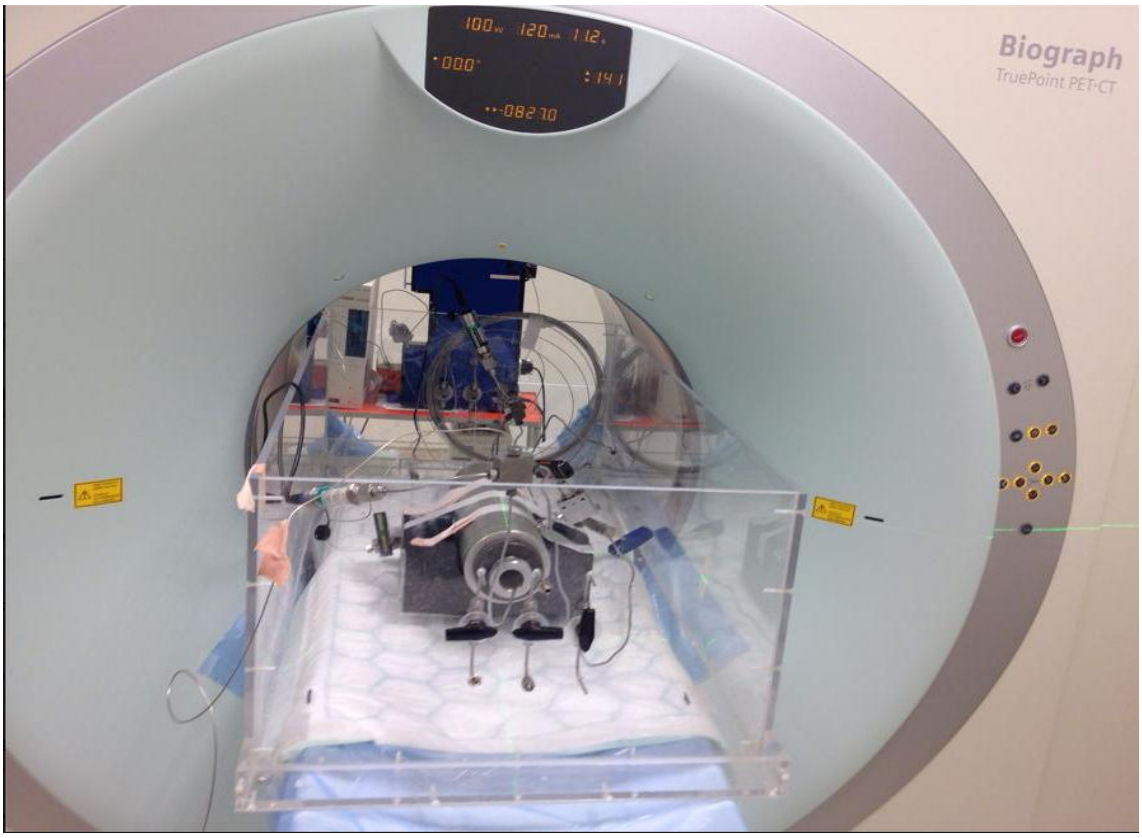

Figure 3.8 Siemens Biograph TruePoint PET/CT scanner with core holder at Haukeland University Hospital in Bergen.

The PET/CT mainly consists of three parts: the PET scanner, the CT scanner, and the table where the patients or in this case the core holder is placed. By combining images from the PET scanner and the CT scanner high-spatial-resolution 3D visualization of in-situ fluid flow can be obtained. The CT-scan maps the initial variation of X-ray attenuation within the object, whereas the PET scan utilizes the annihilation radiation produced during decay of the radioactive isotope/tracer continuously to develop in-situ images. (Jakoby et al., 2006)

CT scanning

Computed tomography (CT) scanning uses computer-processed x-rays to produce tomographic images of an object at different angles. The CT scanner consists of an X-ray source and detectors that measure how much the X-ray signals are attenuated as they pass through material with different densities. The CT value is the attenuation of the X-ray, and increases with increasing density, and is influenced by absorption and scattering which affect the intensity of the X-ray beam. The series of images produced in CT can be viewed individually as two-dimensional pictures or by combining the entire series as a three-dimensional visualization (Ketcham and Carlson, 2001).

PET

Positron emission tomography (PET) is a nuclear imaging technique to obtain a three-dimensional image volume of an object by using the unique decay characteristics of radionuclides that decay by positron emissions (Cherry and Dahlbom, 2006). A PET scanner consists of a set of detectors that surround the object to be imaged and are designed to convert these high-energy photons into an electrical signal that can be fed to subsequent electronics. Labeled tracers (in this case ^{11}C was used to label CO_2) are introduced to the object, and when the radioactive atom on a particular molecule decays, a positron is ejected from the nucleus, ultimately leading to the emission of high-energy photons that have a good probability of escaping from the object. In a PET scan the decays will be detected and reconstructed into a tomographic image using mathematical algorithms to obtain a three-dimensional image. The signal intensity in a particular image is proportional to the amount of the radionuclide (Cherry and Dahlbom, 2006).

Best Practice for saturation shale cores

Different methods have been investigated in order to find a "best practice" for re-saturating dry reservoir shale cores with crude oil. Two saturation methods have been implemented for shale core SC_A and SC_B; 1) flowing crude oil through the cores for two weeks (dynamic) and 2) soaking the cores in crude oil under pressure in one week (static). Both experiments were conducted in a heating cabinet at 60 °C. During the first dynamic method, crude oil was injected from an accumulator through the cores by a differential pressure of 100 bar, keeping the net confinement pressure at 50 bar. The samples were weighed during the test. The second method used for re-saturation was a static method, where the cores were placed inside an accumulator filled with crude oil under high pressure (200 bar) for a longer period of time (1-2 weeks) to force crude oil into the matrix. The added surface area could increase saturation.

4 Results and discussion

This chapter will present and discuss the experimental results, and compare them with similar studies. From a total of 52 cores prepared, 28 cores were used for experiments conducted with CO_2 and/or CO_2 foam injection, in addition to visual studies of structure and flow behavior on shale cores in a PET/CT scanner.

4.1 Routine core analysis

Basic core properties were measured experimentally on the core plugs as described in section 3.3. Porosities, permeabilities, pore volumes and dimensions for all core plugs are listed in Table 4.1 – Table 4.4.

Table 4.1 Basic properties for outcrop cores used in CO_2 and CO_2-foam experiments.

Core ID	Core Material	Length [cm]	Diameter [cm]	Porosity [%]	Pore volume [ml]	S_{wi} [%]	K_{matrix} [mD]
RIK_1	Chalk	6.21	3.84	46.2	33.22	28.7	4.27
RIK_3	Chalk	6.04	3.80	45.3	31.06	29.2	3.79
RIK_4	Chalk	5.92	3.82	45.9	31.10	30.9	3.77
RIK_7	Chalk	6.04	3.83	45.9	31.96	30.7	4.67
RIK_9	Chalk	6.25	3.79	48.3	34.07	25.2	2.94
RIK_13	Chalk	5.97	5.10	44.8	54.58	22.7	4.21
KIR_1	Chalk	5.99	3.78	46.6	31.35	30.8	4.99
KIR_4	Chalk	5.85	3.80	47.3	31.38	28.6	4.04
L_5	Limestone	7.59	4.95	23.1	33.76	22.7	23.31
RI_2	Limestone	7.31	3.75	23.3	18.83	23.0	27.23
RI_3	Limestone	7.76	3.76	23.4	20.22	25.8	21.93
RI_4	Limestone	7.21	3.76	23.1	18.50	24.3	26.95
RI_5	Limestone	7.33	3.76	22.3	18.15	24.5	20.19
RI_6	Limestone	7.150	3.770	21.3	17.01	23.6	12.64
RI_7	Limestone	7.45	3.77	22.7	18.83	25.6	19.11
RI_8	Limestone	7.598	3.772	20.9	17.72	23.8	12.20
RI_10	Limestone	7.384	3.778	23.6	19.56	23.3	21.41
L_28	Limestone	7.67	4.96	24.0	35.67	24.3	19.88
L_33	Limestone	7.05	4.97	24.9	34.01	29.4	33.55
L_14[1)]	Limestone	7.27	4.96	23.4	32.84	28.5	28.20
L_30[2)]	Limestone	7.41	3.78	22.6	18.82	24.5	-

[1)]Neutral-wet
[2)]Obtained from Anders Christoffersen (2011), no permeability information available

Table 4.2 Basic properties for reservoir carbonate cores used in tertiary CO_2 experiments.

Core ID	Core Material	Length [cm]	Diameter [cm]	Porosity [%]	Pore volume [ml]	S_{wi} [%]	K_{matrix} [mD]
RC_A	Carbonate	6.17	4.70	15.0	16.05	46.4	17.94
RC_B	Carbonate	6.56	4.73	14.1	16.25	51.7	9.14
RC_C	Carbonate	6.75	4.79	9.3	11.32	47.0	4.69
RC_D	Carbonate	6.61	4.74	10.8	12.56	74.9	2.32

Table 4.3 Basic core properties for reservoir shale cores used for permeability and saturation investigation.

Core ID	Core Material	Length [cm]	Diameter [cm]	Porosity [%]	Pore volume [ml]	S_{wi} [%]	K_{matrix} [mD]
SC_A	Shale	3.80	3.80	-	-	-	-
SC_B	Shale	3.92	3.80	-	-	-	-
SC_C	Shale	2.45	3.82	-	-	-	-

Table 4.4 Basic core properties for additional core samples.

Core ID	Core Material	Length [cm]	Diameter [cm]	Porosity [%]	PV [ml]	S_{wi} [%]	K_{matrix} [mD]
RIK_2	Chalk	6.10	3.84	45.8	32.35	15.0	3.99
RIK_6	Chalk	5.94	3.80	44.2	31.96	19.3	3.45
RIK_8	Chalk	5.650	3.820	45.2	29.25	12.8	3.55
RIK_10	Chalk	6.040	3.800	48.1	32.93	30.2	3.93
RIK_11	Chalk	6.400	5.080	48.9	63.41	28.2	4.35
RIK_12	Chalk	5.830	5.100	48.2	57.40	26.8	4.80
RIK_15	Chalk	6.080	4.950	47.8	55.96	12.4	4.56
RIK_16	Chalk	5.850	4.830	47.1	50.46	13.8	5.09
RIK_18	Chalk	6.020	5.090	47.2	57.81	27.3	5.97
RIK_20	Chalk	5.960	4.940	47.0	53.67	27.0	4.71
KIR_2	Chalk	5.93	3.80	47.5	31.91	-	4.02
KIR_5	Chalk	5.90	3.80	47.6	31.82	27.7	4.80
KIR_6	Chalk	5.89	3.79	48.8	32.44	30.9	4.82
KIR_7	Chalk	6.14	5.16	47.7	61.21	25.7	3.97
KIR_8	Chalk	6.27	5.10	48.2	61.77	26.6	4.40
KIR_9	Chalk	6.02	5.12	46.2	57.31	-	4.86
KIR_10	Chalk	6.29	5.28	45.5	62.70	-	3.99
KIR_11	Chalk	6.12	5.13	48.8	61.75	-	4.93
RI_9	Limestone	7.304	3.774	23.7	19.38	20.0	28.30
L_3	Limestone	7.581	4.981	21.4	31.56	22.7	12.48
L_8	Limestone	7.265	4.948	22.1	30.81	24.4	17.70
L_11	Limestone	7.057	4.959	23.0	31.37	-	21.12
L_12	Limestone	7.641	4.961	22.6	33.43	26.4	14.27
L_13	Limestone	8.029	4.955	21.6	33.50	26.3	12.49

Fracture permeability was only measured on two core samples and was calculated to be 643mD ± 245mD. The uncertainty is calculated by standard deviation as several measurements were conducted on each core sample. The high uncertainty is a result of: 1) low differential pressure and 2) large uncertainties in the pressure gauges.

Figure 4.1 illustrates the relationship between the measured porosity and the measured permeability for the different cores used in this thesis. The chalk cores are more homogenous, whereas Edward limestone cores and the reservoir carbonate core are more heterogeneous with respect to permeability and porosity.

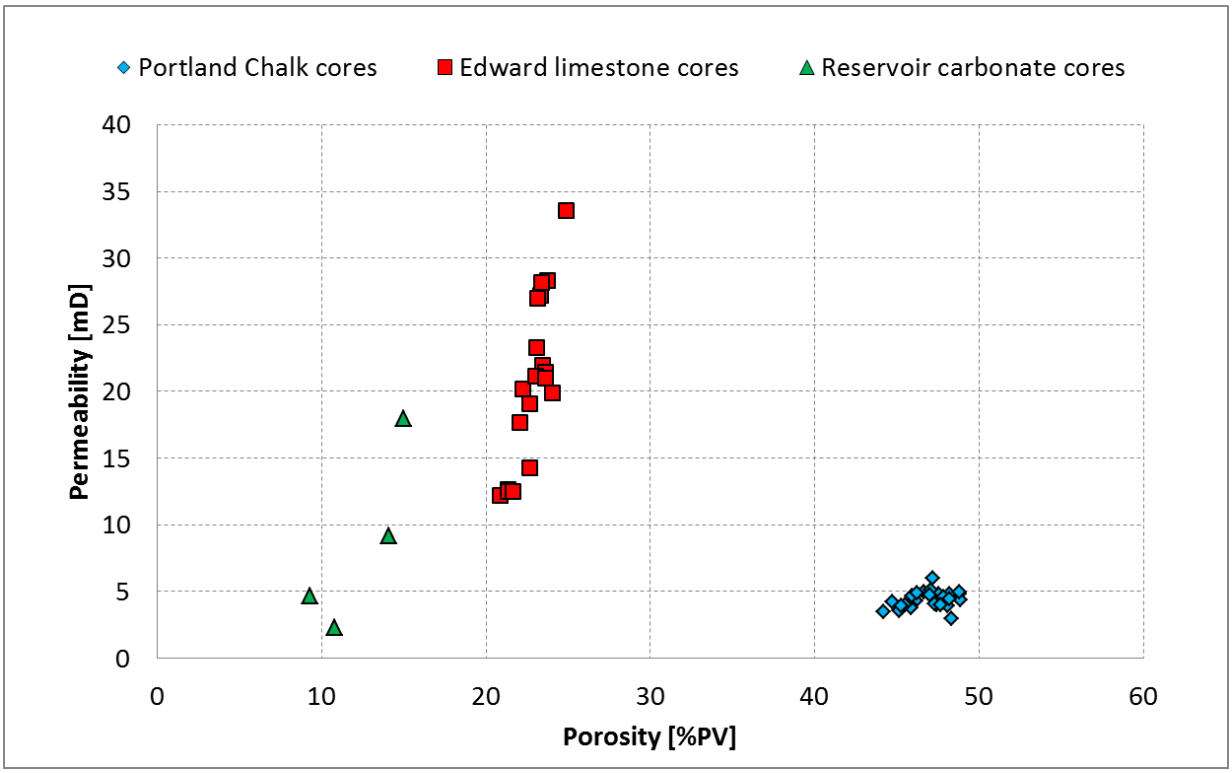

Figure 4.1 Measured permeability as a function of measured porosity for Portland chalk cores, Edward limestone cores and reservoir carbonate cores.

4.2 Experimental processes

Recovery mechanisms by CO_2 and CO_2-foam, in both liquid and supercritical state, have been studied in fractured and non-fractured core material, in addition to visual studies of rock structure and flow behavior on shale cores in a PET/CT scanner. The results will be discussed in detail in the following sub-sections, in the same sequence as it is described in the procedure in section 3.5.

4.2.1 Supercritical CO_2 injection in whole and fractured core plugs

Supercritical CO_2 experiments were conducted on outcrop carbonate cores to investigate oil recovery mechanism by CO_2 diffusion. The experimental procedure is outlined in section 3.5.1. The chalk cores were all saturated with n-Decane, and the limestone cores were saturated with refined paraffinic oil, except core plug L_5 to determine the influence of mineral oil type during oil recovery by CO_2 diffusion. All experiments were conducted above the MMP between CO_2 and mineral oil (n-Decane or refined paraffinic oil). Key numbers are listed in Table 4.5 and include the system permeabilities, K_{total}, average pore pressure, irreducible water saturations, endpoint oil saturation after CO_2 injection, $S_{or,CO2}$, and the recovery factor, R_f.

Table 4.5 Experimental conditions and results from experiments with supercritical CO_2 injection.

Core ID	Core Material	Oil	Frac	K_{total} [mD]	Avg. pressure [bar]	S_{wi} [%]	$S_{or,CO2}$ [%]	R_f [%]
RIK 1	Chalk	n-Decane	No	4.27	91.06	28.7	13.2	81.5
RIK 3	Chalk	n-Decane	Yes	3.79	91.47	29.2	22.4	68.4
RIK 9[1)]	Chalk	n-Decane	No	2.94	91.48	25.2	-	-
RIK 13	Chalk	n-Decane	No	4.21	95.18	22.7	12.4	84.0
L 5	Limestone	n-Decane	No	23.31	93.79	22.7	9.1	88.2
RI 2	Limestone	Paraffinic	No	27.23	91.29	23.0	7.9	89.8
RI 3	Limestone	Paraffinic	Yes	21.93	95.06	25.8	31.0	57.5
RI 4	Limestone	Paraffinic	No	26.95	94.68	24.3	1.9	97.5

[1)] RIK 9 was aborted because the development in oil saturation versus time cannot be used due to fluctuations in back pressure regulator during experiment.

Figure 4.2 shows the development in oil saturation as a function of pore volume of supercritical CO_2 injected and Figure 4.3 illustrates the recovery factor versus pore volumes injected. All of the whole cores, expect RI_2, obtained a recovery above 80% of OOIP after 2 PV of CO_2 injected. The outlier, core plug RI_2, had an end point residual oil saturation of 31% after 7 PV injected. The reason is unclear, but was suspected to be related to the incident that the paraffinic oil used for this experiment was not filtered in advance, and thus the polar components was still present in the oil. This experiment will therefore not be discussed any further. The end point oil saturation for the whole cores was reached after 3-5 PV injected, with a total recovery of 81.5-97.5% of OOIP. From Figure 4.2 it may look like core plugs RIK_13 and L_5 would follow the same development in oil saturation as core plug RI_4 if more CO_2 was injected.

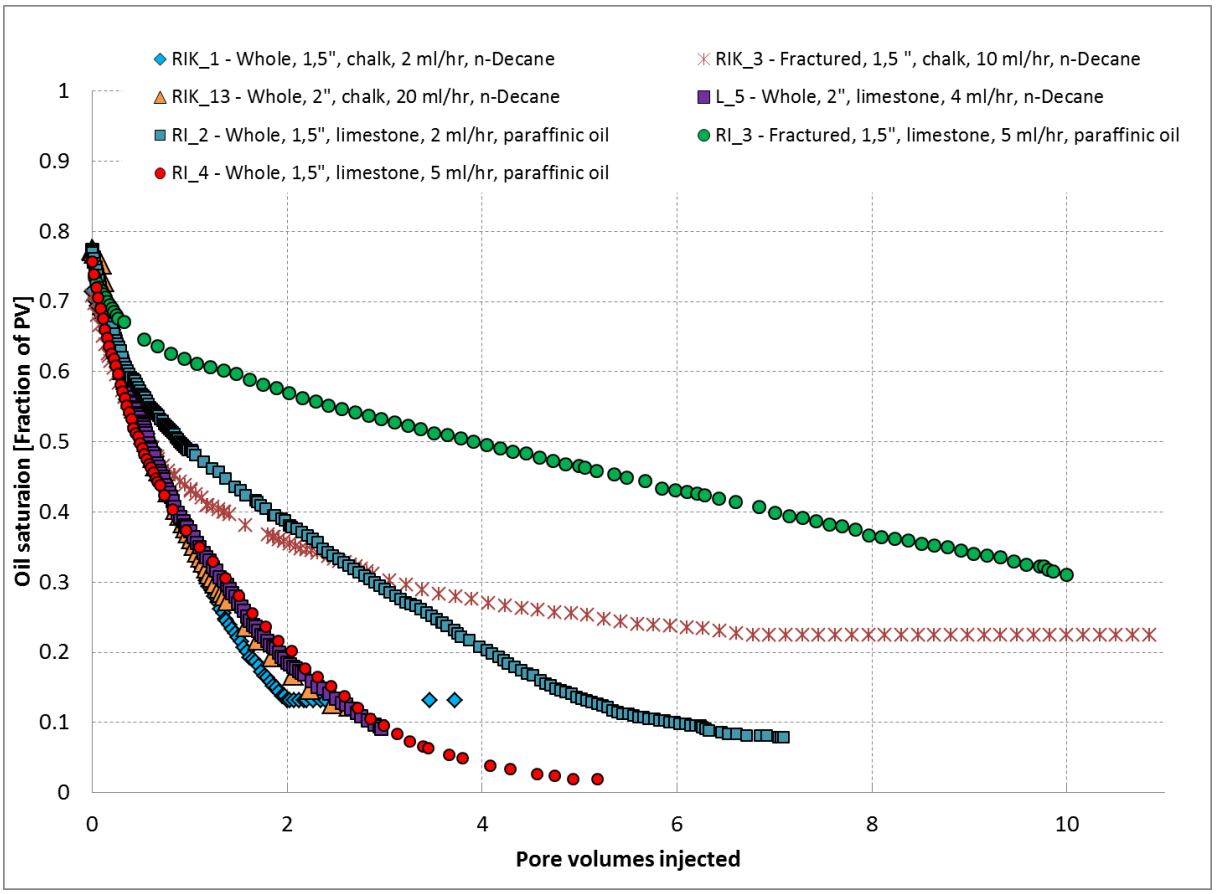

Figure 4.2 Development in oil saturation as a function of pore volume of supercritical CO_2 injected for strongly water-wet outcrop core plugs at S_{wi}.

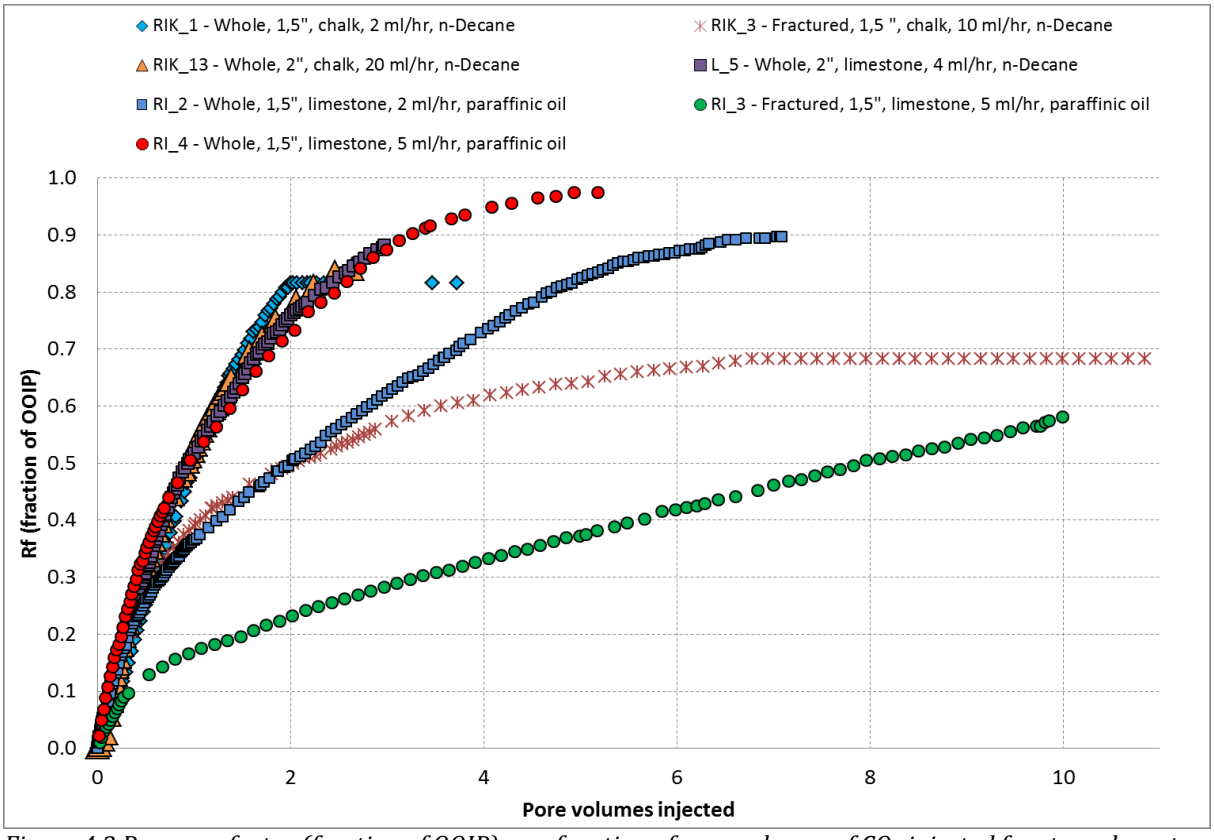

Figure 4.3 Recovery factor (fraction of OOIP) as a function of pore volumes of CO_2 injected for strongly water-wet outcrop core plugs at S_{wi}.

It was observed that the differential pressure in the whole cores was higher than for the fractured cores before CO_2 breakthrough, indicating that viscous forces have a more prominent impact on the displacement, partly stabilized by diffusion. Because of the low viscosity of CO_2 compared to n-Decane and refined paraffinic oil at experimental conditions (P = 90 and T =35 °C) one could also expect viscous fingering to occur. However, this effect is suspected to be less pronounced in these experiments, due to the small size of the system and displacement front stabilized by viscous diffusion leading to high total recoveries.

A good reproducibility between the non-fractured cores was observed, regardless of core material. The small discrepancies in oil production rate were suspected to be caused by small differences in pore pressures and core heterogeneities. The type of mineral oil did not seem to have any effect on the CO_2 injection. Comparing the n-Decane saturated core plug L_5 with the refined paraffinic oil saturated core plug RI_4, no major differences was observed, and one may conclude that both oils develop first contact miscibility and may be interchanged when study CO_2 EOR for these conditions.

Compared to the strongly water-wet whole cores, both the fractured cores (core plug RIK_3 and RI_3) only obtained a total recovery of 68.4 and 57.5 % of OOIP respectively after 7 PV of CO_2 was injected. A larger amount of CO_2 was injected in the fractured cores because diffusion was the only displacement mechanism. The fractured cores had a slower oil production rate and earlier CO_2 breakthrough than the whole cores, and collaborates with earlier work conducted at the Department of Physics and Technology (Lie, 2013). The early breakthrough of CO_2 in the fractured cores may be caused by a higher injection rate than diffusion rate through the high conductive fracture saturated with CO_2. The frontal velocity was equivalent for both fractured cores, but the oil production rate showed large discrepancies and was suspected to be caused by different core material utilized. The diffusion efficiency seemed to be more effective in the chalk core than for the limestone core for these experiments. This may be explained by smaller pore size and higher pore volume present in chalk, and thereby assume that a larger surface contact area is present in chalk. Because the efficiency of diffusion is depending on the total surface contact area of the porous media that is, the larger surface contact area the more efficient, this may explain the higher recovery by CO_2 diffusion in the chalk core compared to the limestone core.

In this work it was observed that the oil recovery for the whole cores (core plugs RIK_1, RIK_13, L_5 and R_I4) was more efficient than for the fractured cores (core plugs RIK_3 and RI_3), and corresponds to previous studies conducted at the Department of Physics and Technology (Svenningsen, 2011). In contrast, other results have shown a higher recovery from fractured

water-wet cores than for non-fractured water-wet cores (Haugen, 2012), and it has also been shown nearly identical recoveries independent of weather the cores were fractured or not (Fosse, 2012, Langlo, 2013, Ydstebø, 2013). These results indicate that no general conclusion about higher recoveries for whole cores can be made, and further investigation should be performed.

The relationship between injection rate and oil production for the whole cores showed that the core with the lowest injection rate (core plug RIK_1) has the highest oil production rate, and reached residual oil saturation first after 2 PV of CO_2 injected compare to an average of 3.5 PV for the other whole core plugs. This may be explained by the lower injection rate that may influence the recovery by a less dispersed front stabilized by viscous diffusion before breakthrough. Injection rate influence the recovery in the sense that the efficiency of diffusion is affected by the contact time, as discussed in section 1.6.1.

4.2.2 Supercritical CO_2 and CO_2-foam injection in fracture cores plugs

Six supercritical CO_2 and CO_2-foam experiments were conducted to investigate the potential of CO_2-foam in improving sweep efficiency in fractured carbonate cores. One experiment of direct foam injection (core plug KIR_1) was conducted and used as reference. The experimental procedure is outlined in section 3.5.2. All experiments were conducted above the minimum miscibility pressure between CO_2 and mineral oil (n-Decane and paraffinic oil) and equivalent frontal velocity were used for all cores samples (10ml/h for chalk cores and 5 ml/h for limestone cores). The results from the pure CO_2 injection presented in section 4.2.1 showed that the production rate in the fractured cores started to level out at approximately 1 PV injected. Based on this observation 1-2 PV of supercritical CO_2 were injected prior to the CO_2-foam injection in these experiments. A summary of end-point oil saturations and the enhanced oil recovery from the CO_2-injection and subsequent CO_2-foam injection for all experiments is listed in Table 4.6. The residual oil after primary drainage was 69% for the chalk cores and ranged between 74.4 - 75.5% for the limestone cores.

Table 4.6 Production data that include end-point oil saturations and the enhanced oil recovery from the CO_2-injection and subsequent CO_2-foam injection.

Core ID	Core Material	Oil Type	$S_{o,wi}$ [%PV]	$S_{or,\ CO2}$ [%PV]	$R_{f,\ CO2}$ [%OOIP]	$S_{or,CO2\text{-}foam}$ [%PV]	$R_{f,\ CO2,foam}$ [%OOIP]	$R_{f,\ total}$ [%OOIP]
RIK_4	Chalk	n-Decane	69.1	32.9	52.4	15.8	24.8	77.2
RIK_7	Chalk	n-Decane	69.3	32.3	53.3	16.5	22.9	76.2
KIR_1	Chalk	Paraffinic	69.2	-	-	18.1	73.8	73.8
RI_5	Limestone	Paraffinic	75.5	60.7	34.2	10.3	52.1	86.3
RI_7	Limestone	Paraffinic	74.4	54.8	26.4	15.6	52.6	79.0

Figure 4.4 shows the development in oil saturation versus pore volumes injected for experiments with CO_2 and subsequent CO_2-foam injection. The results presented in Table 4.6 and Figure 4.4 show that the subsequent CO_2-foam injection provided an additional oil recovery of 22 – 52% of OOIP and that all experiments obtained high total recoveries of 73.8-86.3% of OOIP after 6-10 PV of injection. Oil was mainly recovered by diffusion during the CO_2 injection, due to the high transmissibility of the fractures. The following CO_2-foam injection caused an additional pressure drop, and a viscous compound was added to the transport of CO_2 from the fracture to the matrix, and provided additional production, not only governed by diffusion.

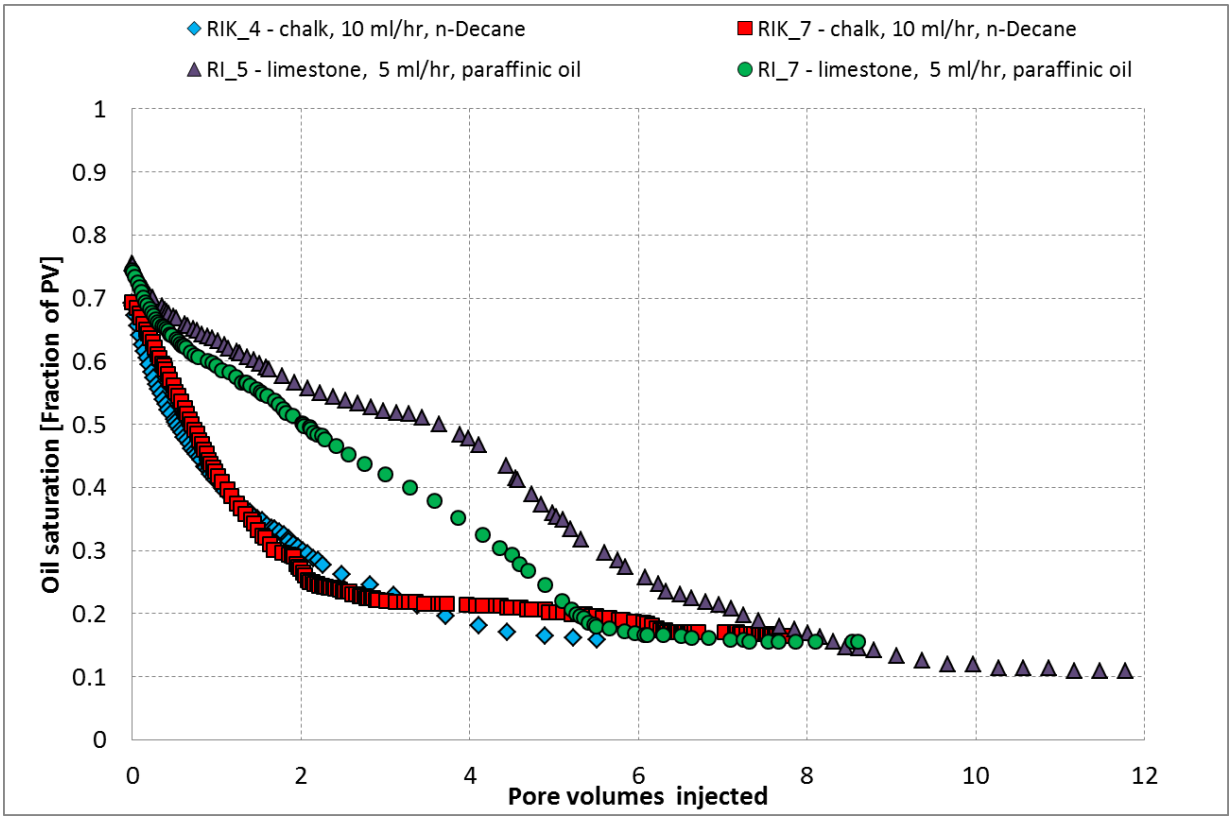

Figure 4.4 Development in oil saturation as a function of pore volumes for secondary CO_2 with subsequent CO_2-foam experiments in fractured 1.5" strongly water-wet core plugs at S_{wi}.

It is worth noticing that the pure CO_2 injection was more efficient in the chalk cores, and recovered about 20-25% more oil by diffusion compared to the limestone cores, with equivalent frontal velocity. The subsequent CO_2 foam injection was more pronounced in the limestone cores and twice the amount of oil was recovered compared to the chalk cores. Hence, the impact of the core material utilized clearly influence the oil production from the different recovery mechanism.

Figure 4.5 shows the development in oil saturation as a function of pore volumes injected for limestone core RI_7 and chalk core RIK_4. The higher differential pressure observed from the limestone core also emphasizes the conclusion that stronger foam is developed in this core, as the strength of the foam is directly related to the magnitude of the pressure drop measured along the core (Kovscek et al., 1995, Zinati et al., 2008, Zitha and Du, 2010). The finer the texture of the foam, the smaller the foam bubbles, and the pressure drop will be larger.

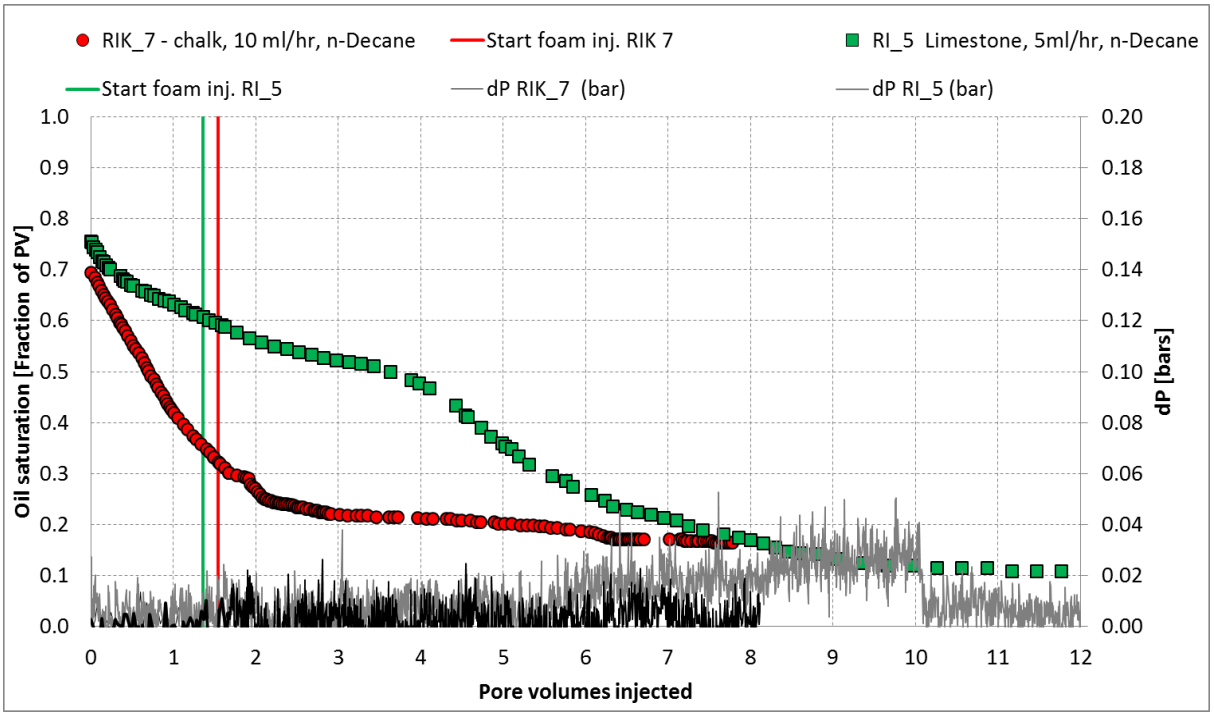

Figure 4.5 Development in oil saturation as a function of pore volumes injected to see the impact of core material between a limestone core (RI_7) and a chalk core (RIK_4).

To investigate the impact of core material in CO_2 and CO_2-foam flooding experiments, a summary of end-point oil saturations and enhanced oil recovery for chalk and limestone material are listed in Table 4.7 and Table 4.8 respectively. The tables also include experiments with pure CO_2 injection in fractured material, presented in section 4.2.1 for comparison. All experiments were conducted at same experimental conditions (P= 90 bar and T = 35 °C) and the CO_2 was in a supercritical state.

Table 4.7 End-point oil saturations and enhanced oil recoveries from CO_2-injection and/or CO_2-foam injection experiments on fractured chalk cores.

Core ID	Oil Type	$S_{o,wi}$ [%PV]	$S_{or,\ CO2}$ [%PV]	$R_{f,\ CO2}$ [%OOIP]	$S_{or,CO2\text{-}foam}$ [%PV]	$R_{f,\ CO2,foam}$ [%OOIP]	$R_{f,\ total}$ [%OOIP]
KIR _1	Paraffinic	69.2	-	-	18.1	73.8	73.8
RIK_3	n-Decane	70.8	22.4	68.4	-	-	68.4
RIK_4	n-Decane	69.1	32.9	52.4	15.8	24.8	77.2
RIK_7	n-Decane	69.3	32.3	53.3	16.5	22.9	76.2

Table 4.8 End-point saturations and enhanced oil recoveries from CO_2-injection and/or CO_2-foam injection experiments on fractured limestone cores.

Core ID	Oil Type	$S_{o,wi}$ [%PV]	$S_{or,\ CO2}$ [%PV]	$R_{f,\ CO2}$ [%OOIP]	$S_{or,CO2\text{-}foam}$ [%PV]	$R_{f,\ CO2,foam}$ [%OOIP]	$R_{f,\ total}$ [%OOIP]
RI_5	Paraffinic	24.5	60.7	34.2	10.3	52.1	86.3
RI_3	Paraffinic	25.8	31.0	57.5	-	-	57.5

Figure 4.6 shows the development in oil saturation for pure CO_2 and/or CO_2-foam injection in fractured chalk cores. The results present in Table 4.7 and Figure 4.6 show that the core samples with CO_2-foam injection provided an additional oil recovery of 5-9% of OOIP compared to pure CO_2 injection, suggesting that CO_2-foam may have had an effect on oil recovery compared to pure CO_2 injection in fractured chalk core systems. This corresponds to earlier laboratory studies conducted with CO_2-foam injection in fractured chalk cores (Zuta et al., 2009). Observations from the differential pressure during foam injection in chalk, see Figure 4.5, showed no major increase in differential pressure when foam is introduced to the system, which indicate that no foam or low quality foam have been present in the chalk cores, and make it difficult to conclude. Most likely, if one had increased the size of the system, the foam would provide a greater effect. This is because pure CO_2 injection through high permeable fracture system is governed by diffusion that depends on contact time, concentration and diffusion length. As the size of the system is increased, the efficiency of diffusion decreases. Collaborative work have been conducted to study the effect of diffusion and up-scaling and supports this assumption (Fernø et al., 2014). One may therefore conclude that at core size resolution in fractured chalk material, the foam effect will not be significant, because recovery mechanism is controlled by diffusion.

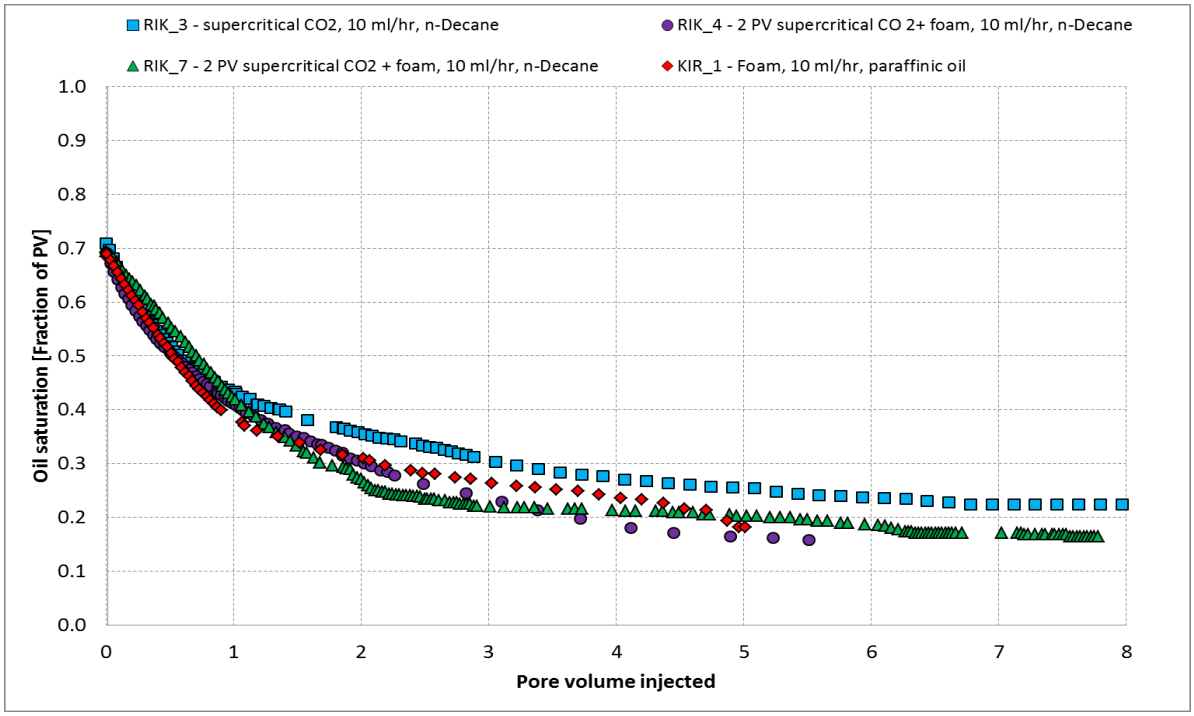

Figure 4.6 Development in oil saturation as a function of pore volumes injected for fractured 1.5" chalk core plugs at S_{wi} by different recovery mechanism.

Figure 4.7 shows the development in oil saturations for two limestone core samples: one core with secondary CO_2 injection, RI_3, and one core with secondary CO_2 injection with subsequent CO_2-foam injection, RI_5. In contrast to the chalk cores, the development in oil saturation diverged when CO_2-foam was introduced to the system, and the effect of CO_2-foam seemed to accelerate the oil production rate which was expected due to the additional pressure drop observed, as illustrated in Figure 4.5.

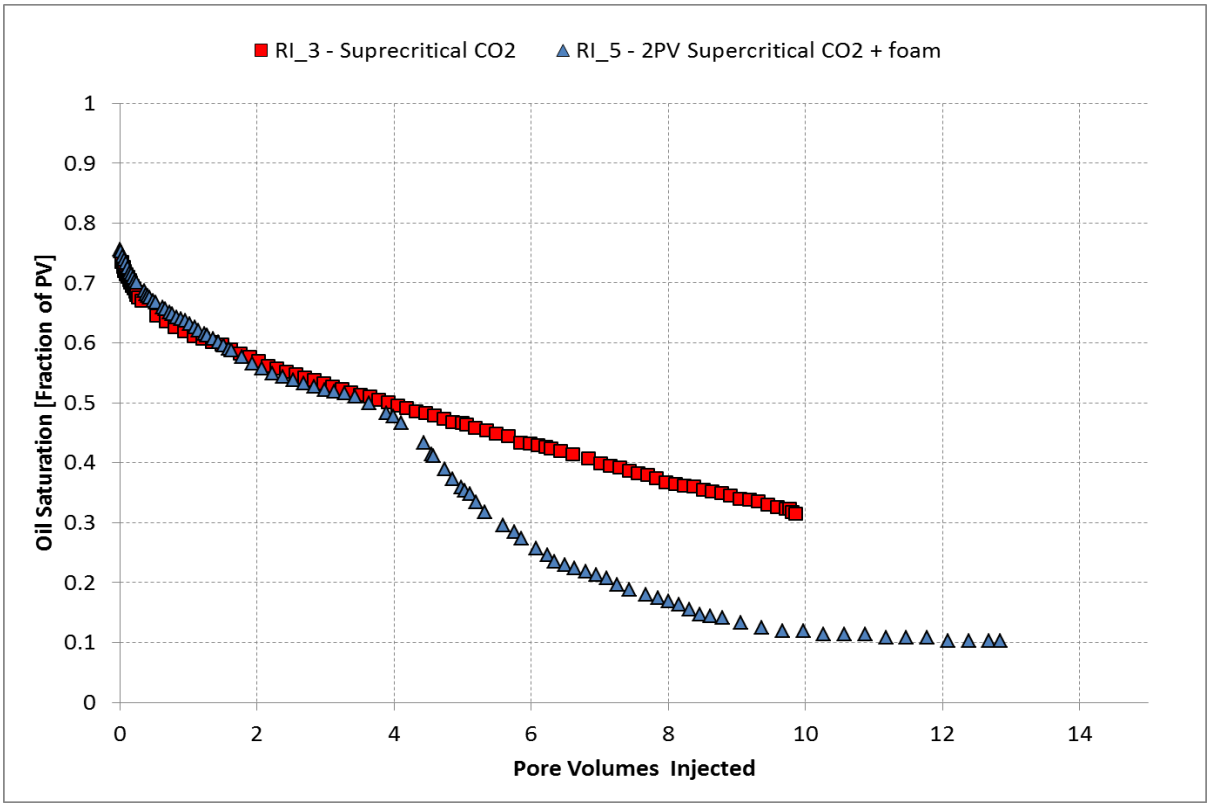

Figure 4.7 Development in oil saturation as a function of pore volumes injected for fractured 1.5" chalk core plugs saturated with refined paraffinic oil at S_{wi}, for two different recovery mechanism: secondary CO2 injection and secondary CO2 with subsequent CO2-foam injection. Injection rate of 5ml/h were used for both core plugs.

The suggested theory that recovery by CO_2 diffusion is more efficient in chalk cores and subsequent CO_2-foam injection is more effective in limestone cores are difficult to explain, as very limited information is available about CO_2-foam processes in fractured carbonate cores. Chalk material has smaller pore size and higher pore volume than limestone material, and thus one may assume that a larger surface contact area is present in chalk. As the efficiency of diffusion is depending on the total surface contact area of the porous media that is, the larger surface contact area the more efficient, this may explain the high recovery by CO_2 diffusion in chalk cores compared to limestone cores. This observation may also support the fact that CO_2-foam is more pronounced in limestone cores, suggesting that recovery performance by CO_2 in limestone is less dependent on diffusion. The prominent foam effect in the limestone cores compared to chalk cores may also be explained by the concept of disjoining pressure, as

discussed in section 2.2.2. The film rupture will be more pronounced in porous media with smaller pores due to higher disjoining pressure, and thus foam films will behave more stable in the bigger limestone pores compared to the smaller chalk pores (Hirasaki, 1991).

The production rate as a function of time for chalk core sample RIK_4 and limestone core sample RI_5 are illustrated in Figure 4.8. A significantly higher increase in production rate may be observed after foam is introduced to the system in the limestone core compared to the chalk core, and thus supports the observation mentioned above, regarding better foam effect in the limestone cores.

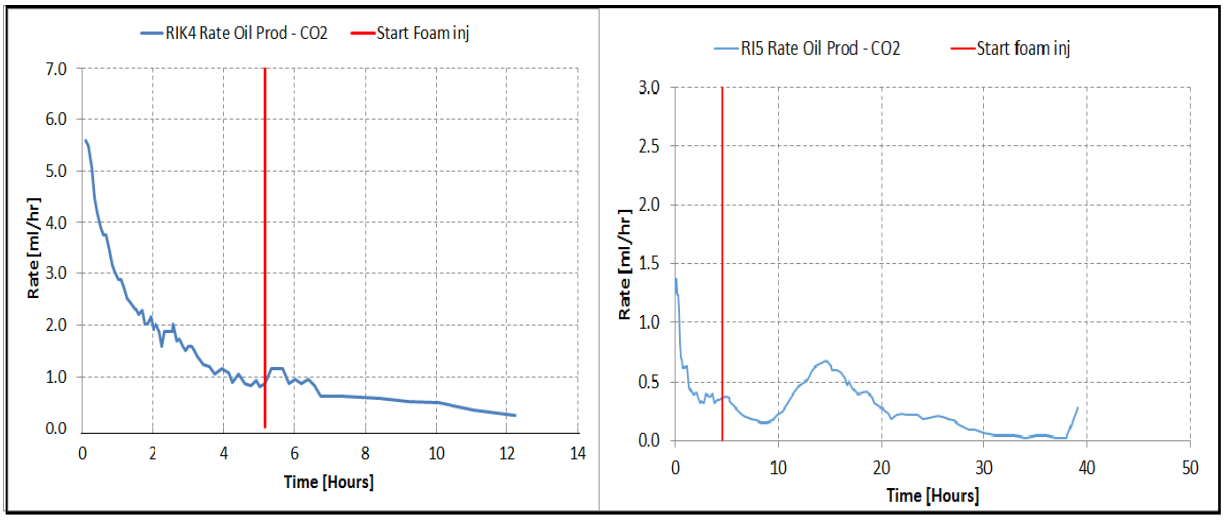

Figure 4.8 Oil production rate as a function of time (hours). The rate is an average calculation of 5 points of production data. Left: Chalk core RIK4. Right: Limestone core RI5. The injection rate is twice as high for the chalk core than for the limestone core to account for differences in porosity and achieve equal frontal velocity.

Another factor that may impact the foam stability is the influence of oil type. Because paraffinic oil consists of alkanes of higher molecular weight than n-Decane, they may be too large to be solubilized in the micelles, and the molecules may therefore have less ability to be transported out of the foam and oil seems to stabilize the foam (Vikingstad et al., 2005). However, by looking at Figure 4.6 that shows CO_2 and CO_2-foam injection in chalk cores saturated with different mineral oil, the type of oil did not seem to have affected the production. The impact of oil in presence of foam may be more pronounced when introduction longer chain alkanes to the system. The foam generation ability is also connected with surfactant concentration, but will not be discussed further as the same surfactant solutions were used in all these experiments.

4.2.3 Secondary Liquid CO_2-foam injection in whole core plugs

Three experiments were conducted with liquid CO_2-foam injection in whole carbonate cores at Texas A&M University in collaboration with Stig Langlo and Tom Ydstebø. The objective was to study recovery mechanism by CO_2-foam for mobility control at both strongly water-wet (SWW) and neutral-wet (NW) conditions. All experiments were conducted above the minimum miscibility pressure between n-Decane and CO_2 and assumed first contact miscible. The experimental procedure is described in section 3.5.3. A summary of the end-point oil saturations and the enhanced oil recovery from the liquid CO_2-foam injection is listed in Table 4.9.

Table 4.9 Production data for CO_2-foam experiments conducted at Texas A&M University.

Core ID	Wettability	$S_{o,wi}$ [%PV]	$S_{or,CO2\text{-}foam}$ [%PV]	$R_{f,\ CO2,foam}$ [%OOIP]
L_28	SWW	24	27	65
L_33	SWW	29	6	91
L_14	NW	29	1	95

Figure 4.9 shows the development in oil saturation versus pore volumes injected for the liquid CO_2-foam experiments. The neutral wet, core plug L_14 obtained the highest oil recovery of 95% of OOIP after 2.5 PV injected, despite low differential pressure during foam injection. In contrast, other observations have found oil recovery to be low during co-injection of surfactant solution and gas into fractured, oil-wet limestone samples. (Haugen et al., 2012). The high recoveries in core plug L_33 and L_14 indicate that the liquid CO_2 is fully miscible with n-Decane.

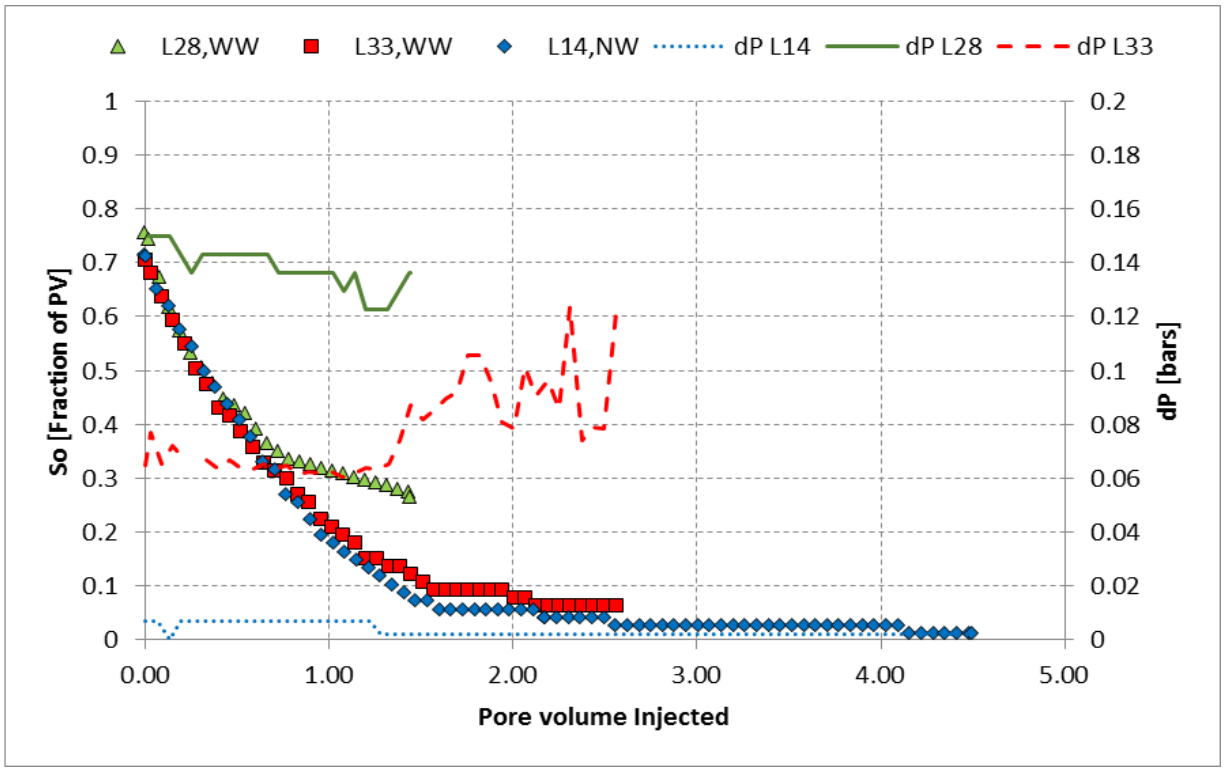

Figure 4.9 Development in oil saturation as a function of pore volumes injected for CO_2-foam experiments conducted at Texas A&M University.

The two water-wet cores (L28 and L33) have equivalent oil production rate up to approximately 0.7 PV injected, where L_28 reaches an earlier CO_2-foam breakthrough and starts to level out. Core plug L_28 obtained a total recovery of only 65% of OOIP, which is unreasonably low, and indicate that the material balance is incorrect, and will therefore not be discussed further.

The production rate of core plug L_33 is similar to L_14, despite different wettability. However, the differential pressure for the water-wet core L_33 is 1 magnitude higher than the differential pressure for the neutral wet core plug L_14, and indicate that higher foam stability is formed in this core as the strength of the foam is directly related to the magnitude of the pressure drop measured along the core (Kovscek et al., 1995, Zinati et al., 2008, Zitha and Du, 2010). The differential pressure for core plug L_33 increases as oil saturation decreases, which may be explained by reduced foam stability in the presence of oil, as discussed in section 2.2.2.

4.2.4 Tertiary CO_2 injection and CO_2 foam injection in fractured core systems

Three experiments were designed to investigate Integrated Enhanced Oil Recovery (IEOR) performance by utilizing three different injection steps; 1) waterflooding, 2) supercritical CO_2 injection and 3) CO_2-foam injection. The experimental procedure is outlined in section 3.5.4. A summary of end-point oil saturations and the enhanced oil recovery from waterflood, CO_2-injection and CO_2-foam injection for all experiments are listed in Table 4.10.

Table 4.10 Production data for tertiary CO_2 and CO_2-foam injection in fractured core systems.

Core ID	$S_{o,wi}$ [%PV]	$S_{or,water}$ [%PV]	$R_{f,water}$ [%OOIP]	$S_{or,\ CO2}$ [%PV]	$R_{f,\ CO2}$ [%OOIP]	$S_{or,CO2\text{-}foam}$ [%PV]	$R_{f,\ CO2,foam}$ [%OOIP]	$R_{f,\ total}$ [%OOIP]
AC_1	76.3	48.3	36.6	20.7	36.3	16.0	6.2	79.1
AC_2[1)]	76.5	-	-	-	-	-	-	-
AC_3	75.8	55.8	26.3	38.4	23.0	31.7	8.9	58.2
COJ2[2)]	77.9	37.2	52.2	29.9	9.4	-	-	61.6

[1)] Experiment AC_2 was aborted because of system leakage
[2)] Reference experiment by (Brautaset, 2009)

Figure 4.10 and Figure 4.11 show the development in oil saturation and the recovery factor as a function of pore volume injected for core samples AC_1 and AC_3, respectively. The vertical green line denotes start of CO_2 injection and the red line indicates start of CO_2-foam injection. Similar oil production patterns was observed for core sample AC_1 and core sample AC_3. However, the overall recoveries from the different injection steps are somewhat different. Because the matrix permeability, porosity, injection rate and S_{wi} are close to identical for the two cores, and the fractured permeability was measured to be twice as high for core sample AC_3 than for core sample AC_1, the discrepancy in oil production was suspected to be caused by heterogeneous characteristics in Edward limestone material. Previous work have also suggest a heterogeneous nature of Edward limestone rock material (Johannesen et al., 2007, Riskedal et al., 2008).

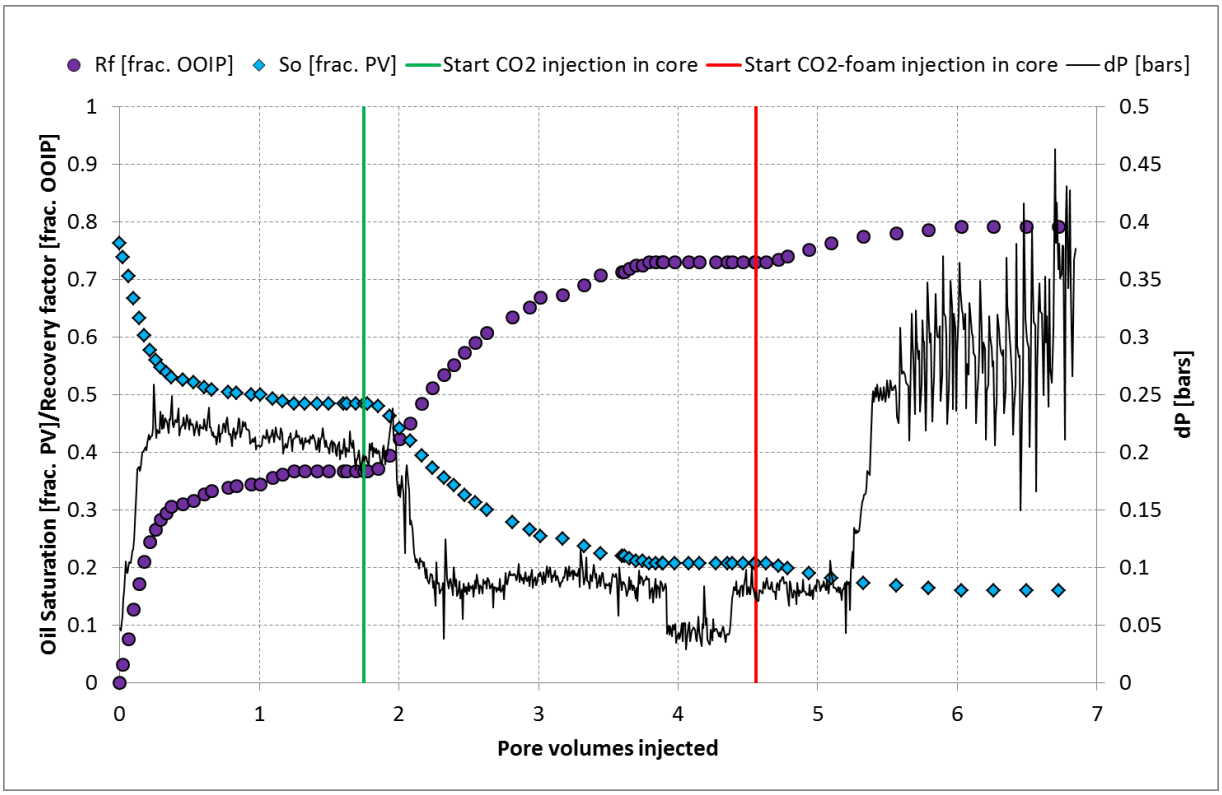

Figure 4.10 Development in oil saturation and recovery factor as a function of pore volumes injected for core sample AC_1. Start of CO_2 and CO_2-foam injection are denoted by the green and red vertical lines respectively. The sudden pressure drop towards the end of the CO_2 injection (around 4 PV injected) was caused by an unintentional temporary low CO_2 injection rate.

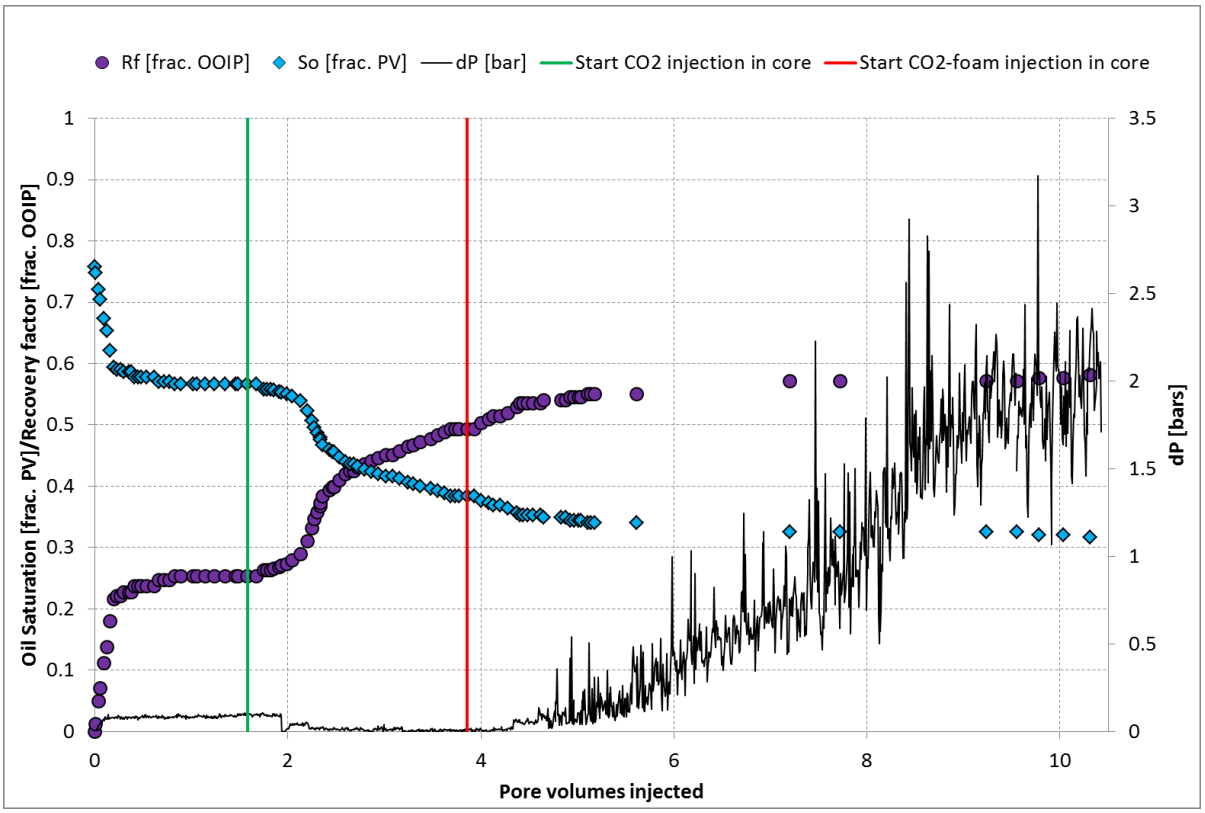

Figure 4.11 Development in oil saturation and recovery factor as a function of pore volumes injected for core sample AC3. Start of CO_2 and CO_2-foam injection are denoted by the green and red vertical lines respectively.

During water injection a rapid decrease in oil saturation was observed until water breakthrough for both experiments. Only minor oil production was contributed to the transient period after water breakthrough, as a consequence of increased water saturation in the cores that prevent oil to flow through the media due to reduced capillary forces. The oil recovered by water injection was assumed to originate from all the core pieces as the core material was strongly water wet and spontaneous imbibition was the main driving force. It has earlier been shown that there is essentially no difference in total oil recovery for a strongly water-wet block between waterfloods on whole core and a fractured core (Viksund et al., 1996, Viksund et al., 1997, Graue et al., 1999b). A total of 1.8 pore volumes of water were injected in both experiments, with recoveries of 36% and 26% of OOIP for core plug AC_1 and AC_3, respectively, and was lower than anticipated as the core materials are strongly water wet.

Subsequent injection of CO_2 caused a significant increase in production, and provided an additional 36% oil recovery in core sample AC_1 and 23% oil recovery in core sample AC_3. Most of the additional oil recovered from the CO_2 injection was believed to be attributed to the unfractured inlet core piece, due to observations presented in section 4.2.1, regarding CO_2 injection in fractured and non-fractured cores, where it was observed that CO_2 displaced nearly all the oil in the whole cores, whereas less oil was recovered in the fractured cores. However, because the total oil recovery by CO_2 was very high, some oil was assumed to be attributed to the two subsequent fractured cores. Observations from the differential pressure indicated that the displacement of oil by pure CO_2 was governed by viscous force in the beginning, and as the CO_2 reached the fracture network the differential pressure decreased and diffusion became the dominating drive mechanism. The oil production rate started to level out towards the end of CO_2-injetion in both experiments, but to a smaller degree for core sample AC_3, which may be a result of less CO_2 injected in this experiment.

The co-injection of surfactant and CO_2 through the cores resulted in a significant increase in differential pressure that indicates that foam was formed in the first whole core, forcing CO_2 from the fracture into matrix, and provided an additional oil production, mechanism not only governed by diffusion. The differential pressure is one order of magnitude higher for core sample AC_3 than for core sample AC_1, which indicate that more stable foam of higher quality is formed in this experiment, as the strength of the foam is directly related to the magnitude of the pressure drop measured (Kovscek et al., 1995, Zinati et al., 2008, Zitha and Du, 2010). It has been shown that generation of foam increase with increasing permeability (Tanzil et al., 2000), and may explain the higher foam stability in core sample AC_3, as the fractured permeability for this core was measured to be significantly higher than for core plug AC_1. The CO_2-foam

injection provided an additional recovery of 6.2% of OOIP for core sample AC_1 and a slightly higher recovery of 8.9% of OOIP for AC_3, likely caused by the stronger foam generated in the latter core. The combined total oil recovery from all injection steps was 79.1% of OOIP for core sample AC_1 and 58.2 % of OOIP for core sample AC_3.

Tertiary CO_2 injection visualized with MRI (reference experiment)

A tertiary CO_2 injection test was conducted on a strongly water-wet Portland chalk core (COJ2) and visualized in the Magnetic Resonance Imaging (MRI) at the ConocoPhillips Research Centre in Bartlesville, USA, to study local fluid flow behavior and recovery mechanism in a fractured core system and previously reported in (Brautaset, 2009). The experiment were conducted at liquid CO_2 conditions (T= 23 °C, P = 83 bar) and the CO_2 was assumed first contact miscible with the mineral oil. Core COJ2 was cut and resembled the same way as for core plug AC_1 and AC_3, as described in section 3.5.4, to obtain a fracture core system. Several factors differ from the other experiments described in this section: 1) Portland chalk cores were used, 2) CO_2 was injected at a liquid state, 3) no foam was injected after the CO_2 flooding, 4) a lower injection rate (2ml/h) was used and 5) n-Decane was used instead of paraffinic oil. The brine in COJ2 was exchanged with deuterium oxide (D_20) brine and n-Decane was injected to obtain irreducible water saturation (S_{wi}). The water signal is attenuation by D_2O infusion, and thus the MRI images only obtain signals from the oil phase.

Figure 4.12 shows the development in oil saturation as a function of pore volumes injected for core sample COJ2 compared to core sample AC_1 and AC_2. Similarities in oil saturation development were observed between core sample AC_1, AC_3 and COJ2. During the water flooding, a linear decline in oil saturation before water breakthrough was also observed for core sample COJ2, and the clean-cut after breakthrough may be explained by the strongly water-wet homogenous chalk material. The end-point oil saturation during the CO_2 injection was not established as the test was terminated prematurely, but the observed production rate was low and decreasing when the experiment was terminated at $S_{or,CO2}$ = 29.9%.

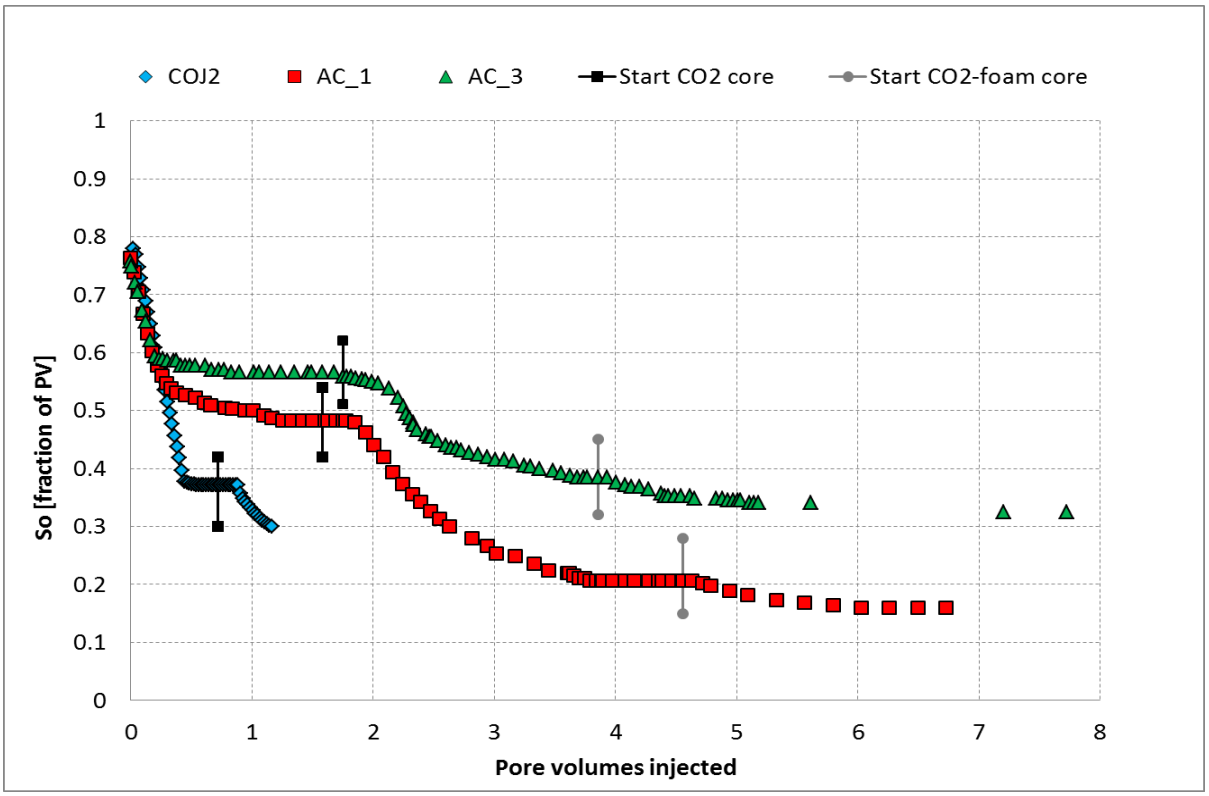

Figure 4.12 Development in oil saturation as a function of pore volumes injected for core sample COJ2 modified from (Brautaset, 2009) compared to core sample AC_1 and AC_3.

During the waterflood the MRI images, illustrated in Figure 4.13, showed capillary dominated block-by-block displacement and no recovery after the end-point for the spontaneous imbibition had been reached at 37.2% after approximately 0.4 pore volumes injected for COJ2. The total recovery by water injection was 52.2% of OOIP for core sample COJ2 and much higher than for core samples AC_1 and AC_3. The main reason for this is suspected to be caused by different core material utilized. Chalk is more homogenous (Graue et al., 1999a), whereas limestone cores tend to be very heterogeneous (Johannesen et al., 2007, Riskedal et al., 2008) and can also be observed by the discrepancies between core AC_1 and AC_3 as discussed earlier. Differences in injection rate may also have influenced the recovery by water injection as increasing the flow rate has been shown to produce a less dispersed waterfront (Lien et al., 1988).

For the subsequent CO_2 flood, a temporal increase in MRI intensity was observed locally in the inlet and middle core piece, indicating an advancing oil bank. As the CO_2 flows through the inlet core piece and reaches the fracture network, the CO_2 channels through the fracture, and only small amounts of oil is recovered from the two fractured core pieces, and thus most of the recovery was from the unfractured inlet core piece. Higher recoveries were observed from the CO_2 injection in the limestone cores than for the chalk core. This might may be caused by: 1) Less CO_2 injected in the chalk core and it was still in the transition period when the experiment ended and 2) Higher water saturation after waterflooding present in the chalk core compared to the limestone cores, and thus the effect of water shielding may be greater in this core.

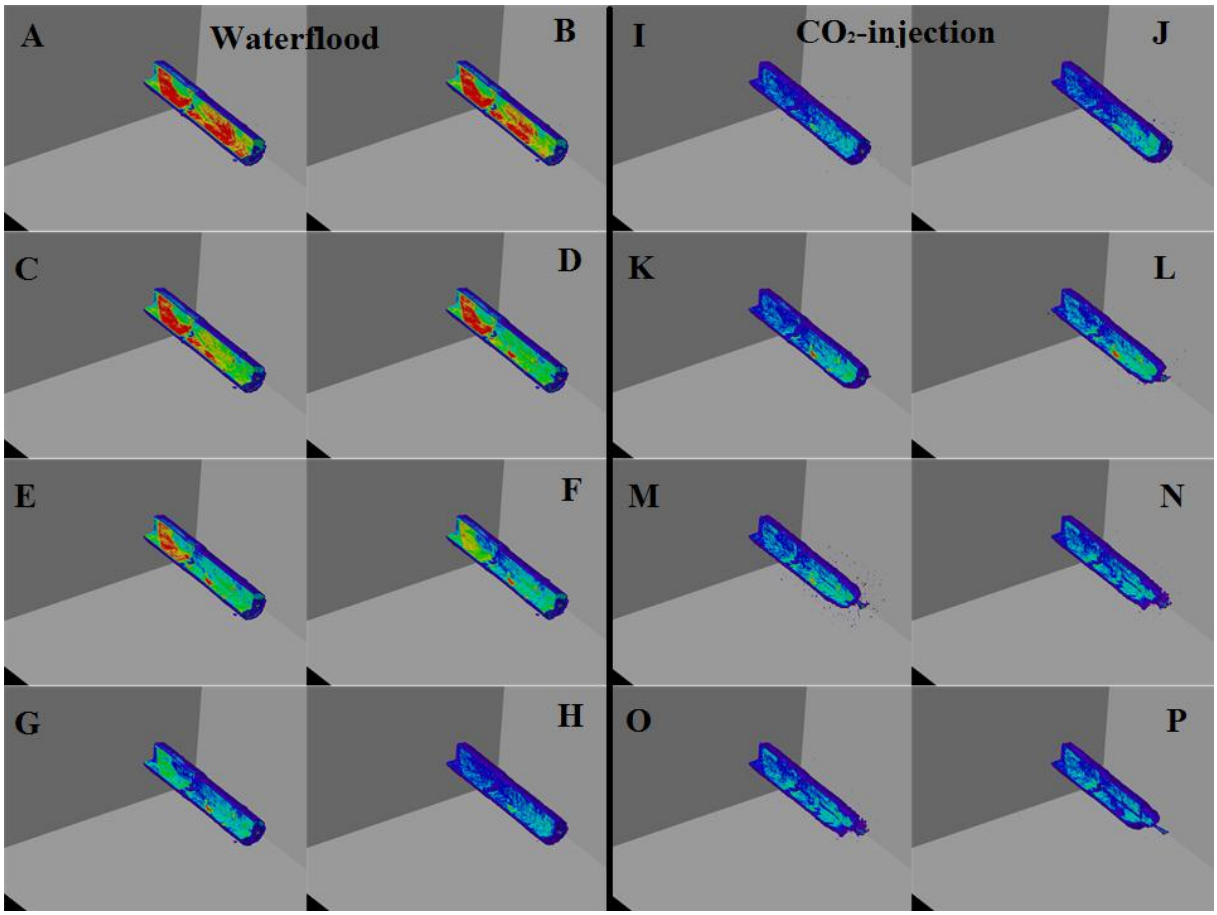

Figure 4.13 MRI image sequence from waterflooding (right) and subsequent CO_2 injection (left) in the fractured, strongly water-wet chalk core COJ2. High intensity areas (warm colors) and low intensity areas (cold colors) indicate high and low oil saturation, respectively (Brautaset, 2009).

The MRI images, see Figure 4.13, showed remaining oil in both isolated matrix blocks after CO_2-injection. For experiments conducted on core sample AC_1 and AC_3 some of this residual oil was believed to be recovered by in-situ foam generation as the effect of foam is clearly emphasized in Figure 4.12. The high pressure drop observed indicated that foam was successfully generated by co-injecting surfactant (Surfonic L24-22) and CO_2 in the whole inlet core, and additional oil was recovered by CO_2-foam injection on AC_1 and AC_3.

4.2.5 Tertiary CO_2 injection in reservoir carbonate cores

Four experiments were designed to investigate oil recovery by tertiary supercritical CO_2 injection in reservoir carbonate rocks. The experimental procedure is outlined in section 3.5.5. For these experiments CO_2 and crude oil are assumed multi-contact miscible as explained in section 1.2. End-point oil saturations and oil recovery from waterflood and CO_2 injection for all experiments are listed in Table 4.11.

Table 4.11 Production data from tertiary CO2 injection in reservoir carbonate cores.

Core ID	$S_{o,wi}$ [%PV]	$S_{or,water}$ [%PV]	$R_{f,water}$ [%OOIP]	$S_{or,\ CO2}$ [%PV]	$R_{f,\ CO2}$ [%OOIP]	$R_{f,\ total}$ [%OOIP]
RC_A	53.6	42.1	21.5	4.0	70.9	92.4
RC_B	48.3	39.7	17.8	4.0	73.9	91.7
RC_C	53.9	29.6	45.1	6.6	42.6	87.7
RC_D	25.1	19.1	23.8	0.8	73	96.8

The results from the tertiary CO_2 experiments conducted in reservoir carbonate cores showed a major potential of a subsequent CO_2 injection in previously waterflooded core systems. Figure 4.14 shows the recovery factor as a function of pore volumes injected for the reservoir carbonate cores. It was observed that tertiary CO_2 injection in whole reservoir carbonate cores at water-wet conditions show similar behavior with respect to development oil production, and a clean water breakthrough was observed for all core samples. The data obtain from these floods at reservoir temperature and pressure, indicate that the CO_2 will be multi-contact miscible with the crude oil, which means that miscibility by CO_2 is generated through multiple-contact equilibrium in which CO_2 is progressively enriched with intermediates from the oil (Rathmell et al., 1971). The overall total recoveries are high for all the reservoir core samples, and in the range 87-96% of OOIP, and are similar to the mineral oil displacement by CO_2 at first contact miscible conditions presented in section 4.2.1. Previous work has shown that extracting hydrocarbons from crude oil by CO_2 in a miscible (first or multiple-contact) displacement promotes a displacement efficiency approaching 100% on core scale (Holm and Josendal, 1974, Haugen, 2012).

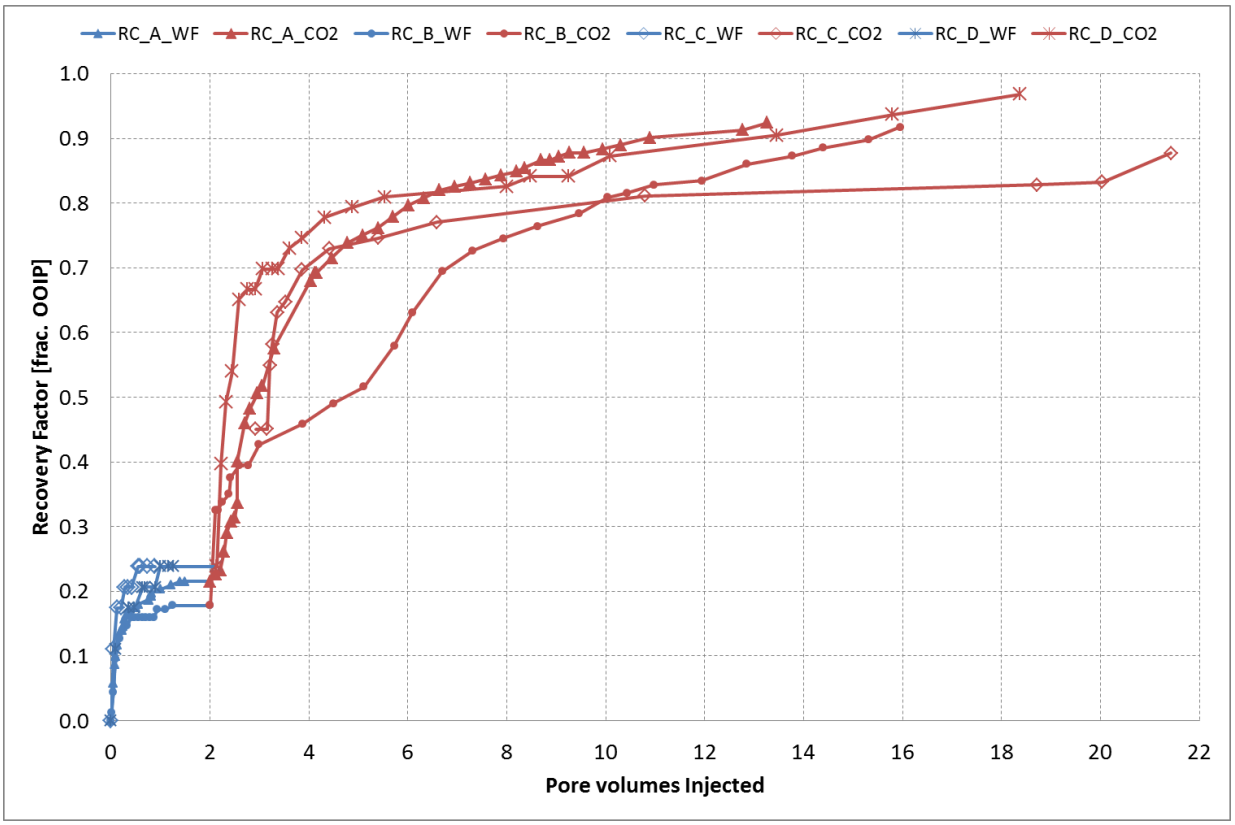

Figure 4.14 Recovery factor as a function of pore volumes injected for tertiary supercritical CO_2 injection in reservoir carbonate cores.

Core sample RC_A, RC_B and RC_D obtained oil recoveries of approximately 20% of OOIP by waterflooding, whereas core sample RC_C obtained a higher oil recovery of 45% of OOIP from the water injection. During the following CO_2 injection a small increase in the differential pressure was observed before CO_2 breakthrough, indicating that viscous force governs the displacement. A significant increase in oil production by CO_2 injection was attained for all core samples. For core sample RC_A, RC_B and RC_D the CO_2 injection provided an additional recovery above 70% of OOIP. The high recovery by CO_2 may be caused by CO_2 dissolving into the water phase, which again depends on the partial pressure of CO_2, brine composition and temperature. It have been reported observations that dissolution of carbonates at reservoir conditions during co- injection of CO_2 and brine increase porosity and permeability whereas deposition of carbonates indicated reduction of porosity and permeability (Grigg and Svec, 2003). Dissolution of CO_2 may cause oil to swell up to 50-60% and thereby increases the contact area between the oil and CO_2 in which increase diffusion rate and recovery efficiency for the supercritical CO_2 injection (Moortgat et al., 2011). Swelling of the oil is also more dominant in crude oils with heavier components than in mineral oil (n-Decane and paraffinic oil).

Core sample RC_C obtained a higher oil recovery from the waterflood, and the lowest oil recovery from the following CO_2 injection. This may be partly caused by the high water saturation obtained prior to the CO_2 injection, and thus, the effect of water shielding may have

greater influence for this core. It has been found that the presence of water reduces the amount of CO_2 available for mixing with the hydrocarbon phase (Pollack et al., 1988). This effect increases with increasing pressure and amount of aqueous phase whereas it decreases with increasing water salinity or temperature (Wiebe and Gaddy, 1940).

A large uncertainty in this experiment is the recording in the beginning of the production by CO_2 injection, as a result of crude oil in contact with CO_2 causing the extraction of heavier hydrocarbons and viscous crude oil is produced firstly.

4.2.6 Reservoir shale rock experiments

Several experiments have been conducted on three shale core samples (SC_A, SC_B, SC_C), from a shale reservoir in the USA to developed a "best practice" to measure permeability using CO_2 and re-saturate unpreserved reservoir shale core plugs with crude oil. A PET/CT scanner was used to evaluate shale rock structure and flow behavior during CO_2 injections. The experimental procedure is described in section 3.5.6.

Permeability Measurements

Permeability measurements by supercritical and liquid CO_2 injection was performed on core sample SC_B and SC_C, and additional information of fluid flow behavior was obtained in the PET/CT scanner at HUS on core sample SC_B by tracing the CO_2 marked with radioactive ^{11}C. Experiments conducted on core sample SC_A was aborted because of leaks from confinement pressure. The average effective permeability results from the tests are listed in Table 4.12, and include the net confinement pressure and the uncertainty in the permeability measurements given by standard deviation.

Table 4.12 Experimental conditions and results from permeability measurements.

Core ID	CO_2 state	Temperature T [°C]	Pore and net confinement pressure [bar]	Average effective permeability, k [µD]
SC_B	Liquid	27	160 / 40	902 ± 74
			160 / 80	671 ± 32
SC_B	Supercritical	80	165 / 35	498 ± 80
			165 / 85	508
SC_B	Supercritical	115	150 / 50	218 ± 55
			150 / 100	142 ± 25
			200 / 50	156 ± 39
			200 / 100	133 ± 18
SC_C	Supercritical	80	200 / 100	0.38

Observations showed that temperature and net confinement pressure have a large impact on the effective permeability. An increase of net confinement pressure results in a decrease of the effective permeability, and is reasonable as it make it harder for the CO_2 to escape around the core sample. Increasing the temperature caused the effective permeability to decrease.

The summary table exhibits large variation in permeability measurements for core sample SC_B, and is suspected to be caused by a phase change of the CO_2 state, as viscosities of supercritical fluids are subjected to change when pressure or temperature varies. This is what may have happened during the experiment conducted in a heating cabinet (CO_2 at supercritical state), where constant outlet pressure was maintained using retracting pump, located at room temperature outside the heating cabinet (CO_2 at liquid state). The higher discrepancy in the first experiment conducted at 80 °C is suspected to be caused by the fact that a Back Pressure Regulator (BPR) was used at the outlet, and might have caused instabilities in the outlet flow.

Figure 4.15 illustrates the various pressures measured (outlet, inlet and differential pressure) and the injection rate as a function of time for core sample SC_B at 80 °C. When varying the injection rate, the outlet pressure remains stable, whereas the inlet pressure increases, and thus a higher differential pressure is observed, and indicates that the core sample is very tight and has a low permeability. One may also notice that by increasing the pressure more pressure fluctuations are observed, and is likely due to the back pressure regulator used in this experiment.

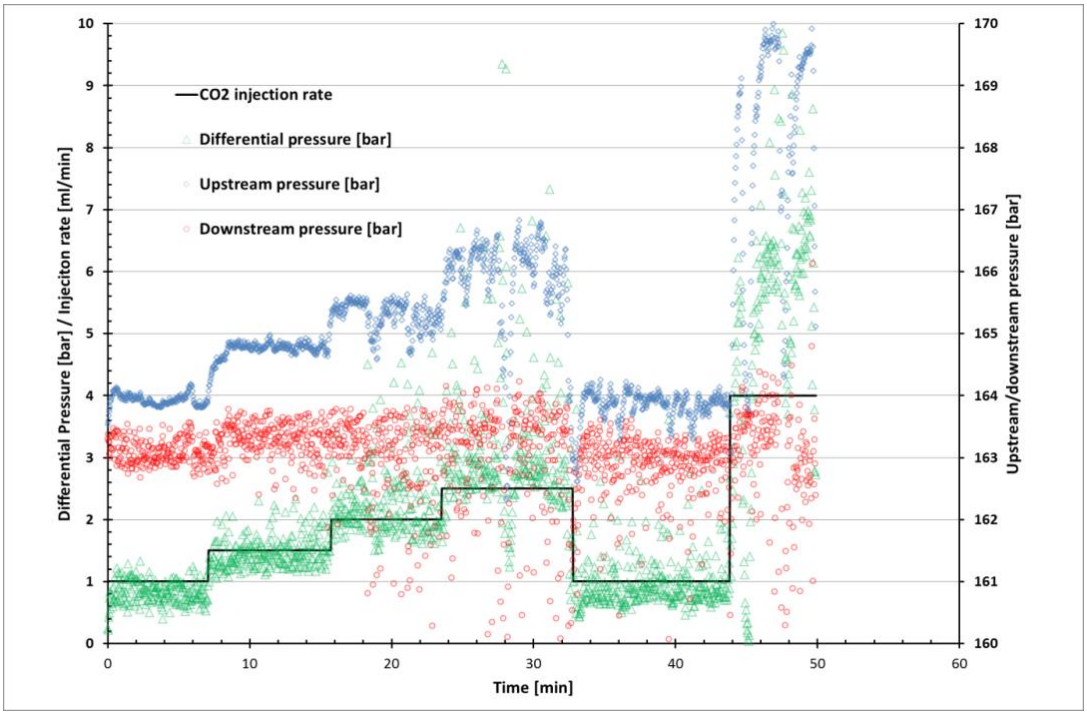

Figure 4.15 Various pressures measured and injection rate as a function of time, for shale core sample SC_B at 80 °C.

The images obtained from the PET/CT scan, see Figure 4.16, showed that the injected CO_2 may have escaped around the core sample, between the core and the aluminum foil protection, because of the consolidated nature of the shale matrix, and adds an uncertainty to all the effective permeabilities measured. Further experiment was conducted on core sample SC_C at 80 °C, without aluminum foil to investigate if this could improve CO_2 flow through the core. Observation showed a significantly lower effective permeability of 0.38 µD and is more realistic compared to unconventional reservoirs that usually have permeability in the range of 0.1-10µD (CSUR, 2014).

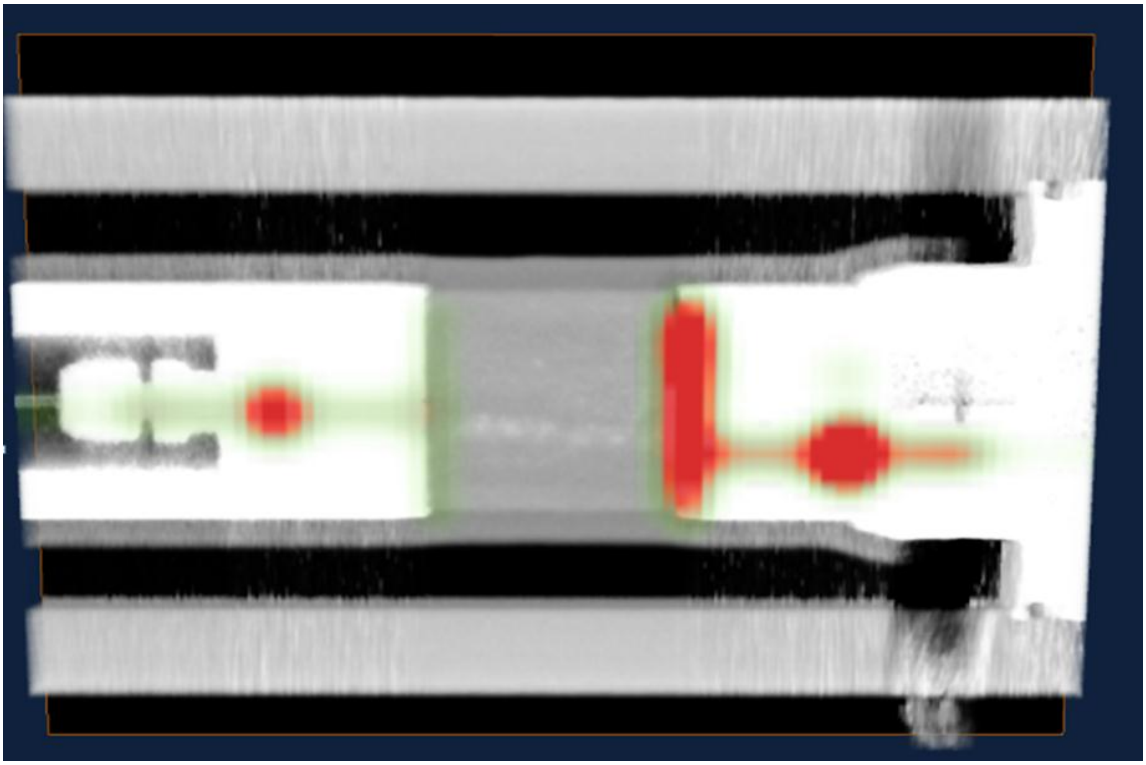

Figure 4.16 Image obtained from the PET/CT scan after 5 minutes of CO_2 injection from right. Light grey box in the middle denotes the core sample and warm (red) color denotes the labeled CO_2 phase. Initially, the CO_2 phase was not present on the left side of the core, but after short time of injection, CO_2 is observed on the outlet side, suggesting CO_2 to have escaped around the core sample.

Rock structure

Dry scan of all the core samples, SC_A, SC_B and SC_C, was also conducted in the CT scanner and the images obtained are illustrated in Figure 4.17. A layered structure was observed in core sample SC_A and SC_B, whereas a more heterogeneous structure was observed from core sample SC_C. One reason for this could be that the core samples are taken from different parts of the reservoir.

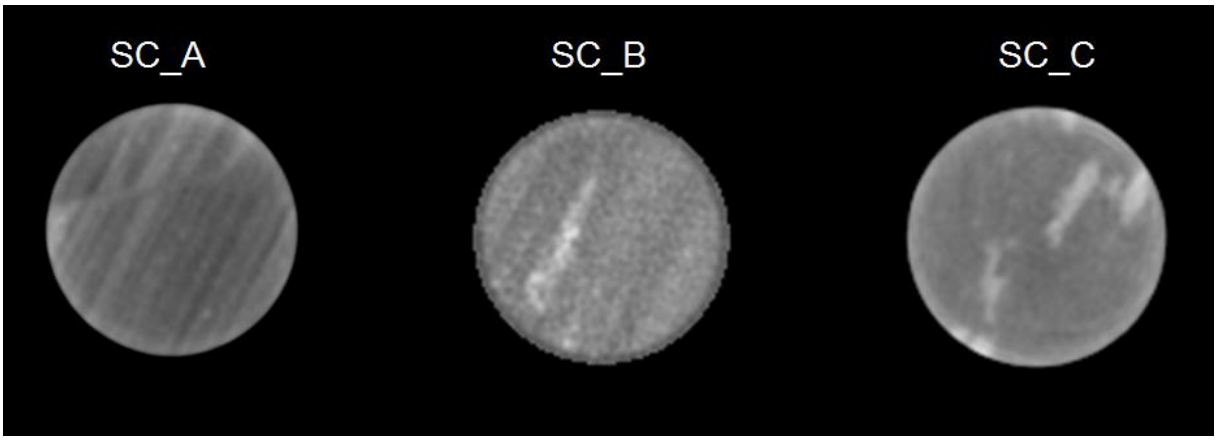

Figure 4.17 Dry scan of SC_A, SC_B and SC_C. Suggesting a layered structure for core sample SC_A and SC_B and a more heterogeneous structure for core sample SC_C. The images are based on CT-values obtained from the scan and are vertical sliced from top left to the right. Darker areas indicate lower density, whereas lighter areas indicate higher density.

Best Practice for saturation shale cores

An investigation of a best practice for re-saturating reservoir shale cores was conducted on the two unpreserved core samples SC_A and SC_B. The two different methods that have been studied include: 1) dynamic method, by flowing crude oil through the core and 2) static method, by soaking the cores in crude oil under pressure. The oil saturation was calculated by:

$$S_o = \frac{m_s - m_d}{V_{bulk} \cdot \rho_o \cdot \varphi} \quad (4.1)$$

where S_o is the oil saturation, m_d and m_s before and after saturation respectively, V_{bulk} is the bulk volume, ρ_o is the density of the oil and φ is the porosity.

The results from the saturation methods are listed in Table 4.13. The average porosity of unconventional shale reservoirs ,~5% (CSUR, 2014), was used to calculate the oil saturation, in addition to weight of dry and saturated core. Properties of the crude oil are listed in Table 3.1.

Table 4.13 Results from the two saturations methods conducted on core samples SC_A and SC_B.

Core ID	Saturation[%PV] (Dynamic method)	Saturation[%PV] (Static method)	Total saturation [PV%]
SC_A	65.2 ± 33	9.0 ± 33	74.2 ± 33
SC_B	71.1 ± 33	7.6 ± 33	78.7 ± 33

The results from the dynamic saturation method provided an oil saturation of 65.2 % for shale core SC_A and 71.1% for shale core SC_B. The uncertainties are calculated to be 33% and the high uncertainty in the porosity is the main contribution to this large number. The static method provided an additional increase in oil saturation of 9.0 and 7.6 % of core sample SC_A and SC_B respectively. It is worth noticing that approximately the same saturation percentage was obtained for both the dynamic and static method, and may indicate that the core structure is similar for the two cores, which was shown from the CT-scan illustrated in Figure 4.17.

4.2.7 Uncertainties related to experiments

Uncertainties related to the experimental tests performed in this thesis may be discussed in two categories that include: 1) experimental uncertainties and 2) uncertainties in experimental equipment. Generally, the experimental uncertainties are greater than the uncertainties in the instruments.

Experimental uncertainties

There are two main sources to the experimental uncertainties, and include limitations and simplification of the experimental procedure and uncontrolled changes to the environment.

Several assumption have been made during the experiments, such as supposing 100% water saturated core in the porosity measurements, neglecting gravity force by aligning the core holder horizontal, and assumed miscibility between CO_2 and oil , which all may have influenced the experimental results to some degree.

Uncertainties related to changes in environment may be electrical noise, leaks and air in the system as well as thermal variation in the system. For experiments where CO_2 is in a supercritical state, the system may be more exposed to leakage as the CO_2 is in gas phase. Such leaks are difficult to detect. For most experiments conducted in this thesis the back pressure regulator and injection pumps were located outside the heating cabinet, and thus thermal variation may have caused fluctuation of the CO_2 phase, and adds an uncertainty to the results. To minimize the experimental uncertainties, it is necessary to reproduce experiments for more reliable results.

Uncertainties in experimental equipment

All the instruments used in the experimental work, such as pumps, pressure gauges and calipers, have uncertainties related to them. The errors related to the injection rate for the pumps are ± 5% and for the pressure gauges (ESI) the uncertainty is ±0.25% of 250 bar (full scale). The calipers have an uncertainty of 0.002mm and the weight error is ±0.002g. The equations used to calculate the uncertainties in permeability, porosity, pore volume etc. are given in Appendix A.

Figure 4.17 shows the recovery factor as a function of pore volumes injected for one of the supercritical CO_2 experiments (RIK_3), and contains error bars. Uncertainties related to oil recovery includes error in pore volume calculations before and after fracturing, production uncertainties, such as production recordings, and uncertainties regarding amount of pore volume of CO_2 injected, which again include errors in injection rate from the pumps and accurate measurement of the dead volume in addition to influence of thermal variation in the system.

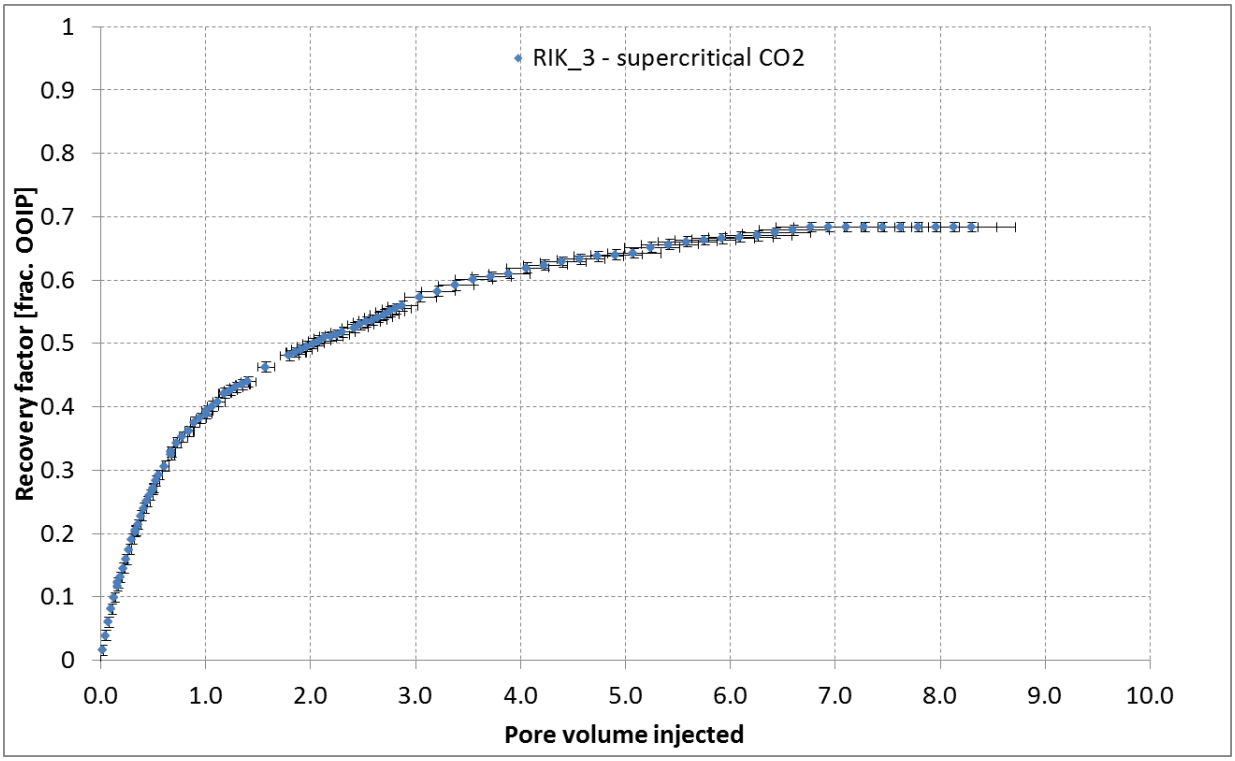

Figure 4.17 Oil recovery as a function of pore volumes injected including error bars for supercritical CO_2 injection in core sample RIK_3.

-

5 Concluding remarks

5.1 Conclusion

Based on the experimental study on CO_2 injection for EOR in fractured and whole core plugs the following key observations were made:

- High recoveries in the range of 81.5 – 89.9 % of OOIP were observed by secondary CO_2 injection for the whole cores and lower recoveries in the range of 57.5 – 68.4 % of OOIP were observed in the fractured cores.
- Less amount of CO_2 was required to reach end point oil saturation in the whole cores than for the fractured cores as diffusion is the only recovery mechanism in fractured cores.
- Supercritical CO_2 injection in fractured chalk cores were more efficient than in fractured limestone cores, with equivalent frontal velocity, because the larger surface contact area in chalk increased the efficiency of diffusion.
- In fractured limestone cores the CO_2-foam injected accelerated oil recovery compared with pure CO_2 injection by a significant increase in differential pressure and thus increased apparent viscosity. No such effect was observed in the chalk cores, and may be related to differences in pore characteristics although no clear conclusions have been drawn in this study. The presence of oil had a detrimental effect on foam.
- For the tertiary CO_2 and CO_2-foam experiments in fractured core systems, foam was successfully generated in-situ in the first whole inlet core. Lower recoveries from the water flood were observed in the limestone fracture system compared to the reference experiments (Brautaset, 2009) performed on a fractured chalk system, whereas higher recoveries where observed from the CO_2-injection in the limestone cores.
- Tertiary CO_2 experiments conducted on reservoir carbonate cores showed a major potential of a subsequent CO_2 injection in previously waterflooded core systems. Most cores obtain a recovery of 21.5 -23.8% of OOIP during the waterflood, and more than 70% of OOIP was recovered from the subsequent CO_2-flood. High total oil recoveries in the range of 87.7 - 96.8 % of OOIP were achieved for all core samples.
- When minimizing the undesired bypass of injected CO_2 , a reasonable permeability measurement of 0.38 µD was achieved for the semi-preserved shale sample SC_C
- A “best practice” for re-saturation the reservoir shale cores with crude oil was established using high pressure and temperature.

5.2 Future work

- Additional experiments should be performed with secondary CO_2 injection on whole and fractured cores before a general conclusion about higher recoveries can be made.
- Secondary CO_2 experiments should be performed at various initial water saturations for further investigation of how the presence of water affects the recoveries.
- In future experiments, equipment such as injection/retracting pumps and Back Pressure Regulator should preferentially be at experimental conditions to avoid volume fluctuations of CO_2 and to improve flow control.
- Additional experiments should be conducted to investigate the impact of core material in the presence of foam as limited information is available.
- As Edward limestone cores are very heterogeneous, further experiments should be conducted by limiting the variation of parameters to better single out different effects that impact recovery.
- To study the effect of CO_2-foam by the impact of oil type, additional experiments should be conducted by exchanging mineral oil with different types of crude oil.
- Further investigation of in-situ foam generation in both chalk and limestone material should be performed.
- Investigate how different types of surfactant solutions impact the foam quality.
- Up-scaling experiments should be implemented to study recovery mechanism of CO_2 and CO_2-foam toward more realistic field scale.
- Apply different visualization techniques like MRI or PET/CT to image CO_2 and CO_2-foam injection in water and oil saturated whole and fractured cores to better understand flow behavior.
- It would be interesting to study more realistic and torturous fracture networks, in both the laboratory and by imaging techniques.
- For permeability measurements on tights shale cores it may be possible to use noble gas instead of CO_2 as it will not damage the sleeve and thus it will not be necessary to wrap the cores in aluminum foil.
- Inject CO_2 in the re-saturated shale core sample to investigate recovery performance.
- The impact of wettability should be studied in similar systems.

6 Nomenclature

EOR	Enhanced Oil Recovery
IEOR	Improved Enhanced Oil Recovery
IFT	Interfacial tension
NCS	Norwegian Continental Shelf
CCS	Carbon capture and sequestration
CCUS	Carbon capture, utilization and sequestration
MMP	Minimum miscibility pressure
OOIP	Original Oil In Place
MRF	Mobility reduction factor
PET	Positron Emission Tomography
CT	Computed Tomography
MRI	Magnetic Resonance Image
PV	Pore volume
R_f	Recovery factor
Q	Fluid flow rate
μ	Fluid viscosity
A	Cross sectional area of the core sample
L	Sample length
Δp	Differential pressure across the core sample
K	Absolute permeability
$k_{r,i}$	Relative permeability of a fluid i
S_i	Fluid saturation of a fluid i
S_{wi}	Irreducible water saturation
V_p	Pore volume
V_b	Bulk volume
D_e	The effective diffusion coefficient
D_a	The absolute diffusion coefficient
ϕ	Porosity
θ	Wettability
m	Cementation factor
σ	Interfacial tension or stress
λ_i	Mobility of phase i
M	Mobility ratio
f_g	gas fractional flow
P_c	Capillary pressure
Π	Disjoining pressure

7 References

ABRISHAMI, Y. & HATAMIAN, H. 1996. Phase Behaviour of Fluids in Multiple Contact Processes with CO2, N2 and their Mixture. *In:* ENGINEERS, S. O. P. (ed.) *Abu Dhabi International Petroleum Exhibition and Conference, 13-16 October.* Abu Dhabi, United Arab Emirates: Society of Petroleum Engineers.

ADMINISTRATION, U. S. E. I. 2014. Annual Energy Outlook 2014 with projection to 2040. EIA.

ALVAREZ, J. M., RIVAS, H. J. & ROSSEN, W. R. 1999. Unified Model for Steady-State Foam Behavior at High and Low Foam Qualities. *SPE Annual Technical Conference and Exhibition, 3-6 October,.* Houston, Texas: Society of Petroleum Engineers.

AMOTT, E. 1959. Observations Relating to the Wettability of Porous Rock. Society of Petroleum Engineers.

ANDERSON, W. 1986a. Wettability Literature Survey- Part 2: Wettability Measurement. *Journal of Petroleum Technology,* 38**,** 1246 - 1262.

ANDERSON, W. G. 1986b. Wettability Literature Survey- Part 1: Rock/Oil/Brine Interactions and the Effects of Core Handling on Wettability. *Journal of Petroleum Technology,* 38**,** 1125 - 1144.

ANDERSON, W. G. 1987. Wettability Literature Survey- Part 4: Effects of Wettability on Capillary Pressure. *Journal of Petroleum Technology,* 39**,** 1283 - 1300.

ARDÈVOL, L. & GUTMANIS, J. 2008. Pyrenees Hold Clues to Fractured Carbonate Reservoirs. *GEO ExPro*.

ASPENES, E., GRAUE, A. & RAMSDAL, J. 2003. In situ wettability distribution and wetting stability in outcrop chalk aged in crude oil. *Journal of Petroleum Science and Engineering,* 39**,** 337-350.

BERNARD, G. G. & HOLM, L. W. 1964. Effect of Foam on Permeability of Porous Media to Gas. *Society of Petroleum Engineers Journal,* 4**,** 267 - 274.

BERNARD, G. G. & JACOBS, W. L. 1965. Effect of Foam on Trapped Gas Saturation and on Permeability of Porous Media to Water. *Society of Petroleum Engineers Journal,* 5**,** 295 - 300.

BIKERMAN, J. J. 1973. *Foams,* New York, Springer-Verlag

BIRD, R. B., STEWART, W. E. & LIGHTFOOT, E. N. 1976. *Transport Phenomena,* Wiley, New York.

BIRKEDAL, K. A. 2013. *Empirical and Numerical Evaluation of Mechanisms in Gas Production from CH4-Hydrates.* PhD, University of Bergen.

BOUD, D. C. & HOLBROOK, O. C. 1958. Gas drive oil recovery process. U.S.A.: Google Patents.

BRATTON, T., CANH, D. V., VAN QUE, N., DUC, N. V., GILLESPIE, P., HUNT, D., LI, B., MARCINEW, R., RAY, S. & MONTARON, B. 2006. The nature of naturally fractured reservoirs. *Oilfield Review,* 18**,** 4-23.

BRAUTASET, A. 2009. *In situ fluid dynamics and CO2 injection in porous rock.* PhD, University of Bergen.

BRITANNICA, E. 2014. *Shale* [Online]. Encyclopaedia Britannica. Available: http://www.britannica.com/EBchecked/topic/538082/shale.

BROCK, W. R. & BRYAN, L. A. 1989. Summary Results of CO2 EOR Field Tests, 1972-1987. *In:* ENGINEERS, S. O. P. (ed.) *Low Permeability Reservoirs Symposium, 6-8 March.* Denver, Colorado Society of Petroleum Engineers.

BROWNLEE, M. H. & SUGG, L. A. 1987. East Vacuum Grayburg-San Andres Unit CO2 Injection Project: Development and Results to Date. *In:* ENGINEERS, S. O. P. (ed.) *SPE Annual Technical Conference and Exhibition, 27-30 September.* Dallas, Texas: Society of Petroleum Engineers.

CAMPBELL, B. T. & ORR, F. M., JR. 1985. Flow Visualization for CO2/Crude-Oil Displacements. *Society of Petroleum Engineers Journal,* 25**,** 665 - 678.

CHERRY, S. & DAHLBOM, M. 2006. PET: Physics, Instrumentation, and Scanners. *In:* PHELPS, M. E. (ed.) *PET.* New York: Springer

CHI, S. M., MORSI, B. I., KLINZING, G. E. & CHIANG, S. H. 1988. Study of interfacial properties in the liquid CO2-water-coal system. *Energy Fuels 2***,** 141-145.

CHRISTIANSEN, R. L. & HAINES, H. K. 1987. Rapid Measurement of Minimum Miscibility Pressure With the Rising-Bubble Apparatus. *SPE Reservoir Engineering,* 2**,** 523 - 527.

COUNCIL, N. R. 2010. *Advancing the Science of Climate Change,* Washington, DC, The National Academies Press.
CRAIG, F. F. 1971. *The reservoir engineering aspects of waterflooding*, H. L. Doherty Memorial Fund of AIME.
CRAWFORD, H. R., NEILL, G. H., BUCY, B. J. & CRAWFORD, P. B. 1963. Carbon Dioxide - A Multipurpose Additive for Effective Well Stimulation. *Journal of Petroleum Technology*.
CSUR, C. S. F. U. R. 2014. Understanding Tight Oil. *CSUR, Canadian Society for Unconventional Resources*.
DA SILVA, F. V. & BELERY, P. 1989. Molecular Diffusion in Naturally Fractured Reservoirs: A Decisive Recovery Mechanism. *In:* ENGINEERS, S. O. P. (ed.) *SPE Annual Technical Conference and Exhibition, 8-11 October.* San Antonio, Texas Society of Petroleum Engineers.
DONALDSON, E. C., THOMAS, R. D. & LORENZ, P. B. 1969. Wettability Determination and Its Effect on Recovery Efficiency. *Society of Petroleum Engineers Journal,* 9**,** 13 - 20.
DOWNS, H. H., HOOVER, P. D., BORCHARDT, J. K. & YEN, T. F. 1989. Oil Field Chemistry: Enhanced Oil Recovery and Production Simulation. *American Chemical Society*.
ELSHARKAWY, A. M., POETTMANN, F. H. & CHRISTIANSEN, R. L. 1992. Measuring Minimum Miscibility Pressure: Slim-Tube or Rising-Bubble Method. *In:* ENGINEERS, S. O. P. (ed.) *SPE/DOE Enhanced Oil Recovery Symposium, 22-24 April.* Tulsa, Oklahoma: Society of Petroleum Engineers.
ENICK, R. M., OLSEN, D. K., AMMER, J. R. & SCHULLER, W. 2012. Mobility and Conformance Control for CO2 EOR via Thickeners, Foams, and Gels - A Literature Review of 40 Years of Research and Pilot Tests. *In:* ENGINEERS, S. O. P. (ed.) *SPE Improved Oil Recovery Symposium, 14-18 April.* Tulsa, Oklahoma, USA Society of Petroleum Engineers.
ERSLAND, G. 2008. *Studies of flow mechanisms and hydrate phase transitions in fractured rocks.* PhD, University of Bergen.
EXEROWA, D. & KRUGLYAKOV, P. M. 1997. *Foam and Foam Films: Theory, Experiment, Application*, Elsevier Science.
FARAJZADEH, R., ANDRIANOV, A., BRUINING, H. & ZITHA, P. L. 2009. Comparative Study of CO2 and N2 Foams in Porous Media at Low and High Pressure− Temperatures. *Industrial & Engineering Chemistry Research,* 48**,** 4542-4552.
FARAJZADEH, R., ANDRIANOV, A., KRASTEV, R., HIRASAKI, G. J. & ROSSEN, W. R. 2012. Foam–oil interaction in porous media: Implications for foam assisted enhanced oil recovery. *Advances in Colloid and Interface Science,* 183–184**,** 1-13.
FERNØ, M., BULL, Ø., SUKKA, P. & GRAUE, A. 2009. Capillary Pressures by Fluid Saturation Profile Measurements During Centrifuge Rotation. *Transport in Porous Media,* 80**,** 253-267.
FERNØ, M. A., EIDE, Ø., AHMED, A., AHMED, K. & GRAUE, A. 2014. Enhanced Oil Recovery and Foam Mobility Control Fractured Rocks manuscript in preparation. *Manuscript in preparation*.
FOSSE, E. 2012. *Et Eksperimentelt Studie av CO2-injeksjon for Oljeutvinning i Kalk.* MSc, University of Bergen.
FREUND, P. Progress in Understanding the Potential Role Of CO2 storage. Fifth International Conference on Greenhouse Gas Control Technologies, 2000. Greenhouse Gas Control Technologies.
FRIED, A. N. 1961. Foam-drive process for increasing the recovery of oil. Washington D.C.: UNT Digital Library.
GARDNER, J. W., ORR, F. M. & PATEL, P. D. 1981. The Effect of Phase Behavior on CO2-Flood Displacement Efficiency. *Journal of Petroleum Technology,* 33**,** 2067 - 2081.
GCCSI. 2014. *Sleipner CO2 Injection* [Online]. Global CCS Institute. Available: http://www.globalccsinstitute.com/project/sleipner%C2%A0co2-injection.
GOLF-RACHT, T. D. V. 1982a. Chapter 9 Fluid Displacement Process in A Single Matrix Block. *In:* GOLF-RACHT, T. D. V. (ed.) *Developments in Petroleum Science.* Elsevier.
GOLF-RACHT, T. D. V. 1982b. Chapter 10 Production Mechanism of A Fractured Reservoir. *In:* GOLF-RACHT, T. D. V. (ed.) *Developments in Petroleum Science.* Elsevier.

GRAUE, A., ASPENES, E., BOGNØ, T., MOE, R. W. & RAMSDAL, J. 2002. Alteration of wettability and wettability heterogeneity. *Journal of Petroleum Science and Engineering,* 33**,** 3-17.

GRAUE, A., VIKSUND, B. G. & BALDWIN, B. A. 1999a. Reproducible Wettability Alteration of Low-Permeable Outcrop Chalk. *SPE Reservoir Evaluation & Engineering,* 2**,** 134 - 140.

GRAUE, A., VIKSUND, B. G., BALDWIN, B. A. & SPINLER, E. 1999b. Large Scale Imaging of Impacts of Wettability on Oil Recovery in Fractured Chalk. *In:* ENGINEERS, S. O. P. (ed.) *SPE Annual Technical Conference and Exhibition, 5-8 October.* San Antonio, Texas: Society of Petroleum Engineers.

GRAUE, D. J. & BLEVINS, T. R. 1978. Sacroc Tertiary CO2 Pilot Project. *SPE Symposium on Improved Methods of Oil Recovery, 16-17 April.* Tulsa, Oklahoma Society of Petroleum Engineers.

GRIGG, R. B. & SVEC, R. K. 2003. Co-injected CO2-brine interactions with Indiana Limestone. *In:* ANALYSTS, S. O. C. (ed.) *International Symposium of the Society of Core Analysts.* Pau, France: New Mexico Petroleum Recovery Research Center.

GROGAN, A. T. & PINCZEWSKI, W. V. 1987. The Role of Molecular Diffusion Processes in Tertiary CO2 Flooding. *Journal of Petroleum Technology,* 39**,** 591 - 602.

HAND, J. L. & PINCZEWSKI, W. V. 1990. Interpretation of Swelling/Extraction Tests. *SPE Reservoir Engineering,* 5**,** 595 - 600.

HAUGEN, M. 2012. *CO2 injection in Fractured Chalk for Enhanced Oil Recovery.* MSc, University of Bergen.

HAUGEN, Å., FERNØ, M. A., GRAUE, A. & BERTIN, H. J. 2012. Experimental study of foam flow in fractured oil-wet limestone for enhanced oil recovery. *SPE Reservoir Evaluation & Engineering,* 15**,** 218-228.

HIRASAKI, G. J. 1991. Wettability: Fundamentals and Surface Forces. *SPE Formation Evaluation,* 6**,** 217 - 226.

HIRASAKI, G. J. & LAWSON, J. B. 1985. Mechanisms of Foam Flow in Porous Media: Apparent Viscosity in Smooth Capillaries. *Society of Petroleum Engineers Journal,* 25**,** 176 - 190.

HOLM, L. 1968. The mechanism of gas and liquid flow through porous media in the presence of foam. *Old SPE Journal,* 8**,** 359-369.

HOLM, L. W. 1986. Miscibility and Miscible Displacement. *Journal of Petroleum Technology,* 38**,** 817 - 818.

HOLM, L. W. & JOSENDAL, V. A. 1974. Mechanisms of Oil Displacement By Carbon Dioxide. *Journal of Petroleum Technology,* 26**,** 1427 - 1438.

HUANG, D. D., NIKOLOV, A. & WASAN, D. T. 1986. Foams: basic properties with application to porous media. *Langmuir,* 2**,** 672-677.

INSTITUTE, E. 2010. *Good Plant Design and Operation for Onshore Carbon Capture Installations and Onshore Pipelines: A Recommended Practice Guidance Document*, Energy Institute.

JAKOBY, B. W., BERCIER, Y., WATSON, C. C., RAPPOPORT, V., YOUNG, J., BENDRIEM, B. & TOWNSEND, D. W. Physical Performance and Clinical Workflow of a new LSO HI-REZ PET/CT Scanner. Nuclear Science Symposium Conference Record, Oct. 29 2006-Nov. 1 2006 2006. IEEE, 3130-3134.

JENSEN, J. A. & FRIEDMANN, F. 1987. Physical and Chemical Effects of an Oil Phase on the Propagation of Foam in Porous Media. *SPE California Regional Meeting, 8-10 April, Ventura, California.* Society of Petroleum Engineers.

JHA, R. K., BRYANT, S. & LAKE, L. W. 2011. Effect of Diffusion on Dispersion. *SPE Journal,* 16**,** 65 - 77.

JOHANNESEN, E., RISKEDAL, H., TIPURA, L., HOWARD, J. & GRAUE, A. Wettability characterization by NMR T2 measurements in Edwards limestone rock. International Symposium of the Society of Core Analysts, 10-13 September 2007, Calgary, Canada, 2007.

KATZ, M. L. 1980. Outlook For Enchanced Recovery Operations In The 80's. *Annual Meeting Papers, Division of Production, 13-16 April.* Dallas, Texas: American Petroleum Institute.

KETCHAM, R. A. & CARLSON, W. D. 2001. Acquisition, optimization and interpretation of X-ray computed tomographic imagery: applications to the geosciences. *Computers & Geosciences,* 27**,** 381-400.

KHATIB, Z. I., HIRASAKI, G. J. & FALLS, A. H. 1988. Effects of Capillary Pressure on Coalescence and Phase Mobilities in Foams Flowing Through Porous Media. *SPE Reservoir Engineering,* 3**,** 919-926.

KLEPPE, J. & MORSE, R. A. 1974. Oil Production from Fractured Reservoirs by Water Displacement. *In:* ENGINEERS, S. O. P. (ed.) *Fall Meeting of the Society of Petroleum Engineers of AIME, 6-9 October.* Houston, Texas Society of Petroleum Engineers.

KOLB, G. E. 1964. *Several Parameters Affecting the Foam-Drive Process for the Removal of Water from Consolidated Porous Media*, Pennsylvania State University.

KOVAL, E. J. 1963. A Method for Predicting the Performance of Unstable Miscible Displacement in Heterogeneous Media. *Society of Petroleum Engineers Journal,* 3**,** 145 - 154.

KOVSCEK, A. R. & BERTIN, H. J. 2002. Estimation of Foam Mobility in Heterogeneous Porous Media. *In:* ENGINEERS, S. O. P. (ed.) *SPE/DOE Improved Oil Recovery Symposium, 13-17 April.* Tulsa, Oklahoma: Society of Petroleum Engineers.

KOVSCEK, A. R., PATZEK, T. W. & RADKE, C. J. 1995. A mechanistic population balance model for transient and steady-state foam flow in Boise sandstone. *Chemical Engineering Science,* 50**,** 3783-3799.

KOVSCEK, A. R. & RADKE, C. J. 1996. Gas bubble snap-off under pressure-driven flow in constricted noncircular capillaries. *Colloids and Surfaces A: Physicochemical and Engineering Aspects,* 117**,** 55-76.

LAKE, L. W. 1989. *Enhanced Oil Recovery,* University of California, Prentice Hall Incorporated.

LANGLO, S. 2013. *Enhanced Oil Recovery by CO2 and CO2-foam Injection in Fractured Limestone Rocks.* MSc, University of Bergen.

LIE, M. 1995. *Evaluering av dagbruddsbergarter som analoger til kalksteinsreservoarer i Nordsjøen.* MSc, Univeristy of Bergen.

LIE, S. H. 2013. *Diffusion as an Oil Recovery Mechanism During CO2 Injection in Fractured Reservoirs.* MSc, University of Bergen.

LIEN, J. R., GRAUE, A. & KOLLTVEIT, K. 1988. A nuclear imaging technique for studying multiphase flow in a porous medium at oil reservoir conditions. *Nuclear Instruments and Methods in Physics Research Section A: Accelerators, Spectrometers, Detectors and Associated Equipment,* 271**,** 693-700.

LIU, E., PAYNE, M. A., XU, S., BAECHLE, G. & HARRIS, C. E. 2009. Carbonate Rock Physics Issues. *International Petroleum Technology Conference, 7-9 December.* Doha, Qatar: International Petroleum Technology Conference.

MANNHARDT, K., NOVOSAD, J. & SCHRAMM, L. Foam/oil interactions at reservoir conditions. *In:* ENGINEERS, S. O. P., ed. SPE/DOE Improved Oil Recovery Symposium, 19-22 April, 1998 Tulsa, Oklahoma Society of Petroleum Engineers, 287-300.

MATHIASSEN, O. M. 2003. CO2 as Injection Gas for Enhanced Oil Recovery and Estimation of the Potential on the Norwegian Continental Shelf. Norwegian University of Science and Technology.

MOORTGAT, J., SUN, S. & FIROOZABADI, A. 2011. Compositional modeling of three-phase flow with gravity using higher-order finite element methods. *Water Resources Research,* 47**,** 5511.

MORROW, N. R. 1990. Wettability and Its Effect on Oil Recovery. *Journal of Petroleum Technology*.

MORROW, N. R. & BUCKLEY, J. 2006. Wettability and Oil Recovery by Imbibition and Viscous Displacement from Fractured and Heterogeneous Carbonates. Wyoming: University of Wyoming.

NASIR, F. M. & AMIRUDDIN, N. A. 2008. Miscible CO2 Injection: Sensitivity to Fluid Properties. *In:* ENGINEERS, S. O. P. (ed.) *SPE Asia Pacific Oil and Gas Conference and Exhibition, 20-22 October.* Perth, Australia Society of Petroleum Engineers.

NASRABADI, H., FIROOZABADI, A. & AHMED, T. K. 2009. Complex Flow and Composition Path in CO2 Injection Schemes from Density Effects in 2 and 3D. *In:* ENGINEERS, S. O. P. (ed.) *SPE Annual Technical Conference and Exhibition, 4-7 October.* New Orleans, Louisiana Society of Petroleum Engineers.

NELSON, R. A. 2001. *Geologic analysis of naturally fractured reservoirs.,* Woburn, Gulf Professional Publishing.
NGUYEN, D. N. 2003. Carbon Dioxide Geological Sequestration: Technical and Economic Reviews. *In:* ENGINEERS, S. O. P. (ed.) *SPE/EPA/DOE Exploration and Production Environmental Conference, 10-12 March.* San Antonio, Texas Society of Petroleum Engineers.
ORR, F. M. 2007. *Theory of gas injection processes*, Tie-Line Publications.
ORR, F. M. & TABER, J. J. 1983. Displacement of Oil by Carbon Dioxide: Annual Report for the Period October 1981-September 1982. New Mexico Energy Research and Development Institute, United States. Department of Energy.
OSTERLOH, W. T. & JANTE JR., M. J. 1992. Effects of Gas and Liquid Velocity on Steady-State Foam Flow at High Temperature. *In:* ENGINEERS, S. O. P. (ed.) *SPE/DOE Enhanced Oil Recovery Symposium, 22-24 April.* Tulsa, Oklahoma: Society of Petroleum Engineers
PERKINS, T. K. & JOHNSTON, O. C. 1963. A Review of Diffusion and Dispersion in Porous Media. *Society of Petroleum Engineers Journal,* 3**,** 70 - 84.
PLUG, W.-J., MAZUMDER, S. & BRUINING, J. 2008. Capillary Pressure and Wettability Behavior of CO2 Sequestration in Coal at Elevated Pressures. *SPE Journal,* 13**,** 455 - 464.
POLLACK, N. R., ENICK, R. M., MANGONE, D. J. & MORSI, B. I. 1988. Effect of an Aqueous Phase on CO2/Tetradecane and CO2/Maljamar-Crude-Oil Systems. *SPE Reservoir Engineering,* 3**,** 533 - 541.
RAO, D. N. & LEE, J. I. 2003. Determination of gas–oil miscibility conditions by interfacial tension measurements. *Journal of Colloid and Interface Science,* 262**,** 474-482.
RATHMELL, J. J., STALKUP, F. I. & HASSINGER, R. C. 1971. A Laboratory Investigation of Miscible Displacement by Carbon Dioxide. *In:* ENGINEERS, S. O. P. (ed.) *Fall Meeting of the Society of Petroleum Engineers of AIME, 3-6 October.* New Orleans, Louisiana Society of Petroleum Engineers.
RISKEDAL, H., TIPURA, L., HOWARD, J. & GRAUE, A. NMR monitoring of spontaneous brine imbibition in carbonates. International Symposium of the Society of Core Analysts, 2008 Abu Dhabi, UAE. Society of Core Analysts.
ROSSEN, W. R. & VAN DUIJN, C. J. 2004. Gravity segregation in steady-state horizontal flow in homogeneous reservoirs. *Journal of Petroleum Science and Engineering,* 43**,** 99-111.
SAHIMI, M. 2012. *Flow and transport in porous media and fractured rock: from classical methods to modern approaches*, John Wiley & Sons.
SANDERS, A., JONES, R. M., RABIE, A., PUTRA, E., LINROTH, M. A. & NGUYEN, Q. P. 2012. Implementation of a CO2 Foam Pilot Study in the SACROC Field: Performance Evaluation. *In:* ENGINEERS, S. O. P. (ed.) *SPE Annual Technical Conference and Exhibition, 8-10 October.* San Antonio, Texas, USA Society of Petroleum Engineers.
SCHLUMBERGER. 2014. *Carbonate Rock Properties* [Online]. www.slb.com: Schlumberger. Available: http://www.slb.com/services/technical_challenges/carbonates/near_wellbore/rock_properties.aspx.
SCHRAMM, L. L. & GREEN, W. H. F. 1995. The influence of marangoni surface elasticity on gas mobility reductions by foams in porous media. *Colloids and Surfaces A: Physicochemical and Engineering Aspects,* 94**,** 13-28.
SCHRAMM, L. L. & WASSMUTH, F. 1994. Foams: Fundamentals and Applications in the Petroleum Industry. *In:* COMSTOCK, M. J. (ed.) *Foams: Fundamentals and Applications in the Petroleum Industry.* Washington, DC: American Chemical Society.
SCHUBERT, H. 1982. *Kapillarität in porösen Feststoffsystemen*, Springer-Verlag GmbH.
SHYEH-YUNG, J. G. J. 1991. Mechanisms of Miscible Oil Recovery: Effects of Pressure on Miscible and Near-Miscible Displacements of Oil by Carbon Dioxide. *In:* ENGINEERS, S. O. P. (ed.) *SPE Annual Technical Conference and Exhibition, 6-9 October.* Dallas, Texas: Society of Petroleum Engineers.

SIEMONS, N., BRUINING, H., CASTELIJNS, H. & WOLF, K.-H. 2006a. Pressure dependence of the contact angle in a CO2–H2O–coal system. *Journal of colloid and interface science,* 297**,** 755-761.

SIEMONS, N., BRUINING, H., WOLF, K.-H. & PLUG, W.-J. 2006b. Pressure dependence of the CO2 contact angle on bituminous coal and semi-anthracite in water. *Paper,* 605**,** 22-26.

SIMJOO, M., REZAEI, T., ANDRIANOV, A. & ZITHA, P. L. J. 2013. Foam stability in the presence of oil: Effect of surfactant concentration and oil type. *Colloids and Surfaces A: Physicochemical and Engineering Aspects,* 438**,** 148-158.

SKARRESTAD, M. & SKAUGE, A. 2010. *Reservoarteknikk II. Course compendium PTEK213*, University of Bergen.

SKAUGE, A., SPILDO, K., HØILAND, L. & VIK, B. 2007. Theoretical and experimental evidence of different wettability classes. *Journal of Petroleum Science and Engineering,* 57**,** 321-333.

SKJÆVELAND, S. M. & KLEPPE, J. 1992. *SPOR Monograph, recent Advances in Improved Oil Recovery Methods for North Sea Sandstone Reservoirs,* Stavanger, Norwegian Petroleum Directorate.

SMITH, D. M. & WILLIAMS, F. L. 1984. Diffusional Effects in the Recovery of Methane From Coalbeds. *Society of Petroleum Engineers Journal,* 24**,** 529 - 535.

SORBIE, K. & VAN DIJKE, M. 2004. Fundamentals of three-phase flow in porous media of heterogeneous wettability. *Institute of Petroleum Engineering, Heriot-Watt University, Edinburgh, Scotland*.

SPENCE, A. P., JR. & WATKINS, R. W. 1980. The Effect Of Microscopic Core Heterogeneity On Miscible Flood Residual Oil Saturation. *In:* ENGINEERS, S. O. P. (ed.) *SPE Annual Technical Conference and Exhibition, 21-24 September.* Dallas, Texas: Society of Petroleum Engineers.

STALKUP, F. I. 1970. Displacement of oil by Solvent at High Water Saturation. *Society of Petroleum Engineers Journal,* 10**,** 337 - 348.

STEVENS, J. E., HARPOLE, K. J., ZORNES, D. R. & MARTIN, F. D. 1992. CO2 Foam Field Verification Pilot Test at EVGSAU: Phase II - Foam Injection Design and Operating Plan. *In:* ENGINEERS, S. O. P. (ed.) *SPE Annual Technical Conference and Exhibition, 4-7 October.* Washington, D.C.: Society of Petroleum Engineers.

STEVENS, J. E. E. A. 1995. CO2 Foam Field Verification Pilot Test at EVGSAU: Phase IIIB -Project Operations and Performance Review. *SPE Reservoir Engineering,* 10**,** 266-272.

SVENNINGSEN, S. 2011. *An experimental study of CO2 injection for enhanced oil recovery in chalk and limestone.* MSc, University of Bergen.

TANZIL, D., HIRASAKI, G. J. & MILLER, C. A. 2000. Mobility of Foam in Heterogeneous Media: Flow Parallel and Perpendicular to Stratification. *In:* ENGINEERS, S. O. P. (ed.) *SPE Annual Technical Conference and Exhibition, 1-4 October.* Dallas, Texas: Society of Petroleum Engineers.

TEKLU, T. W., ALHARTHY, N., KAZEMI, H., YIN, X., GRAVES, R. M. & AL-SUMAITI, A. M. 2013. Minimum Miscibility Pressure in Conventional and Unconventional Reservoirs. *In:* ENGINEERS, S. O. P. (ed.) *Unconventional Resources Technology Conference, 12-14 August.* Denver, Colorado, USA: Society of Petroleum Engineers.

VIKINGSTAD, A. K., SKAUGE, A., HØILAND, H. & AARRA, M. 2005. Foam–oil interactions analyzed by static foam tests. *Colloids and Surfaces A: Physicochemical and Engineering Aspects,* 260**,** 189-198.

VIKSUND, B. G., ELIERTSEN, T., GRAUE, A., BALDWIN, B. & SPINLER, E. 1997. 2D-Imaging of the Effect from Fractures on Oil Recovery in Large Blocks of Chalk. *International Symposium of the Scociety of Core Analysts.* Calgary, Canada.

VIKSUND, B. G., GRAUE, A., BALDWIN, B. & SPINLER, E. 2-D Imaging of Waterflooding a Fractured Block of Outcrop chalk. 5th Chalk Research Symposium, Oct. 7-9 1996 1996 Reims, France.

WALSH, M. P., NEGAHBAN, S. & GUPTA, S. P. 1989. An Analysis of Water Shielding in Water-Wet Porous Media. *In:* ENGINEERS, S. O. P. (ed.) *SPE Annual Technical Conference and Exhibition, 8-11 October.* San Antonio, Texas Society of Petroleum Engineers.

WANG, G. C. 1982. Microscopic Investigation of CO2, Flooding Process. *Journal of Petroleum Technology,* 34**,** 1 789 - 1 797.

WANG, G. C. 1984. A Laboratory Study of CO2 Foam Properties and Displacement Mechanism. *In:* ENGINEERS, S. O. P. (ed.) *SPE Enhanced Oil Recovery Symposium, 15-18 April.* Tulsa, Oklahoma: Society of Petroleum Engineers.

WATKINS, R. W. 1978. A Technique For The Laboratory Measurement Of Carbon Dioxide Unit Displacement Efficiency In Reservoir Rock. *In:* ENGINEERS, S. O. P. (ed.) *SPE Annual Fall Technical Conference and Exhibition, 1-3 October.* Houston, Texas Society of Petroleum Engineers.

WELLINGTON, S. & VINEGAR, H. 1985. CT studies of surfactant-induced CO2 mobility control. *In:* ENGINEERS, S. O. P. (ed.) *SPE Annual Technical Conference and Exhibition, 22-26 September.* Las Vegas, Nevada: Society of Petroleum Engineers.

WIEBE, R. & GADDY, V. L. 1940. The solubility of carbon dioxide in water at various temperatures from 12° to 40° and at pressures to 500 atmospheres: Critical phenomena. *Jornal of the American Chemical Society*.

WILLIAMS, C. A., ZANA, E. N. & HUMPHRYS, G. E. 1980. Use Of The Peng-Robinson Equation Of State To Predict Hydrocarbon Phase Behavior And Miscibility For Fluid Displacement. *In:* ENGINEERS, S. O. P. (ed.) *SPE/DOE Enhanced Oil Recovery Symposium, 20-23 April.* Tulsa, Oklahoma: Society of Petroleum Engineers.

YDSTEBØ, T. 2013. *Enhanced Oil Recovery by CO2 and CO2-foam in Fractured Carbontes.* MSc, University of Bergen.

ZINATI, F. F., FARAJZADEH, R. & ZITHA, P. L. J. 2008. Foam Modeling in Heterogeneous Reservoirs Using Stochastic Bubble Population Approach. *SPE Symposium on Improved Oil Recovery, 20-23 April.* Tulsa, Oklahoma, USA Society of Petroleum Engineers.

ZITHA, P. & DU, D. 2010. A new stochastic bubble population model for foam flow in porous media. *Transport in Porous Media,* 83**,** 603-621.

ZOLOTUCHIN, A. B. & URSIN, J.-R. 2000. *Introduction to petroleum reservoir engineering,* Kristiansand, Høyskoleforlaget.

ZUTA, J., FJELDE, I. & BERENBLYUM, R. Oil Recovery during CO2-foam Injection in Fractured Chalk Rock at Reservoir Conditions. Int. Symp. Society of Core Analysts, 2009 Noordwijk, Netherlands. Society of Core Analysts, 26-30.

Appendix A – Uncertainty calculations

The results presented in this thesis required many steps in core preparations and experimental work, in which all has uncertainties related to them, in addition to uncertainties in instruments like pumps and pressure gauges.

The uncertainty for value R given from the variables x, y, z, …, i with respective uncertainties given by S_x, S_y, S_z, …, S_i can be calculated by equation:

$$S_{\bar{R}} = \sqrt{\left(\frac{\partial R}{\partial x} S_{\bar{x}}\right)^2 + \left(\frac{\partial R}{\partial y} S_{\bar{y}}\right)^2 + \left(\frac{\partial R}{\partial z} S_{\bar{z}}\right)^2 + \ \ldots + \left(\frac{\partial R}{\partial i} S_{\bar{i}}\right)^2} \tag{A.1}$$

where $\bar{x}$, $\bar{y}$, $\bar{z}$, …, $\bar{\imath}$, are the arithmetical middle value of the measured variables given by:

$$\bar{x} = \frac{x_1 + x_2 + \cdots + x_N}{N} = \frac{1}{N} = \sum_{i=1}^{N} x_i \tag{A.2}$$

Assuming R as a product of the variables a^2, b^2 and c^2, equation A.1 may be written as:

$$\frac{S_{\bar{R}}}{R} = \sqrt{\left(a\frac{S_{\bar{x}}}{x}\right)^2 + \left(b\frac{S_{\bar{b}}}{x}\right)^2 + \left(c\frac{S_{\bar{c}}}{x}\right)^2} \tag{A.3}$$

The uncertainty related to the permeability measurements based on Darcy's law is calculated by equation A.4, including the error contribution from all various variables: rate (Q), viscosity (μ), Length (L), cross section area (A) and pressure drop (ΔP).

$$\frac{S_{\bar{K}}}{K} = \sqrt{\left(\frac{S_{\bar{Q}}}{Q}\right)^2 + \left(\frac{S_{\bar{\mu}}}{\mu}\right)^2 + \left(\frac{S_{\bar{L}}}{L}\right)^2 + \left(\frac{S_{\bar{A}}}{A}\right)^2 + \left(\frac{S_{\overline{\Delta P}}}{\Delta P}\right)^2} \tag{A.4}$$

Uncertainties regarding porosity include error contribution from the pore volume, $V_p = m/\rho$, where m is the fluid mass and ρ is the density, and the bulk volume ($V_{bulk} = \pi r^2 L$), where r is the radius of the core and L is the length. The uncertainty in the bulk volume is given by:

$$S_{\bar{V}_{bulk}} = \sqrt{(2 \cdot \pi \cdot r \cdot L \cdot S_{\bar{r}})^2 + (\pi \cdot r^2 \cdot S_{\bar{L}})^2} \tag{A.5}$$

The uncertainty related to the pore volume may be calculated by:

$$S_{\overline{V_P}} = \sqrt{\left(m \cdot S_{\bar{\rho}}\right)^2 + (\rho \cdot S_{\bar{m}})^2} \tag{A.6}$$

The uncertainty in the porosity may then be calculated by equation A.7 and including the contribution from the uncertainty calculate from equation A.5 and A.6.

$$S_{\bar{\varphi}} = \sqrt{\left(\frac{1}{\bar{V}_{bulk}{}^2} S_{\overline{V_P}}\right)^2 + \left(-\frac{V_P}{\bar{V}_{bulk}{}^2} S_{\bar{V}_{bulk}}\right)^2} \tag{A.7}$$